FORGE
Fate Of Repository Gases
European Commission FP7

# FORGE Deliverable D1.3

# Progress report on benchmark studies on repository-scale numerical simulations of gas migration

# March 2010


Authored by:

| | |
|---|---|
| Belgium | Li Yu (SCK-CEN), |
| France | Jacques Wendling (ANDRA) |
| | Magdalena Dymitrowska & Delphine Pellegrini (IRSN) |
| Lithuania | Darius Justinavicius (LEI) |
| Switzerland | Manuel Sentis (ENSI) |
| United Kingdom | Simon Norris (NDA RWMD) |
| | Alex Bond (Quintessa) |


| | | |
|---|---|---|
| Compiled by: | Jacques Wendling | Date: 26st March 2010 |
| Checked by: | | Date: |
| Approved by: | | Date: |
| EC Project Officer: | | Date: |


## Euratom 7th Framework project: FORGE 2010

**F**ate **O**f **R**epository **G**as**E**s (FORGE)

The multiple barrier disposal concept is the cornerstone of all proposed schemes for geological disposal of radioactive wastes. The concept is based on a series of passive complementary barriers, both engineered and natural, that act to achieve the required level of safety for radioactive waste disposed in a geological repository.

Demonstrating an appropriate understanding of gas generation and migration is a key component in a safety case for a geological repository for radioactive waste. On the basis of work to date, the overall behaviour of waste-derived gas and its influences on repository system performance require improved understanding. Key issues to be further examined relating to an enhanced understanding of gas-related processes include: dilational versus visco-capillary flow mechanisms; long-term integrity of seals, in particular gas flow along contacts; role of the EDZ as a conduit for preferential flow; and laboratory to field up-scaling. Such issues are the focus of the integrated, multi-disciplinary European Commission FORGE project.

The FORGE project links international radioactive waste management organisations, regulators and academia, and is specifically designed to tackle the key research issues associated with the generation and movement of repository gases associated with waste disposed in a geological repository. Of particular importance are the long-term performance of bentonite buffers, plastic clays, indurated mudrocks and crystalline formations. Further experimental data are required to reduce uncertainty relating to the quantitative treatment of gas in performance assessment.

FORGE will address these issues through a series of laboratory and field-scale experiments, including the development of new methods for up-scaling allowing the optimisation of concepts through detailed scenario analysis. The FORGE partners are committed to training and CPD through a broad portfolio of training opportunities and initiatives which form a significant part of the project.

Further details on the FORGE project and its outcomes can be accessed at www.FORGEproject.org.

*Contact details:*

*EC FORGE Work Package 1 Leader:*

Dr Simon Norris

Nuclear Decommissioning Authority – Radioactive Waste Management Directorate

Tel +44 1925 802891

Fax +44 1925 802948

Email simon.norris@nda.gov.uk

Web address: www.nda.gov.uk

Address NDA Harwell
Building 587
Curie Avenue
Harwell Science and Innovation Campus
Didcot
Oxon OX11 0RH
United Kingdom

# Table of content


**1. Context and introduction 8**

**2. Definition of the benchmark 9**

**3. Summary of the work done by the different teams 11**

***3.1 NDA RWMD contribution 11***

3.1.1 Model Implementation 11
3.1.2 Base Case Results 13
3.1.3 Prescribed Sensitivity Cases 16
3.1.4 Additional Sensitivities 16
3.1.5 References 17

***3.2 SCK-CEN contribution 18***

3.2.1 INTRODUCTION 18
3.2.2 MODELISATION OF THE REPOSITORY 18
3.2.3 Results 22

***3.3 Andra contribution 30***

3.3.1 Simulation program 30
3.3.2 Deviations from the definition of the benchmark and from original version of Tough2-MP 30
3.3.3 Anisotropy: 30
3.3.4 Physical parameters: 30
3.3.5 Boundary conditions: 32
3.3.6 Production term for hydrogen: 32
3.3.7 Outputs: 32
3.3.8 Gas phase relative permeability: 32
3.3.9 Mesh size and refinement 33
3.3.10 Time step management and numerical issues 34
3.3.11 Selected results 35

***3.4 IRSN contribution (M. DYMITROWSKA) 38***

3.4.1 Simulation code 38
3.4.2 Differences with respect to the benchmark definition 40
3.4.3 Simulations results 41
3.4.4 Conclusion and perspectives 43

***3.5 LEI contribution 45***

3.5.1 Numerical code 45
3.5.2 Main Features of TOUGH2/EOS5 45
3.5.3 Modelling approach and the deviations from the definition of the benchmark: 45

***3.6 ENSI/IFSN contribution 49***

3.6.1 Introduction 49
3.6.2 Programs used for the model 49
3.6.3 Implementation of the grid 49
3.6.4 Initial conditions and boundary conditions 52
3.6.5 Installation of TOUGH2-MP and modifications in the code 53
3.6.6 Scope of future work of ENSI in FORGE 55

**4. Global synthesis of the benchmark so far 56**

***4.1 Comparison of the available results and main phenomenological results 56***

*4.2 Sensitivity analysis results 62*
4.2.1 Sensitivity 1 : Permeability of EDZ reduced to permeability of the undisturbed rock 62
4.2.2 Sensitivity 2 : use of different relative permeability curves 63
4.2.3 Sensitivity 3 : Diffusion coefficient of dissolved gas multiplied by 10 65
*4.3 Main problems encountered 66*
4.3.1 Boundary conditions representation 66
4.3.2 Time step management 66
4.3.3 Mesh optimisation 67

**5. Interactions with other FORGE WP's 69**

**6. Future work 70**

**7. ANNEX : Full description of the benchmark 72**
*7.1 CONTEXT AND OBJECTIVES 72*
*7.2 REFERENCE TEST CASE 72*
7.2.1 GEOMETRY 73
7.2.2 PHYSICAL PARAMETERS 74
7.2.3 Initial conditions 76
7.2.4 Boundary conditions 76
7.2.5 Production term for hydrogen 77
7.2.6 Simulation period 78
*7.3 SENSITIVITY ANALYSIS 78*
*7.4 OUTPUT RESULTS 78*
*7.5 MATHEMATICAL MODEL PROPOSED FOR THE EXERCISE 81*

# List of figures

**Definition of benchmark**
Figure 1 : Representation of the axisymmetric calculation domain 9

**NDA-RWMD contribution**
Figure 2: Gridded geometry for the QPAC runs, coloured by material type. The location of prescribed (non no-flow) boundaries are shown in blue. 12
Figure 3: Plot of free gas flow into the drift from the EDZ, plug and interfaces 13
Figure 4: Plot of dissolved gas flux from cell EDZ into the host-rock. 14
Figure 5: Log10 Gas Saturation at selected times for the base case 15
Figure 6: 3D grid using the 'squared off' grid geometry 16

**SCK-CEN contribution**
Figure 7: Problem geometry 18
Figure 8: Mesh of the domain and the imposed boundary conditions 19
Figure 9: Comparison of gas/liquid pressure between benchmark definition and numerical simulation at the boundary of drift 20
Figure 10 : retention curve of interface 21
Figure 11 : Gas flux around the disposal cell at t=330 years (kg/s) 23
Figure 12 : Gas flux vector at t=10000 years 23
Figure 13 : comparison of amount of gaseous gas phase trrough three boundaries 24
Figure 14 : Unsaturated area t=10000 years 24
Figure 15 : of water saturation along line $L_{cell}$ 24
Figure 16 : Liquid flux during resaturation process t=27 years 25
Figure 17 : water pressure contour (thick arrow marks the direction of water flow) 26
Figure 18 : comparison of gaseous gas flux through interface and EDZ for two cases (t=5000 years) 26
Figure 19 : Time variation of gaseous gas flux through $S_{int1}$ 27
Figure 20 : Comparisons of gaseous gas flux at boundaries $S_{EDZ1}$ for two cases 27
Figure 21 : Comparisons of gaseous gas flux at boundaries $S_{cell}$ for two cases 27
Figure 22 : Comparisons between three cases 28

**Andra contribution**
Figure 23: gas phase relative permeability, for interface materials, at lower gas phase saturations 33
Figure 24: Mesh selected for the different simulations 34
Figure 25: Mesh selected for the different simulations (zoom around the access drift) 34
Figure 26: Illustration of influence of the residual gas saturation value 35
Figure 27: Reference Case : evolution with time of gas pressure (left) and liquid saturation (right) 35
Figure 28: Sensitivity case 1: evolution with time of gas pressure (left) and liquid saturation (right) 36
Figure 29: Sensitivity case 2: evolution with time of gas pressure (left) and liquid saturation (right) 36
Figure 30: Sensitivity case 3: evolution with time of gas pressure (left) and liquid saturation (right) 37

**IRSN contribution**

Figure 31 : Effective cappilary pressure on the interface between two materials. 39
Figure 32 : Zoom of the initial saturation field near the beginning the cell 40
Figure 33 : Gas Pressure evolution in observation points 42
Figure 34 : Water saturation evolution in the observation points 42
Figure 35 Water saturation field at t=2.3years near the P3 point (red dot) 43
Figure 36 Zoom of gas pressure and water saturation field at t=1y and t=2.3y 44

**LEI contribution**

Figure 37 : Schematic view of the geometry and mesh of the axisymetrical configuration 46
Figure 38 : Schematic representation of the lines along which results should be given 47
Figure 39 :. Evolution of gas saturation along interface for different time periods 47
Figure 40 : Schematic representation of the point where results should be given 48
Figure 41 : Evolution of gas saturation in different points 48
Figure 42 : Evolution of capillary pressure in different points 48

**ENSI contribution**

Figure 43 Domain of the model proposed for the first exercise. 49
Figure 44 Mesh used for the numerical simulations with TOUGH2 and TOUGH2-MP, the mesh consists of 6200 nodes. 50
Figure 45 Detail of the mesh in the common region of the EDZ, bentonite and access drift. The differences in sizes of the nodes for the different materials are noticeable. 51
Figure 46 Detail of the mesh close to the corner in the interface facing canister. 51
Figure 47 ENSI Results for pressure values for the first hundred years in different points of the model. 53

**Global synthesis**

Figure 48: position of point 4 in the model 56
Figure 49: evolution with time of water pressure at point 4 57
Figure 50: evolution with time of gas pressure at point 4 57
Figure 51: Position of point 9 in the model 58
Figure 52: evolution of water pressure with time at point 9 58
Figure 53: position of mine Lcell in the model 59
Figure 54: evolution with time of the water saturation in the first on and a half meter radially from cell axis along line Lcell at different time. Results from NDA/Quintessa 59
Figure 55: evolution with time of the water saturation in the first on and a half meter radially from cell axis along line Lcell at different time. Results from Andra 60
Figure 56: position of the interface on with gas flux is calcultated 61
Figure 57: evolution with time of the gas flux toward the access drift for both teams 61
Figure 58: Evolution with time of the gas pressure at point 4 62
Figure 59 : comparison of gas flux toward the drift between reference case and sensitivity 1 for andra's results 63
Figure 60 : comparison of gas flux toward the drift between reference case and sensitivity 1 for NDA-RWMD's results 63
Figure 61 : comparison of gas flux toward the drift between reference case and sensitivity 2 for andra's results 64
Figure 62 : comparison of gas flux toward the drift between reference case and sensitivity 2 for NDA-RWMD's results 64

Figure 63 : comparison of gas flux toward the drift between reference case and sensitivity 3 for andra's results 65
Figure 64 : comparison of gas flux toward the drift between reference case and sensitivity 3 for NDA-RWMD's results 65
Figure 65: example of a coarse regular mesh 67
Figure 66: example of a refined unstructered non conform mesh 68

**ANNEX**

Figure 67: Representation of the axisymetric calculation domain 73
Figure 68: Dimensions in the calculation domain 73
Figure 69: schematic representation of the boundary conditions 76
Figure 70: Time variable boundary conditions to be used in the drift 77
Figure 71: schematic representation of the surfaces trough which fluxes will be calculated 79
Figure 72: schematic representation of the lines along which results should be given 80
Figure 73: schematic representation of the point where results should be given 81

# List of tables

**SCK-CEN contribution**
Table 1: Material properties used in calculations for the base case. 22

**ENSI contribution**
Table 2 Changes made in the intrinsic permeabilities in order to fulfil the requirements of the axial symmetry. 55

**ANNEX**
Table 3 : Size of items in the calculation domain 74
Table 4 : Physical characteristics of materials 74

# 1. Context and introduction

This document is the first intermediate report on the work done for FORGE WP1.2 in the context of a benchmark simulation concerning gas generation and migration at repository depth (many hundreds of metres below ground level) and repository scale. The work described has been undertaken during the second semester of 2009. Some of the teams involved in this work package have not yet begun their work as it was planned from the outset that their contribution will initiate in 2010 only. The results presented are therefore only partial and the final aim of the work package is far from being achieved. Nevertheless, some interesting points can already be mentioned.

One of the main problems in dealing with different teams from different countries, who have different disposal concepts, is to find a common representation as a basis for the benchmark. This implies simplifications are necessary to real concepts, in order that they be represented at a basic level that has some degree of consistency to all participants. Another point is to find a common initial benchmark definition that can satisfy any team, so something quite simple is needed at the outset, so that teams can have a first trial and, in comparing the respective results thus obtained, verify that basics are well understood by each team.

At the start of WP1.2 activities, after discussion, there was a general agreement that the reference exercise will be as generic as possible (without targeting precisely on national concepts), with sensitivity analyses making it possible to cover national specificities. The aim here is more to understand the behaviour of the modeled system as underastood by each participant, rather than to undertake an inter-comparison of codes. A second agreement was that, although the final aim of the benchmark studies is to represent repository-scale simulations, the first exercise should be rather simple and at cell scale.

To give some added value to this first exercise, a feature not yet well represented in usual gas simulations was introduced: the explicit representation of the interface between canisters and cell walls.

After a brief description of the benchmark definition (see Section 2), Section 3 of this report collates the results to date of each WP1.2 participant. This is followed (Section 4) by a comparison of the main results produced by each participant. The main problems encountered, and the main conclusions so far, are also discussed. To conclude, the proposed work programme for the first semester of 2010 is also presented.

# 2. Definition of the benchmark

**N.B.** : The complete definition of the benchmark can be found in the Annex

To be able to understand water and gas flow at the repository scale, it is necessary to understand the water and gas flow associated with sub-repository "cell" scale components (e.g. on the scale of a vault or tunnel). Information is needed at an appropriate level of detail in order to upscale from the cell level to the full repository level, via perhaps intermediate modules scales of e.g. several tens of cells.

For this reason, the first benchmark was defined at cell level. The type of cell considered is a somehow generic high level waste cell in a clay host rock. As the scale is quite small, it is possible to represent fine geometric features, and especially the interface between the canister and clay rock as well as interface between bentonite seal and clay rock (considered as a centimetre-thick region). As permeability is increased in the EDZ, this zone is also represented.

To stay as generic as possible, the gas flux rate in this benchmark is represented by a simple step function lasting 10,000 years; the simulation time is limited to 100,000 years. To understand the distinct role of each phenomenon, the reference case is not considering any coupling. This will be done further on in the sensitivity analysis (second 2010 semester).

As most of the materials in ths benchmark are assigned very low permeability, capillary process will be dominant over gravity. Therefore the mesh can be built as axisymmetric without losing any important phenomenology.

Figure 1 gives a representation of the represent area and the type of material defined.

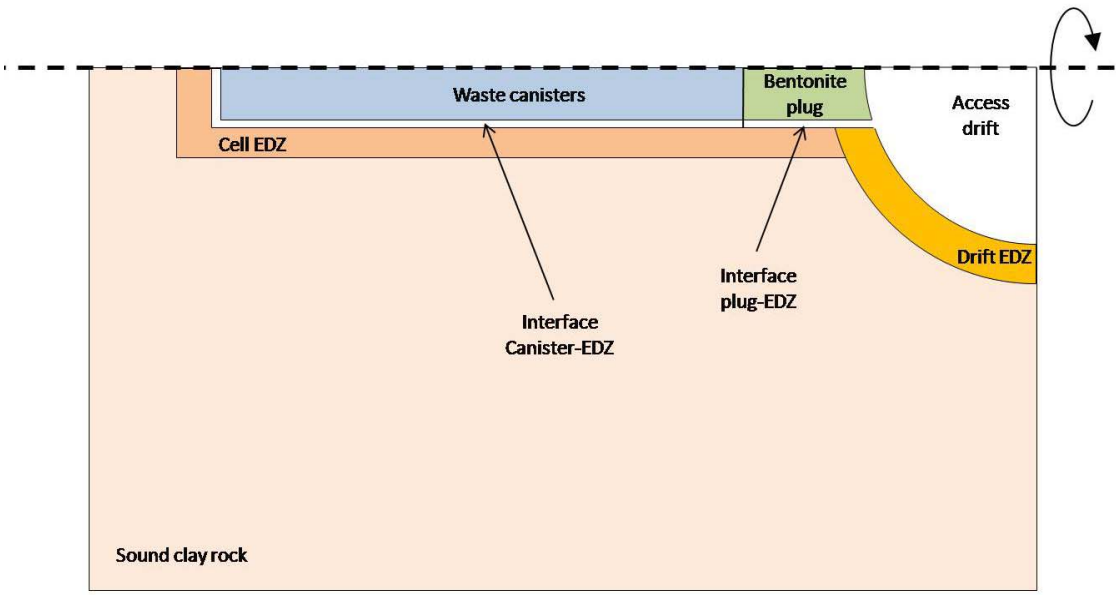


*Figure 1 : Representation of the axisymmetric calculation domain*

More details and the complete benchmark definition can be found in the Annex

# 3. Summary of the work done by the different teams

***N.B.*** *: There is no actual contribution from CEA (France) and CNRS (France) as these two teams have planned from the beginning to initiate work only in 2010*

## 3.1 NDA RWMD contribution

***N.B****. : the simulation work was undertaken by Quintessa on behalf of NDA RWMD*

### 3.1.1 Model Implementation

The model was implemented in the Quintessa multi-physics code "QPAC" using the specification as the only source of input (FORGE, 2009). The standard Multi-Phase-Flow (MPF) QPAC module retains all the process model functionality required by this case (Bond and Benbow, 2009), and hence the process and geometry could be implemented exactly as described, i.e. multiphase flow of water with a gas phase (hydrogen) together with consideration of dissolved hydrogen and water vapour diffusion. Consistent with the specification there is no distinction between the initially present gas (air) and generated hydrogen.

#### 3.1.1.1 Grid

QPAC uses a control volume approach to spatial discretisation, and for the reference case the model geometry was implemented using a simple reclined cylindrical grid (see below), with a single compartment in the angular direction to give a total of 520 compartments. Consistent with the geometrical details in the specification meant that the cylindrical section is effectively horizontal (i.e. out of the plane of gravity), so that buoyancy effects are ignored.

A 3D half-cylinder representation was also set up, as this allowed the possibility of examining the effect of gravity on the results through the use of additional angular discretisation, without forcing the use of a prohibitive number of cells.

For convenience the volume representing the waste was included in the model, but these compartments were isolated from the remainder of the grid, so took no part in the solve. The compartments representing the interfaces between the waste and EDZ, and plug and EDZ were specified as being a single compartment thick, but given the numerical formulation this gave no particular problems in representing the high lateral conductivity along the outside of the waste.

The definition of the anisotropy in the system and the effective assumption of horizontality of the 2D modelling section, meant that no anisotropy was present in the 2D model, although of course material variations were present.

A number of gridding options were available for representing the curve of the access drift and associated EDZ, however it was decided that a simple step-wise approximation to the curve was the most appropriate as it gave addition resolution around the periphery of the disposal cell and made discretising a full 3D version of the case relatively easy to implement.

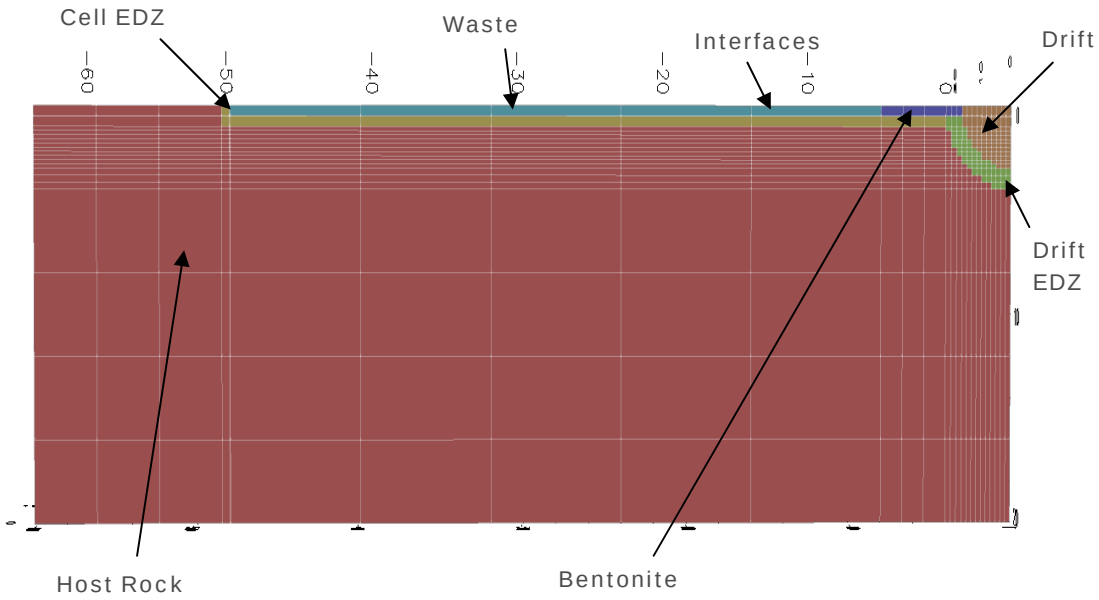


*Figure 2: Gridded geometry for the QPAC runs, coloured by material type. The location of prescribed (non no-flow) boundaries are shown in blue.*

#### 3.1.1.2 Boundary Conditions and Sources

As specified the interface between the waste and EDZ received the generated $H_2$ gas at a total rate of 50 mol/y (equivalent to 100 mol/y for the full model) divided amongst the interface compartments proportional compartmental volume.

The access drift boundary condition for water (total pressure and fluid saturation) was implemented as specified using the tabulated data provided. Full information was not provided on the gas boundary for the access drift. It was decided to adopt a pragmatic approach that allowed the gas pressure to vary sensibly with the water pressure.

At the boundary, a capillary pressure $P_c$ was calculated using the backfill characteristics supplied in the specification using the prescribed water boundary saturation. The gas pressure was calculated using the following algorithm:

$$P_{g0} = P_w + P_c$$

$$P_g = 1e5Pa \quad where \quad P_{g0} \leq 1e5Pa$$

$$P_g = P_{g0} \quad where \quad P_{g0} > 1e5Pa$$

where $P_w$ is the boundary water pressure. Effectively this assumes that the gas pressure is atmospheric until the water pressure rises sufficiently high that the water pressure itself can start increasing while using a sensible capillary pressure.

The outer radial boundary was implemented precisely as described, all other boundaries were designated as no-flow, consistent with the specification.

#### 3.1.1.3 Implementation Issues and Model Stability

There were no particular problems implementing the model as prescribed either in terms of geometry or through processes. The model results were examined for signs of significant numerical instability, but no evidence of problematic behaviour was

observed that wasn't explainable in terms of the time variant boundary conditions or expected behaviour. Solver information also showed no symptoms of particular problems, noting that the most 'difficult' part of the transient appears to be associated with the sudden cessation of gas generation at 10000 years.

### 3.1.2 Base Case Results

The fluid saturation, pressure and flux results appear to be generally consistent with the boundary conditions and initial conditions. In terms of water flow, the access drift acts as a significant sink to water with the generation of a large low pressure zone around the disposal cell which draws water towards this area. This low pressure zone disperses as the access drift pressure boundary conditions rise and is virtually eliminated after approximately 5000 years.

Free gas saturations only reach significant levels in the waste/EDZ interfaces, access drift and some parts of the EDZ (Figure 3). Saturations of free gas never reach more than 1.0e-3 in the host rock and seem to be largely associated with dissolved $H_2$ coming out of solution having diffused away from the EDZ.

The flux results (Figure 3, **Error! Reference source not found.**) show that loss of gas from the disposal is dominated almost completely by losses of free gas via the interfaces into the access drift. The large negative fluxes at early times arise from gas in the drift moving into the EDZ as the water flows towards the low pressure sink at the access drift boundary.

Nearly all of the remaining gas is lost via diffusion of dissolved gas from the EDZ to the host-rock and then on to the outer radial boundary.

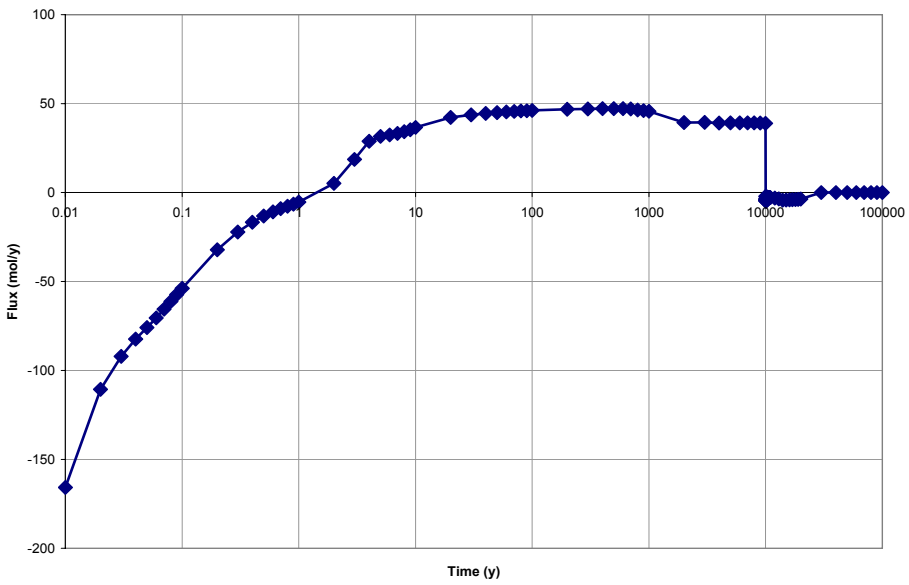


*Figure 3: Plot of free gas flow into the drift from the EDZ, plug and interfaces*

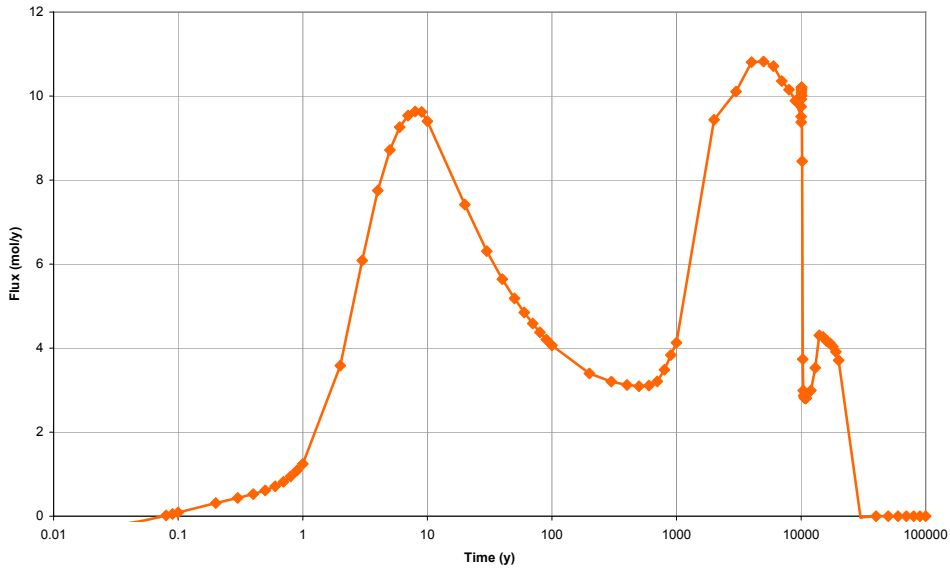


*Figure 4: Plot of dissolved gas flux from cell EDZ into the host-rock.*

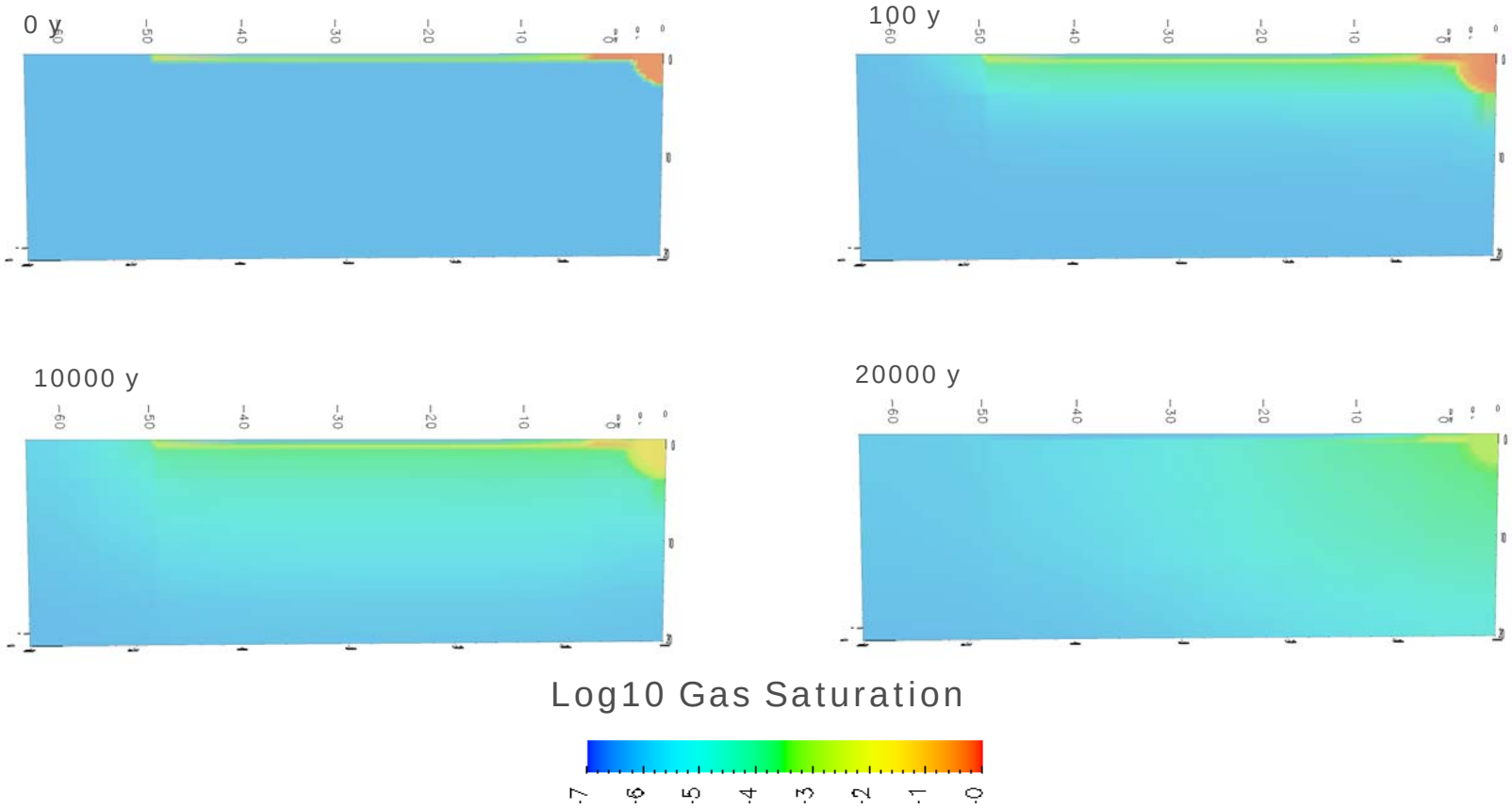


*Figure 5: Log10 Gas Saturation at selected times for the base case*

### 3.1.3 Prescribed Sensitivity Cases

The three sensitivity cases prescribed in the specification, which investigate impacts of effectively removing the EDZ (Case 1), selection of alternative relative permeability curves (Case 2) and enhanced hydrogen diffusivity in water (Case 3) were all run. The summary results were:

- Case 1: Removal of the EDZs had a significant early impact on limiting gas invasion from the access drift and the water pressure distribution in the host-rock, however it did little to change the general characteristics of gas losses from disposal cell, as losses from the interfaces still dominate.
- Case 2: The alternative relative permeability curves for selected media had almost no affect on the bulk fluxes and pressures. This is consistent with the interfaces dominating free gas movement in the model, with most other gas transport in the model being via diffusion of dissolved gas.
- Case 3: The enhancement of gas diffusivity by an order of magnitude had a dramatic effect on the bulk fluxes. It caused loss from the disposal cell due to the radial diffusion of hydrogen to dominate the gas transport processes at later times, and the role of free gas flows via the interfaces to be almost eliminated.

### 3.1.4 Additional Sensitivities

In addition some additional scoping calculations were conducted to examine areas of particular interest to the NDA team. Two related problems were examined:

1. Simplification of the geometry around the drift such that the geometry of the access drift was 'squared off' and a general reduction in resolution around the disposal cell. This results in fewer compartments/unknowns in the problem and hence provides a faster model that can be more effectively used as the basis for sensitivity analysis.
2. Implementation of a full 3D model using angular discretisation of the squared off geometry and hence including gravitational effects.

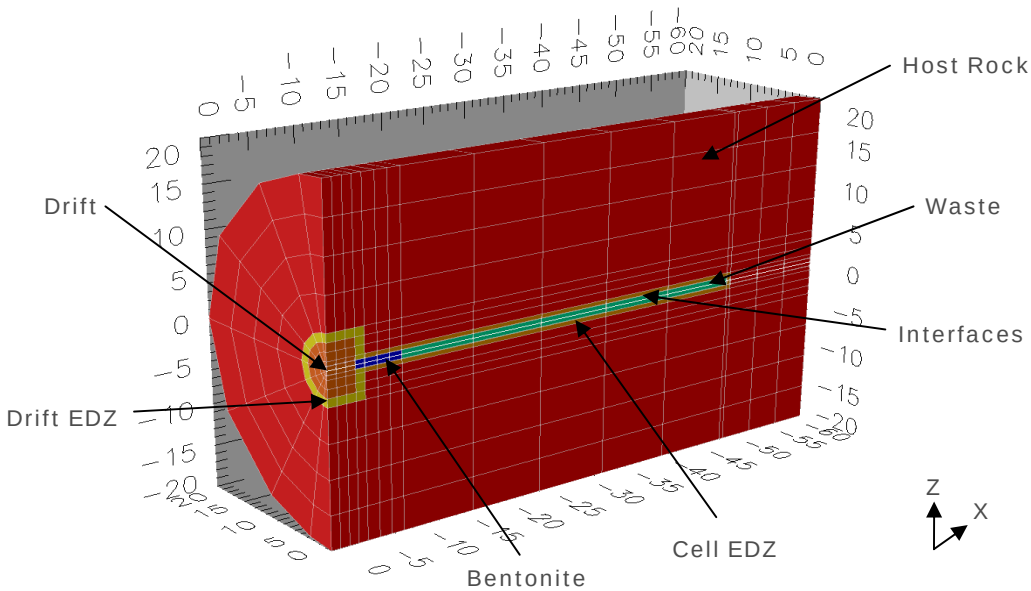


*Figure 6: 3D grid using the 'squared off' grid geometry*

The key results from this analysis were:

1. Inclusion of a simplified 'squared off' geometry for the drift only impacts on pressures and saturations local to the geometrical change and then only to a relatively minor degree – other differences were relatively minor including the bulk fluxes in the model.
2. The 3D model, shows some changes to local pressures and saturations, most notably in causing gas to accumulate at the top of the cell EDZ and interfaces. Otherwise the general fluxes of gas to the host-rock and drift access were largely unchanged. The differences in saturations appeared to average out in some manner to produce a result that is very similar to the equivalent 2D case.

Both of these results are interesting in that they imply quite strong simplifications can be made to system representation without compromising the results themselves. In particular the second result implies , as the case is currently specified, that the specification of the as a 2D section does not compromise the realism of the model in significant fashion, whilst the first result suggest that a fairly simplified representation of the 2D geometry is still appropriate.

### 3.1.5 References

Bond AE. and Benbow SJ. (2009). QPAC Multi-Phase Flow Module Functional Specification and Architectural Design. Quintessa Report QRS-3000C-4 v1.0.

FORGE (2009). FORGE WP1.2 :First step toward a benchmark for 3D Modelling of a disposal area for vitrified waste.

## 3.2 SCK-CEN contribution

### 3.2.1 INTRODUCTION

The aim of the first benchmark is trying to answer some pertinent questions from long-term safety point of view (for example, which component could play the dominant role in the migration of gas, EDZ, interfaces or backfill?). It aims to examine the behaviour of the system and study the influence of the system components, rather than an inter-comparison of codes. Although the final aim of the benchmark studies is to represent repository-scale simulations, the first exercise is at cell scale and as generic as possible.

### 3.2.2 MODELISATION OF THE REPOSITORY

CODE_BRIGHT 3.0 developed by Technical University of Catalunya (UPC) is used for the benchmark calculation. Software GID 8.0 developed by International Center for Numerical Methods in Engineering (CIMNE) is used for the pre and post-processing.

#### 3.2.2.1 Geometry and boundary conditions

The benchmark intends to simulate the gas migration in a disposal cell and a portion of the drift (Figure 7)

The benchmark exercise is a two-dimensional axisymetric problem with isothermal hypothesis at 20°C. In the direction of the disposal cell axis, the extension is assumed to be 50 m which takes into account the length of the cell, the distance between two adjacent cells and a portion of the access drift. The radius of the axisymetric domain is assumed to be 20 m which is a compromise between the inter-cell distance along the access drift and the thickness of the geological layer. For the detailed dimensions of the benchmark problem, please refer to the full definition of the benchmark exercise.

A gas production term is attributed to the disposal cell. It is imposed on the external surface of the cylinder which represents schematically the canisters. The disposal cell is constituted as a material impermeable to both water and gas. The materials to be taken into account in the simulation include the EDZ of both the cell and the access drift, the cell plug, the backfill of the drift, interface and geological medium. Note that the interface at the level of the seal has different properties than the interface between the disposal cell and the cell EDZ.

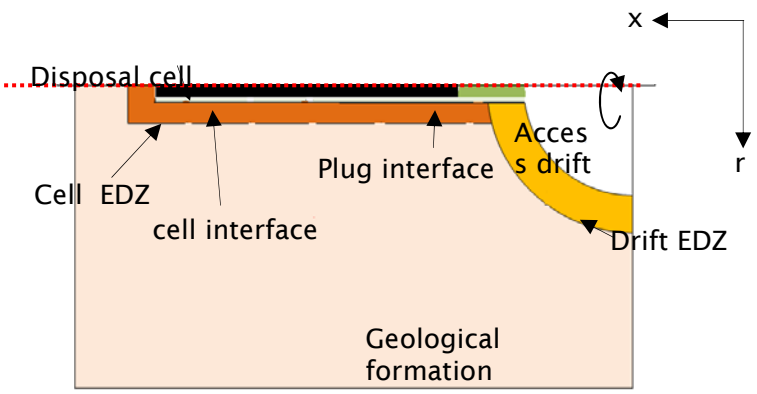


*Figure 7: Problem geometry*

The whole domain is meshed with 2328 quadrilateral linear elements (Figure 8).

The Hydrogen produced from the canister cell is considered uniformly distributed within the cell. In the simulation, cell canister and cell interface are not included considering that the permeability

of cell interface is six orders higher than that of EDZ, gas could be imposed directly on the surface of cell EDZ. Time evolution of hydrogen production is illustrated in Figure 8. A constant hydrogen influx (0<t<10000 years) as $J = Q / S_{cell}$ is imposed directly along the inner surface of the cell EDZ and left end of the plug (red solid line in Figure 8)

where Q=100 mol/year/cell =100*0.002/365/86400=6.34×$10^{-9}$ kg/s/cell;

surface area of the canister cell $S_{cell}$=2*pi*Rc*Lc+2*pi*Rc*Rc=2*3.14*0.5*40+2*3.14*0.5*0.5=127.17 $m^2$/cell;

J=(6.34×$10^{-9}$ kg/s/cell)/(127.17 $m^2$/cell)=5×$10^{-11}$ kg/s/$m^2$.

Except for the outer boundary with fixed gas and liquid pressure (blue dashed line), the other boundaries are all assumed to be no flux boundaries (black line). Although, gas/liquid pressures at the drift boundary (pink line) were assigned to be time variable in the original benchmark definition (dot line in Figure 9), in the actual numerical simulation, the pink line is treated to be a no flux boundary because of convergence problem. However, the comparison of gas/liquid pressure between benchmark definition and numerical simulation at the drift boundary for the base case shows that the difference is not significant especially for the gas pressure (Figure 9).

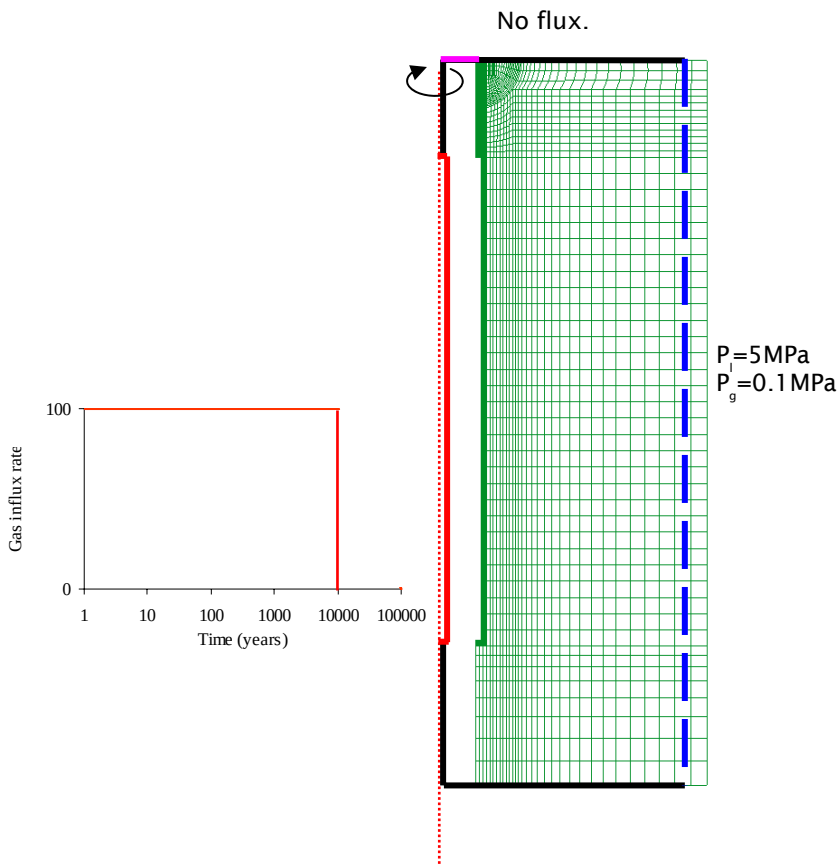


*Figure 8: Mesh of the domain and the imposed boundary conditions*

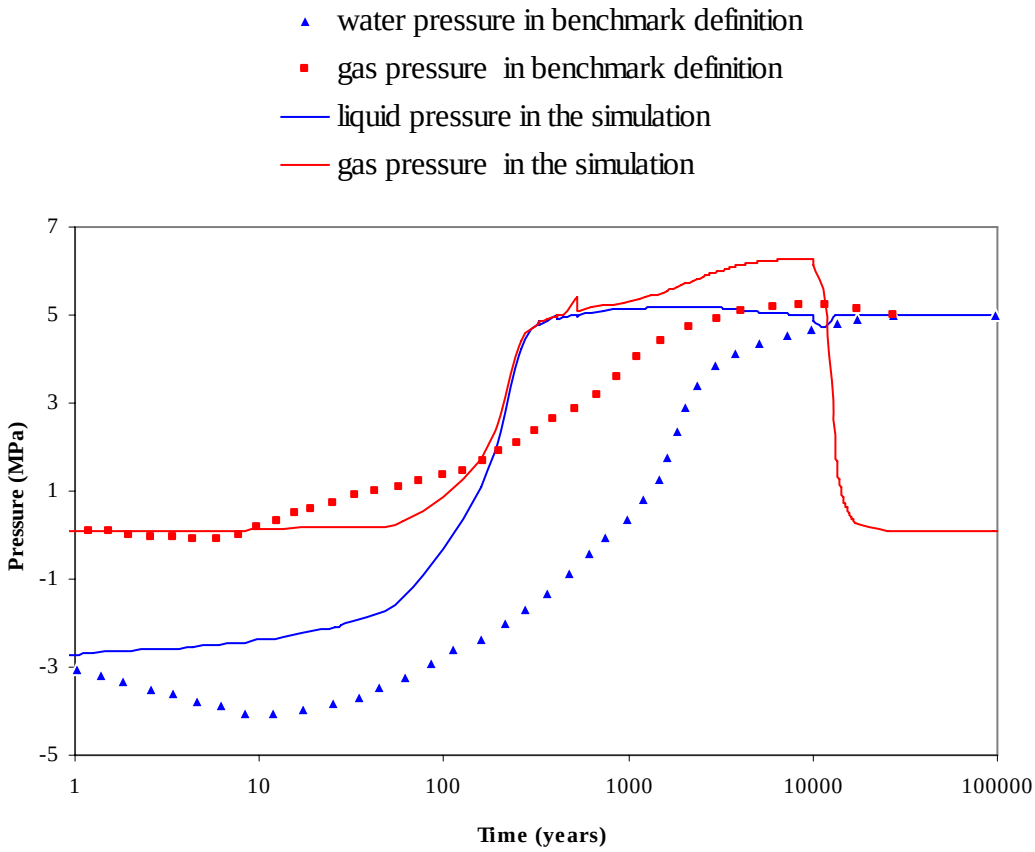


*Figure 9: Comparison of gas/liquid pressure between benchmark definition and numerical simulation at the boundary of drift*

#### 3.2.2.2 Initial conditions

The geological formation and EDZ are considered to be initially saturated with $P_g$=0.1 MPa and $P_l$=5 MPa. The plug is initially 70% saturated with $P_g$=0.1 MPa and $P_l$=-21.27 Mpa. The drift is initially 70% saturated with $P_g$=0.1 MPa and $P_l$=-2.985 MPa. The initial water pressure in the plug interface is assumed to be -40 MPa with the saturation of 15.7%.

#### 3.2.2.3 Constitutive models and parameters

The physical models used in the simulation are defined according to the benchmark definition including viscosity of gas mixture, diffusion coefficient of dissolved hydrogen and gaseous hydrogen, solubility of hydrogen, retention curve and relative permeability of water and gas. The parameters used in the base case are summarized in Table 1.

Besides base case, two sensitivity cases have been done in the exercise:

- Sensitivity analysis 1: all the parameters remain the same as in base case except that intrinsic permeability of EDZ is reduced by one order of magnitude (in the original definition of benchmark, it aims to reduce the permeability by three order of magnitude. Due to convergence problem, only reducing one order of magnitude which is capable of reflecting sufficiently the distinct difference of permeability between two adjacent materials);
- Sensitivity analysis 3: all the parameters remain the same as in base case except that the diffusion coefficient of dissolved $H_2$ in liquid phase is increased by one order of magnitude.

#### 3.2.2.4 Adaption to the original benchmark problem

The following specific constitutive laws are defined in code_BRIGHT for liquid phase properties:

1. liquid density: $\rho_l = \rho_{l0} \exp(\beta(P_l - P_{l0}) + \alpha(T - T_0))$
2. liquid viscosity: $\mu_l = 2.1 \times 10^{-6} \exp\left(\frac{1808.5}{273.15 + T}\right)$ (Pa.s)
3. Saturation pressure for water vapour: $\rho_{v0} = 136075 \times \exp\left(\frac{-5239.7}{273.15 + T}\right)(MPa)$

   At 20°C, saturation pressure for water vapour is 2.35 kPa which is very close to the value given in the benchmark, 2.34 kPa.

Due to the convergence problem, the following modifications to the original benchmark definition have been made in the simulation:

1. Some of the material properties (marked in red in table 1)
2. The initial water pressure in the plug interface is assumed to be -40 MPa which corresponds to $S_l$=15.7% (parameters for retention curve: Pr=1Mpa and λ=0.3333).
3. Time varying boundary at drift is restricted to no flux boundary.

#### 3.2.2.5 Remaining questions

The extremely steep retention curve (green curve in Figure 10) defined for interface in the benchmark definition makes computation very difficult. In the actual calculation, the retention curve of interface is modified significantly (red line in Figure 10)). In the base case, most of the time the saturation of interface remains around 80% with a suction of 1 MPa. Although the relatively higher water saturation in the interface reduces its ability to transport gas, it still serves as an important preferential pathway for the gas migration. The modified retention curve is not the real-world interface properties. In the future, some computational techniques (not known yet) should be taken in order that the suitable properties for interface could be incorporated in the simulation.

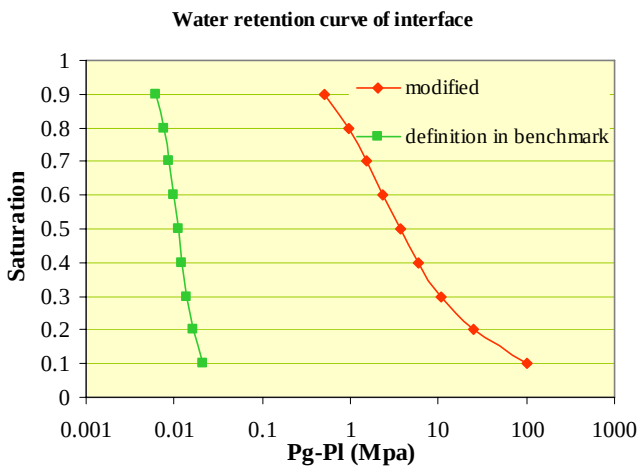


*Figure 10 : retention curve of interface*

When encountered a curvature boundary, such as the circular drift and drift EDZ, the direction of the flux is quite complicated and not straightforward. The comparison between overall flux through drift boundary and other straight boundary seems impossible. In CODE_BRIGHT, the elemental flux is obtained by the gradient of nodal pressure and is separated in X and Y directions. The flux at each boundary shows very much fluctuations with time.

The outer boundary with fixed gas/water pressure at a distance of 20 m ($S_{out}$) will influence the value of the maximum gas pressure triggered in the system. In the reality, 20 m only represents horizontal range and is underestimated in the vertical direction.

*Table 1: Material properties used in calculations for the base case.*

Increasing 2 orders

| | | Unit | Host rock | drift | plug | EDZ | Interface |
|---|---|---|---|---|---|---|---|
| porosity | $\eta$ | - | 0.15 | 0.4 | 0.35 | 0.15 | 0.3 |
| permeability | $k_x$ | $m^2$ | $5\times 10^{-21}$ | $5\times 10^{-17}$ | $1\times 10^{-20}$ | $5\times 10^{-20}$ | $5\times 10^{-20}$ |
| | $K_y$ | $m^2$ | $1\times 10^{-20}$ | $5\times 10^{-17}$ | $1\times 10^{-20}$ | $1\times 10^{-19}$ | $1\times 10^{-19}$ |
| tortuosity | $\tau$ | - | 2 | 2 | 2 (original value is 4.5) | 2 | 1 |
| capillary pressure function | | | | | | | |
| shape parameter | $\lambda$ | - | 0.3333 | 0.3333 | 0.375 | 0.3333 | 0.3333 (original value is 0.75 ) |
| residual w saturation | $S_{lr}$ | - | 0 | 0 | 0 | 0 | 0 |
| maximum w saturation | $S_{ls}$ | - | 1 | 1 | 1 | 1 | 1 |
| air entry pressure | $P_0$ | MPa | 15 | 2 | 16 | 10 (original value is 1.5) | 1 (original value is 0.01) |
| liquid density [a] | | | | | | | |
| Storage coefficient | β | $m^{-1}$ | $2.3\times 10^{-6}$ | $1\times 10^{-5}$ | $4.4\times 10^{-6}$ | $2.3\times 10^{-6}$ | $4.6\times 10^{-6}$ |
| Reference density | $\rho_{l0}$ | $Kgm^{-3}$ | 1002.6 | | | | |
| Reference pressure | $P_{l0}$ | MPa | 0.1 | | | | |
| Volumetric thermal expansion coefficient | $\alpha$ | $°C^{-1}$ | $-3.4\times 10^{-4}$ | | | | |
| Liquid viscosity [b] | | | | | | | |
| A | | MPas | $2.1\times 10^{-12}$ | | | | |
| B | | K | 1808.5 | | | | |

[a] Liquid density: $\rho_l = \rho_{l0}\exp\left(\beta\left(P_l - P_{l0}\right) + \alpha\left(T - T_0\right)\right)$

[b] Liquid viscosity: $\mu_l = A\exp\left(\frac{B}{273.15 + T}\right)$

### 3.2.3 Results

**results of the base case**

The migration pathway of gaseous gas include (Figure 11 and Figure 12):

1)flowing radially through cell EDZ towards host clay (lowest flux rate with largest amount);

2)flowing horizontally along cell EDZ, plug EDZ towards the drift (medium flow rate with smallest amount);

3) flowing through the interface plug-EDZ towards the drift (largest flow rate with medium amount). Although the gas flow rate through the interface plug-EDZ is about one order higher

than along cell EDZ, the total amount of gas transported through $S_{int1}$ is two orders lower than gas transported through $S_{EDZ1}$ because the extremely small volume of interface (Figure 13).

The gas pressure within the drift starts to increase when gas reaches the drift after 80 years, and keeps increasing until the gas production stops after 10000 years. Afterwards, excess gas pressure within the whole domain starts to dissipate through the outer boundary. The whole system recovers to the original state after 47440 years.

Free gas phase exists in an area, including the near field around the disposal cell (about 10 meters), interface plug-EDZ, drift and drift EDZ (Figure 14 and Figure 15). The maximum gas pressure reaches 7.27 MPa in the vicinity of the disposal cell. The gas pressure increase due to gas production is somehow weakened in reality, because at the repository scale, gas will flow through drift towards shaft which cannot be considered in the two dimensional case.

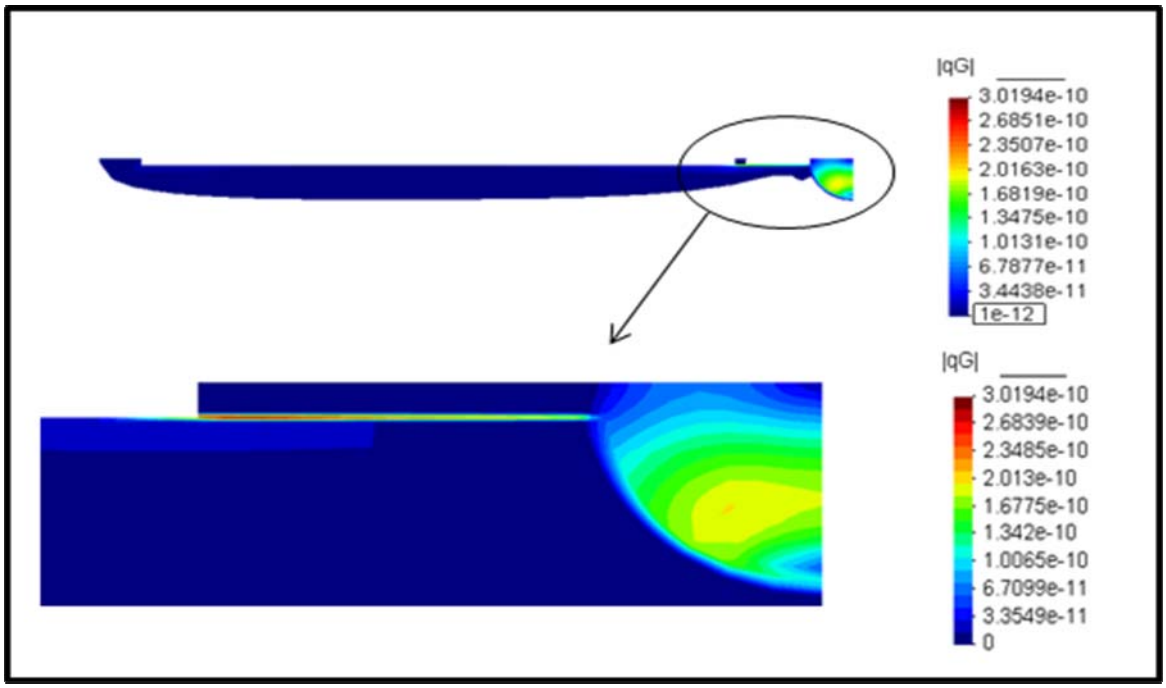


*Figure 11 : Gas flux around the disposal cell at t=330 years (kg/s)*

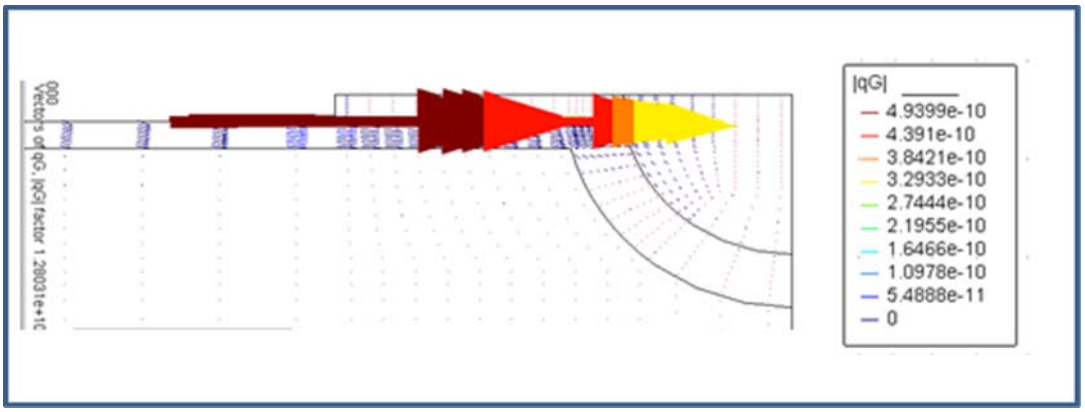


*Figure 12 : Gas flux vector at t=10000 years*

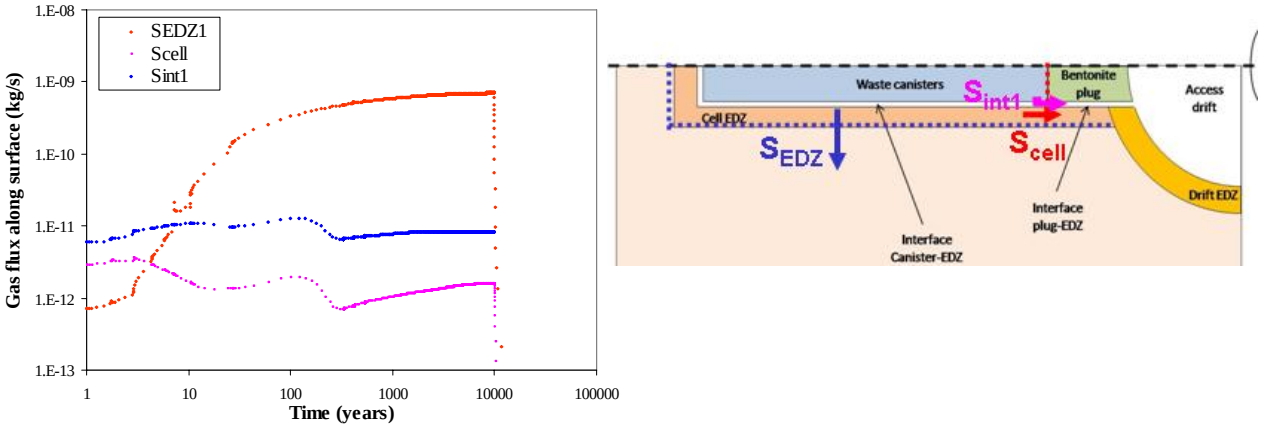


*Figure 13 : comparison of amount of gaseous gas phase trrough three boundaries*

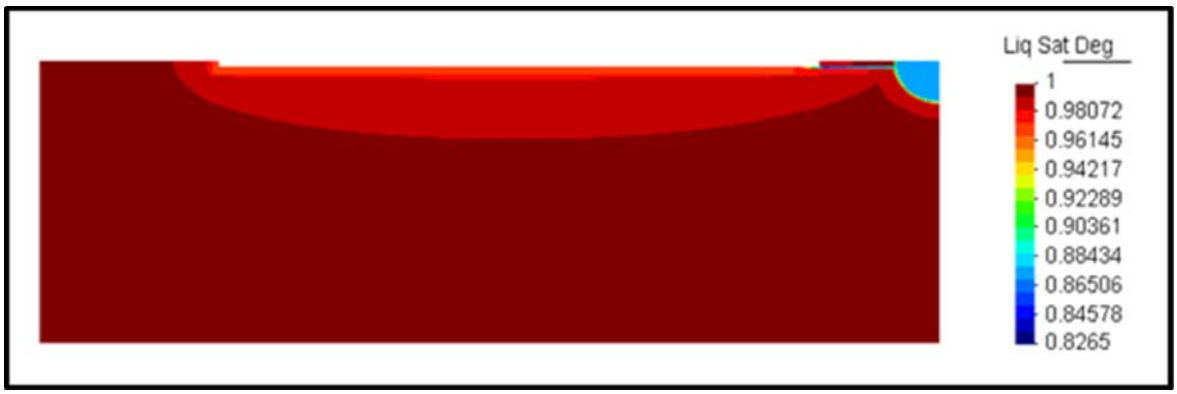


*Figure 14 : Unsaturated area t=10000 years*

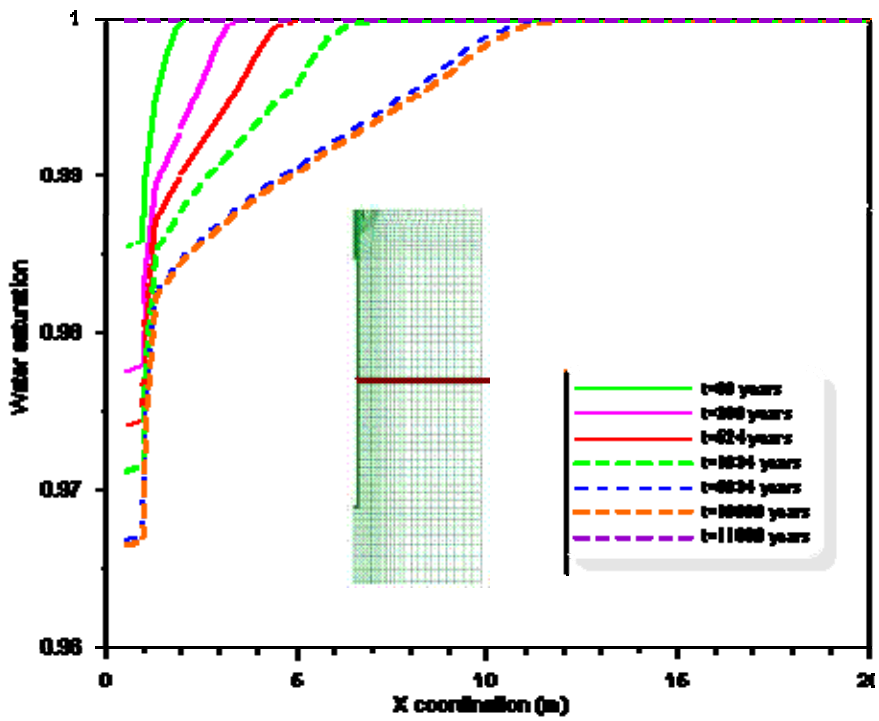


*Figure 15 : of water saturation along line $L_{cell}$*

Because the initial state of the drift and plug is unsaturated, resaturation process of drift and the plug starts from the beginning. From the water pressure fields presented in Figure 16, water flows from the surrounding host clay through drift EZD to resaturate the drift. Besides that, water also flows from initially saturated cell EDZ towards drift under the increased water pressure in cell EDZ induced by the gas production in the vicinity of canister. While at the same time, some portion of the gas flows through the interface plug-EDZ towards the drift to desaturate the drift. At the beginning, the amount of gas flowing into the drift is quite small, thus the resaturation process takes the predominance and the water saturation degree of the drift keeps increasing. These two simultaneous processes, namely the increasing of gas pressure due to gas influx into the drift and increasing of water pressure due to water supply to the drift, prolong the resaturation timescale, and it takes about 200 years for the drift to be fully saturated (Pl=Pw≈4Mpa). After that, water continues flowing from the surrounding host clay into the drift due to the water pressure difference between host clay and the drift (first graph in Figure 17). When t=600 years, water pressure within the drift becomes equal to the drift EDZ, the water exchange between drift EDZ and the drift becomes reversed. In the vicinity of disposal cell, water pressure still keeps increasing due to the gas production, and water still flows from cell EDZ to the drift. Water flux during the whole time scale is quite complex. Time of 600 years, 900 years and 10000 years mark three watersheds for the direction of water exchange between the drift and the surrounding host clay (Figure 17).

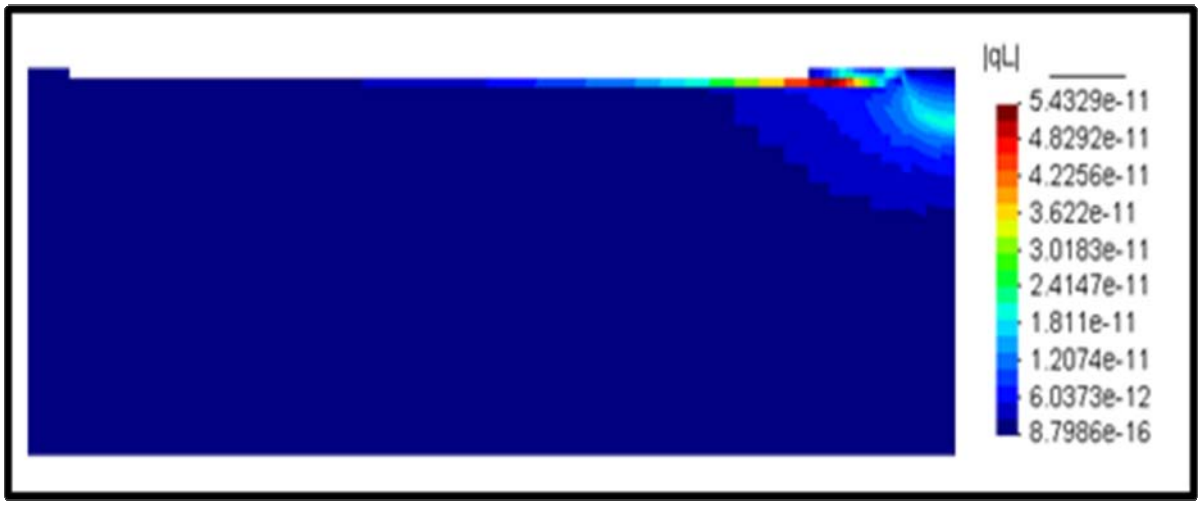


*Figure 16 : Liquid flux during resaturation process t=27 years*

**comparisons among the base case and two sensitivity cases**

In sensitivity analysis 1, gas pressure and water pressure increases more quickly and to higher levels in the vicinity of the canister as a result of the decreased permeability of cell EDZ compared to the base case. The maximum gas pressure in the centre of the disposal cell is 7.42 MPa in the sensitivity case 1 and 7.27 MPa in the base case. The area of unsaturated zone are almost the same for the base case and sensitivity analysis 1. Increasing diffusion coefficient of dissolved gas effectively decreases maximum gas pressure in sensitivity analysis 3. Nearly all the gas generated in the disposal system is evacuated through diffusion. There is no unsaturated area in the whole domain after resaturation process of the first 200 years.

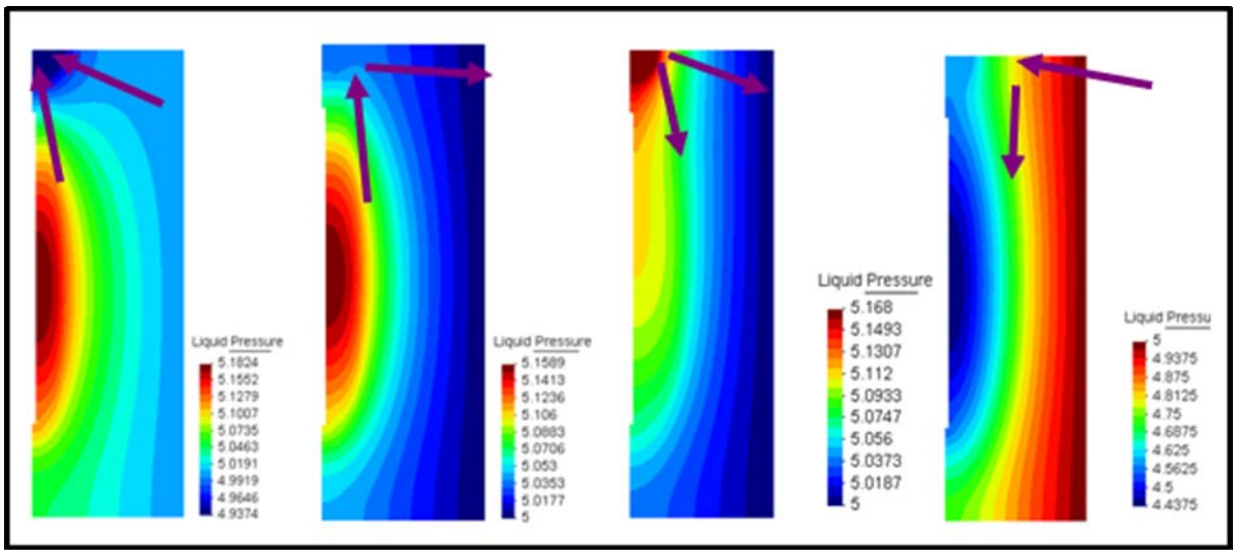


*Figure 17 : water pressure contour (thick arrow marks the direction of water flow)*

Gas flows more preferable through the interface plug-EDZ in sensitivity analysis 1 compared with the base case (Figure 18 and Figure 19), because the decreased permeability of EDZ forces gas to flow more easily along the interface plug-EDZ. The overall gas pressure in drift area is higher in the base case with maximum gas pressure of 6.3 MPa at point 4, while 6.05 MPa in the sensitivity analysis 1. The gas pressure tends to become similar between the base case and sensitivity analysis 1 with time going on.

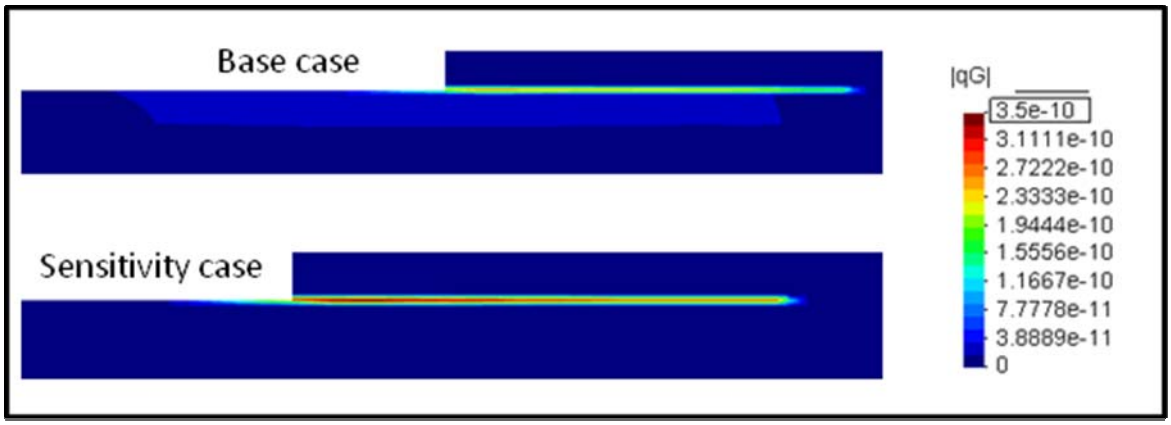


*Figure 18 : comparison of gaseous gas flux through interface and EDZ for two cases (t=5000 years)*

Comparing mass flux at the surface of Scell and SEDZ1, there is more gaseous and dissolved gas flows horizontally along EDZ to drift in the base case than in the sensitivity analysis 1, and less gaseous and dissolved gas flows radially into host rock in the base case (Figure 20 and Figure 21). This implies that increasing the permeability of EDZ could make gas evacuate more easily horizontally along EDZ to the drift and reduce the gas migration to the host rock. At the same time, the increased gaseous mass flux along EDZ is counteracted by the decreased gaseous mass flux through interface. Considering that gaseous gas flux through Scell is one order lower in magnitude than gas flux through Sint1, it is difficult to conclud that the overall horizontal gaseous mass flux could be enhanced significantly by increasing permeability of EDZ. This result is valid only for the permeability of EDZ varying within one order in magnitude.

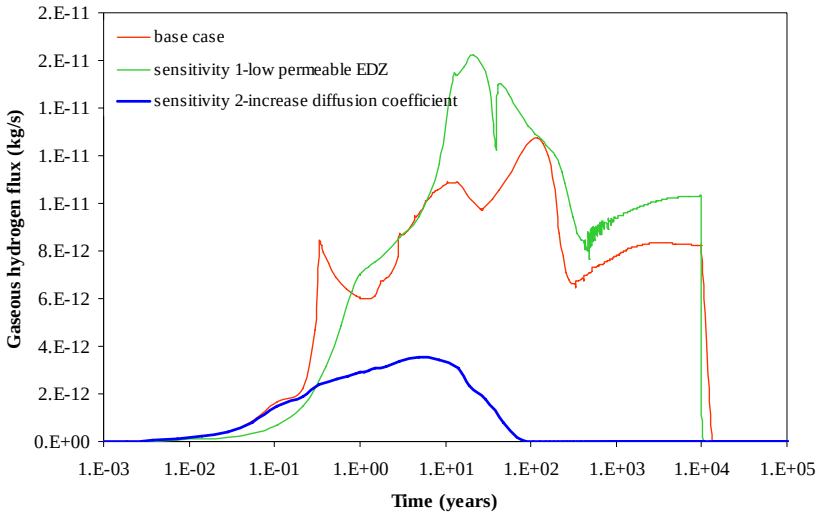


*Figure 19 : Time variation of gaseous gas flux through $S_{int1}$*

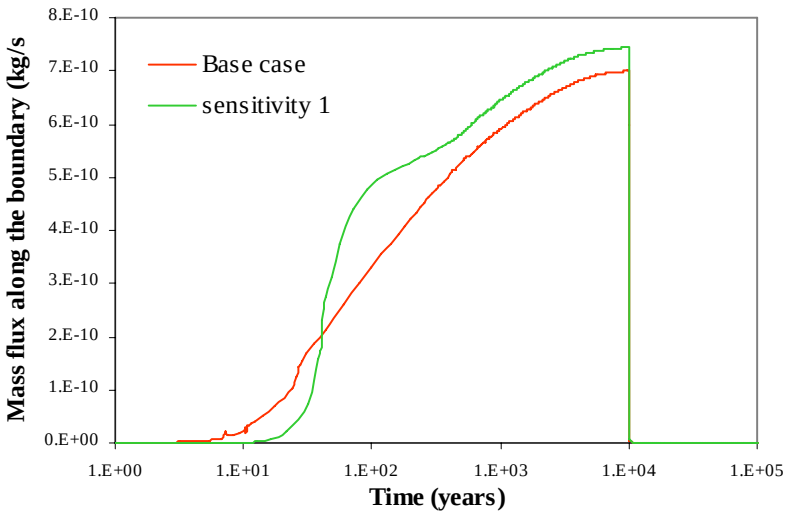


*Figure 20 : Comparisons of gaseous gas flux at boundaries $S_{EDZ1}$ for two cases*

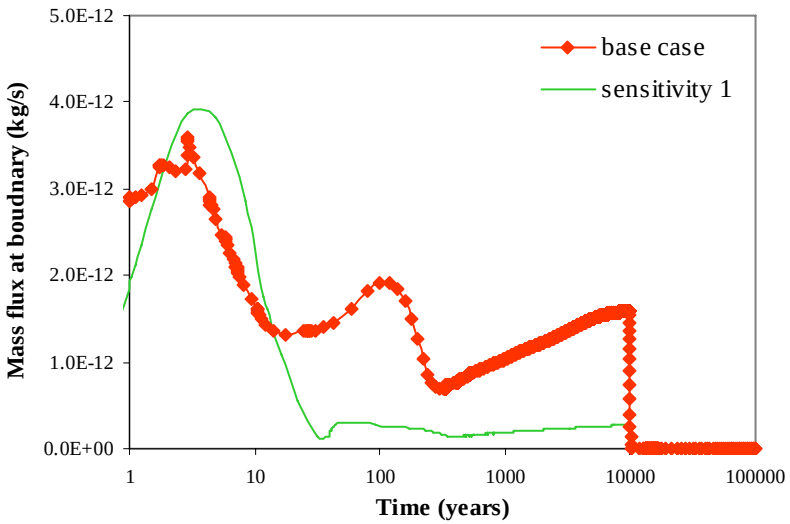


*Figure 21 : Comparisons of gaseous gas flux at boundaries $S_{cell}$ for two cases*

There exist more differences for liquid pressure among the three cases (Figure 22). The time needed to resaturate the drift is much longer in the sensitivity analysis 1 because less permeable EDZ retards the flowing of the liquid phase from the surrounding host clay to the drift. At the end of 10,000 years, the liquid saturation in the drift area is the lowest in the base case. While in the sensitivity analysis 3, gas is dissipated easily through diffusion in the pore water without causing much desaturation within the whole domain.

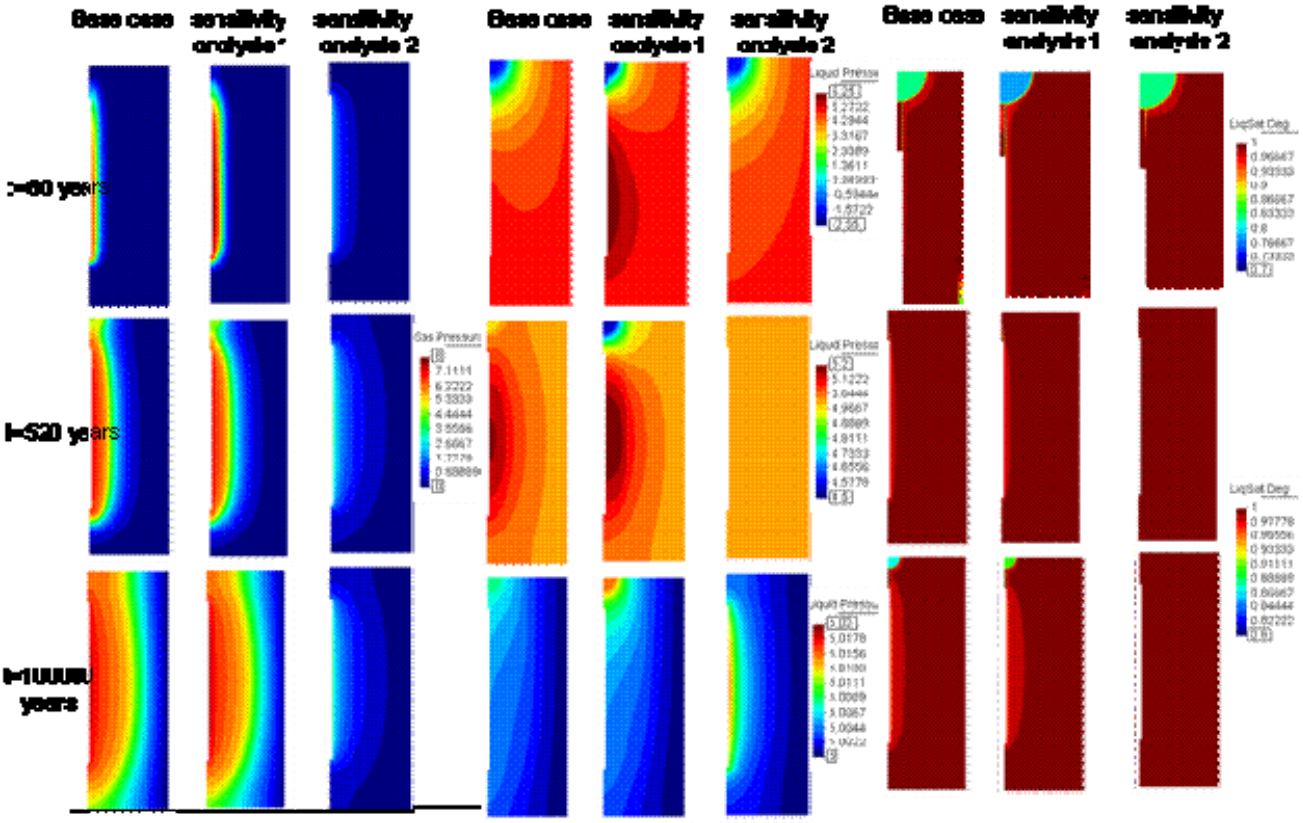


*Figure 22 : Comparisons between three cases*

**Impact of gas on the PA at the HLW cell scale**

The following points are significant to PA:

- The interface plug-EDZ is a important pathway for the transportation of free gas phase from the disposal cell towards the drift. The drift will continue to evacuate gas, to the shaft at repository scale. But due to the extremely small volume of the interface, the total amount of free gas migrated through the interface remains smaller compared to gas migrated through cell EDZ to the host rock.
- Increasing the permeability of EDZ will force gas flow more easily along EDZ zone to the drift, but at the same time decrease the gaseous mass flux through the interface. The overall quantity of gaseous flux along the horizontal direction is not necessarily to be much enhanced by increasing permeability of EDZ by one order in magnitude. The unsaturated area induced by gas production in the whole domain remains almost the same.
- The maximum water pressure triggered in the system is 5.2 MPa (t=2000 years). The maximum gas pressure reaches as high as 7.3 MPa (t=10000 years). This value is comparable to the total pressure in the host clay, thus might induce fractures or fissures.
- Water flux induced by gas production starts to flow out of the outer boundary (20m from disposal cell) after 300 years with maximum value of $6\times10^{-7}$ kg/s (or about 50 ml/day or 18 liters/year as total water flux along a length of 50 m boundary). The outflux will

continue until the gas production stops. During this period, there is risk of advective RN transport out of the boundary if pore water is contaminated.

- Time varying water pressure given at the drift boundary in the benchmark definition (blue triangle in Figure 9) is always lower than the hydrostatic water pressure in the whole time range of gas production (0<t<10000 years). This means water will continuously flow from surrounding host rock through drift towards shaft (in the 2D simulation, water pressure at the drift boundary will reach hydrostatic pressure after 200 years thus there is no such process). As mentioned above, water keeps flowing radially from the canister to outer boundary until gas production stops. So, the flow path of pore water can be canister-host rock-drift-shaft. This might be an additional RN transport pathway, although its significance-in terms of system performance has not been assessed.

## 3.3 Andra contribution

### 3.3.1 Simulation program

Numerical simulations rely on TOUGH2, a general-purpose numerical simulation program for multi-phase fluid and heat flow in porous and fractured media. Tough2 was developed at the Earth Sciences Division of Lawrence Berkeley National Laboratory (LBNL).

Simulations have been performed using Tough2-MP, a massively parallel (MP) version of the Tough2 code, designed for computationally efficient parallel simulation of isothermal and non-isothermal flows of multi-component, multiphase fluids in one, two, and three-dimensional porous and fractured media.

Tough2-MP features several fluid property modules [EOS (Equation Of State) modules].

In the framework of this benchmark, numerical simulations are performed using EOS5 module (water, hydrogen), under isothermal (20°C) conditions.

Further description and more details about Tough2/Tough2-MP codes are available from the Tough2 Homepage on the web, at http://esd.lbl.gov/TOUGH2, and from the Tough2-MP Homepage on the web at http://tough2.com.

### 3.3.2 Deviations from the definition of the benchmark and from original version of Tough2-MP

The different conceptual and physical processes and assumptions are in accordance with the benchmark specifications, and/or the original version of Tough2-MP, except for the following aspects:

### 3.3.3 Anisotropy:

In the axisymmetric configuration as defined in the conceptual model of the benchmark, horizontal $K_H$ and vertical $K_V$ intrinsic permeabilities couldn't be taken into account.

Two configurations could then be considered:

- anisotropic configuration with longitudinal $K_L$ and radial $K_R$ intrinsic permeabilities such as $K_L = K_H$ and $K_R = \sqrt{K_H K_V}$
- isotropic intrinsic permeabilities $K = \sqrt[3]{K_H K_H K_V}$

### 3.3.4 Physical parameters:

Some physical parameters and fluid properties are internally computed and/or tabulated in Tough2/Tough2-MP Fortran source code. They have not been replaced by the mathematical expressions presented in the benchmark description.

#### 3.3.4.1 Water vapor pressure:

In standard EOS5 module of Tough2-MP, vapor pressure is equal to saturated vapor pressure of water. It is not expressed by Kelvin's equation. At a 20°C temperature, this vapor pressure is 2337 Pa.

#### 3.3.4.2 Viscosity of the gas mixture:

Dynamic viscosity of hydrogen is both pressure and temperature dependent in Tough2/Tough2-MP. For the 20°C temperature used in the numerical simulations, values expressed in Pa.s are:

8,8 $10^{-6}$ Pa.s when pressure is lower than 0,1 MPa

8,95 $10^{-6}$ Pa.s at 10,0 MPa and 9,22 $10^{-6}$ Pa.s at 200,0 MPa

Values at intermediate pressures are linearly interpolated.

The dynamic viscosity of hydrogen-vapor mixture is approximated as dynamic viscosity of hydrogen.

#### 3.3.4.3 Diffusion coefficients:

In Tough2/Tough2-MP, diffusive flux of component $\kappa$ (water or hydrogen for EOS5 module) in fluid phase $\beta$ (liquid or gas) is expressed as follows: $f_\beta^\kappa = -\phi\tau_0\tau_\beta\rho_\beta d_\beta^\kappa \nabla X_\beta^\kappa$.

where $\phi$ is porosity, $\tau_0\tau_\beta$ is the tortuosity which includes a porous medium dependent factor, $\tau_0$ and a coefficient that depends on phase saturation $S_\beta$, $\tau_\beta = \tau_\beta(S_\beta)$, $\rho_\beta$ is density, $d_\beta^\kappa$ is the diffusion coefficient of component $\kappa$ in bulk fluid phase $\beta$, and $X_\beta^\kappa$ is the mass fraction of component $\kappa$ in phase $\beta$.

Tortuosity effects have a porous medium-dependent part $\tau_0$ and a saturation-dependent part $\tau_\beta(S_\beta)$, with $S_\beta$ as the fluid phase $\beta$ saturation. The following three alternative formulations are available in Tough2 / Tough2-MP:

- Relative permeability model:
  tortuosity will be taken as $\tau_0\tau_\beta = \tau_0 k_{r\beta}(S_\beta)$.
- Millington-Quirk model:
  $\tau_0\tau_\beta = \phi^{1/3} S_\beta^{10/3}$, with $\phi$ as the porosity.
- Saturation model: s $\tau_0\tau_\beta = \tau_0 S_\beta$ will be used.

#### 3.3.4.4 Solubility of Hydrogen in water:

In Tough2/Tough2-MP, the solubility of hydrogen in liquid water is represented by Henry's law. Henry's constant Kh (expressed in $Pa^{-1}$) for hydrogen dissolution in water is a linear function of temperature, varying from 1,697 $10^{-10}$ $Pa^{-1}$ at 0 °C to 1,379 $10^{-10}$ $Pa^{-1}$ at 25 °C.

For the 20°C temperature used in the numerical simulations, Kh is equal to 1,443 $10^{-10}$ $Pa^{-1}$. This value is equivalent to a Henry's constant of 8,0 $10^{-6}$ expressed in $mol.Pa^{-1}.m^{-3}$ (different from the 7.6 $10^{-6}$ $mol.Pa^{-1}.m^{-3}$ mentioned in the benchmark description).

#### 3.3.4.5 Specific storage coefficient:

Tough2/Tough2-MP codes do not use specific storage coefficient $S_S$ as an input parameter, but pore compressibility. Relation between pore compressibility C, expressed in $Pa^{-1}$, and specific storage coefficient $S_S$ expressed in $m^{-1}$ as follows:

$$C = \frac{S_S}{\rho_w g \phi} - \beta_w$$

With: $\rho_w$ liquid water density ($kg/m^3$)
g magnitude of the gravitational acceleration vector ($m/s^2$)
$\phi$ porosity (-)
$\beta_w$ liquid water compressibility ($Pa^{-1}$)

### 3.3.5 Boundary conditions:

Original version of Tough2 V2.0 does not allow time-dependent boundary conditions.

In the original version of Tough2-MP 2.0, only time dependent pressure boundary conditions are available.

Numerical developments have been performed in the Fortran source code of Tough2-MP to provide additional capabilities for a time-dependent gas saturation boundary conditions (gas saturation is one of the primary variables for EO55 module).

Attention must be paid to assume, at every time, coherence between boundary gas saturation, boundary water pressure, capillary pressure in access drift material, and realistic gas pressure.

### 3.3.6 Production term for hydrogen:

Tough2/Tough2-MP codes do not allow to apply a source term on a surface, as mentioned in the benchmark specifications.

Time-dependent hydrogen production term is then applied on a thin specific volume next to the external surface of the cell, in contact with both “Interface Canister –EDZ” and “Bentonite plug” materials. For the corresponding material a zero capillary pressure is applied for all saturations.

### 3.3.7 Outputs:

In the original version of Tough2-MP 2.0, mass flow rates from diffusion are not printed in the standard output file.

Developments have been performed in the Fortran source code of Tough2-MP to print the diffusive fluxes of each component (water, hydrogen) in both liquid and gas phase. These fluxes are necessary for computing, after the end of the simulation, the total rate of flow for each component.

### 3.3.8 Gas phase relative permeability:

Special attention must be paid to the expression of gas phase relative permeability $k_{rg}$ , in case of relationship after van Genuchten–Mualem.

In the original version of Tough2/Tough2-MP, $k_{rg}$ is then defined by $k_{rg} = 1 - k_{rl}$ [KRG 1] (with $k_{rl}$ as aqueous phase relative permeability), in case of zero residual gas saturation ($S_{gr} = 0.$). For materials with a non-zero $S_{gr}$ , $k_{rg}$ switches to the following. expression: $k_{rg} = (1. - S_{we})^2 (1 - S_{we}^2)$ [KRG 2], with $S_{we}$ .as effective saturation.

In the benchmark specifications, $k_{rg}$ is expressed as follows: $k_{rg} = \sqrt{1 - S_{we}} \left[1 - S_{we}^{1/m}\right]^{2m}$ [KRG 3]

Developments have been performed in the Fortran source code of Tough2-MP to allow this last relation.

Every of these three expressions could then be considered in the Tough2-MP simulations.

Depending on the used expression, $k_{rg}$ values could be very different, especially close to fully saturated conditions ($S_{we} \approx 1.$).

As an example, Figure 23 shows log-scale gas phase relative permeability evolution with gas phase saturation, for both interface materials (m parameter equal to 0.75). At lower gas phase saturations, differences between the three expressions are several orders of magnitude.

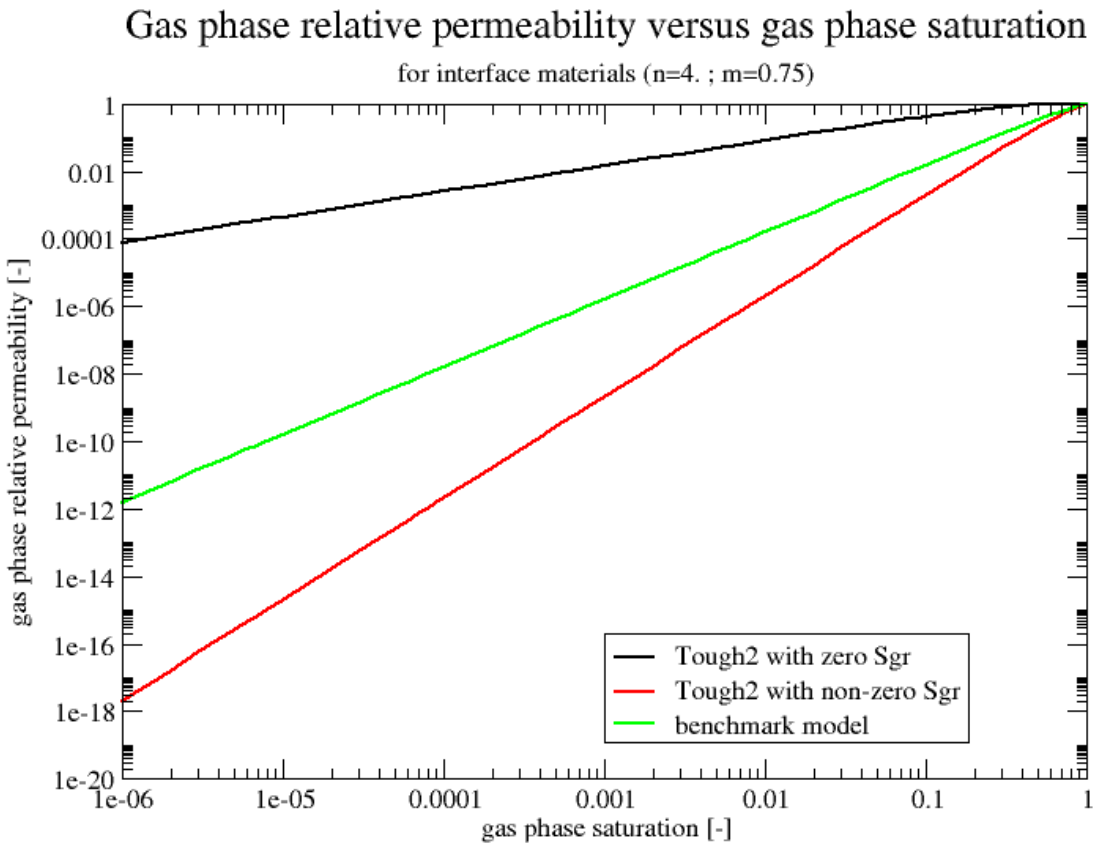


*Figure 23: gas phase relative permeability, for interface materials, at lower gas phase saturations*

### 3.3.9 Mesh size and refinement

Sensitivity runs have been performed with different mesh refinements. This analysis is based on the reference case, with anisotropic permeabilities. Four meshes have been used with different refinements:

26,346 elements, 10 layers in “Drift EDZ”, 13 layers in “Cell EDZ”

12,365 elements, 4 layers in “Drift EDZ”, 13 layers in “Cell EDZ”

6,817 elements, 4 layers in “Drift EDZ”, 4 layers in “Cell EDZ”

1,181 elements, 1 layer in “Drift EDZ”, 1 layer in “Cell EDZ”

The pressure and saturation evolutions with time, at the 12 given points defined in the benchmark description, appear to be very similar for the different meshes, except the 1181 cells one. This last mesh seems to be too much coarse for the numerical simulations.

Thus, mesh with 6817 cells is selected for the different cases. A view of this mesh and a close up around the access drift could be seen respectively on Figure 24 and on Figure 25.

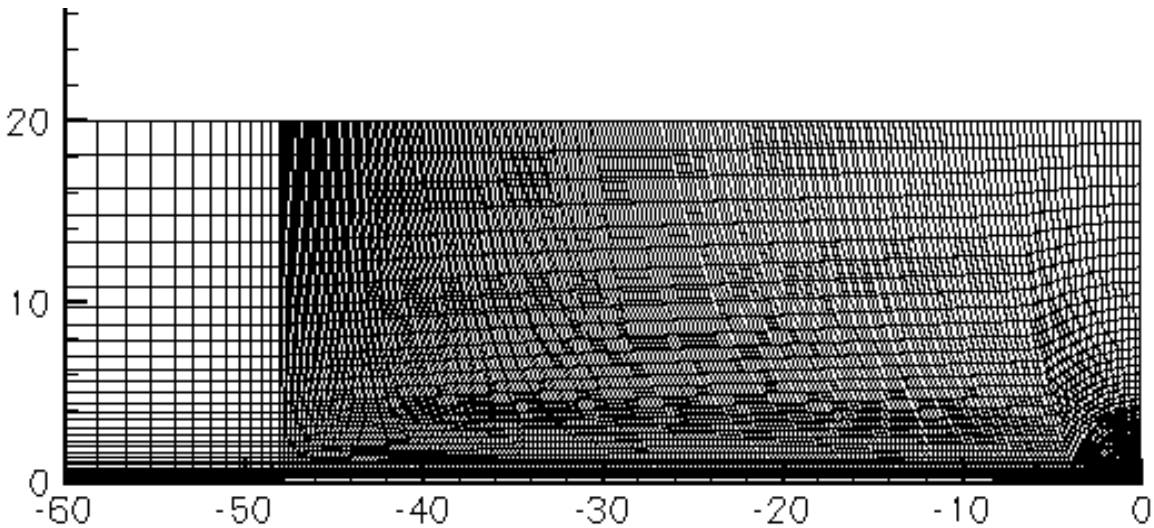


*Figure 24: Mesh selected for the different simulations*

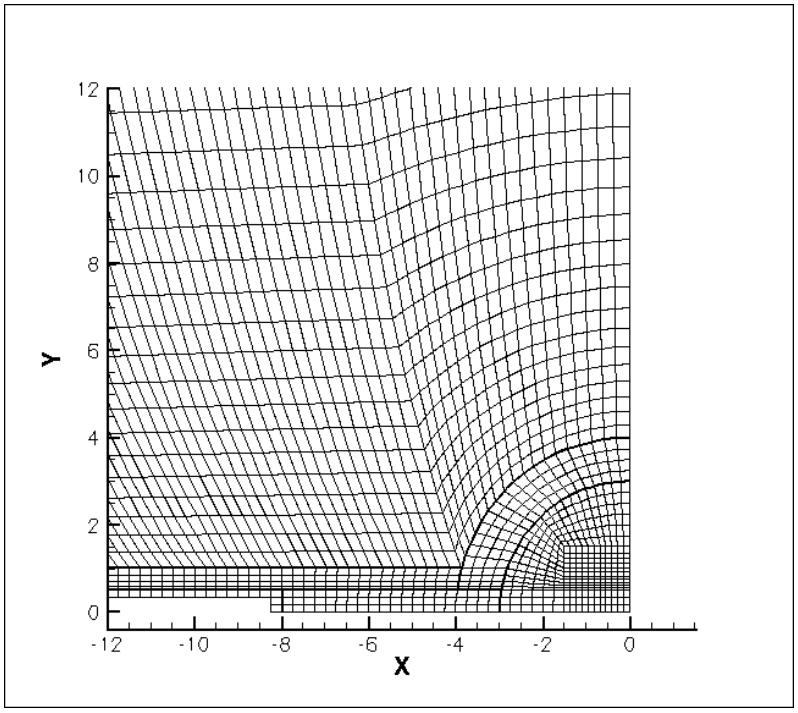


*Figure 25: Mesh selected for the different simulations (zoom around the access drift)*

### 3.3.10 Time step management and numerical issues

- …
- Stop and restart of the simulation, with a large initial time step
- Stop and restart of the simulation, by assigning fully-saturated single phase initial conditions in elements with a very low gas saturation degree at the end of the first run.

Simulations could be performed up to 100,000 years only for cases with gas phase relative permeability $k_{rg}$ expressed as in [KRG 2]. This could be done by assigning a non-zero ($10^{-8}$) residual gas saturation to the different materials.

### 3.3.11 Selected results

Expression of gas phase relative permeability could lead to very large differences in some results.

As an illustrative example, considering the reference case with isotropic intrinsic permeabilities and Millington Quirk model,

Figure 26 shows log-scale gas saturation evolution with time, in an element of “interface facing canister” located at X=9 m. Kinetics of liquid resaturation and desaturation appear then to be very different.

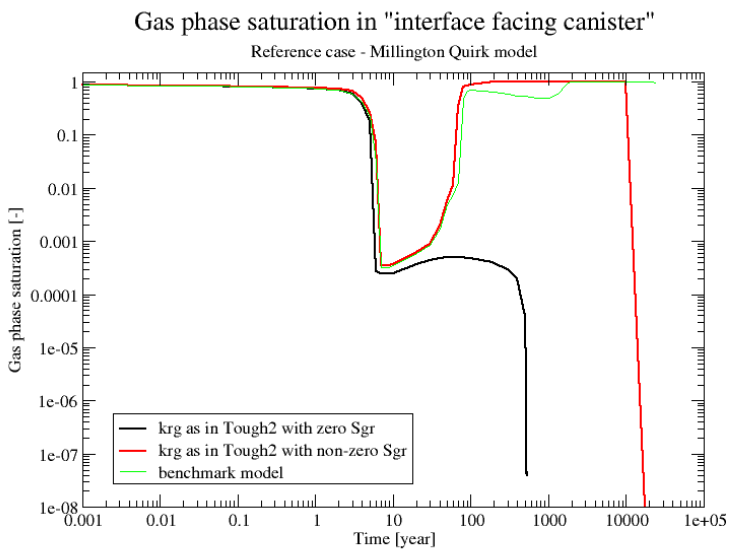


Figure 26: Illustration of influence of the residual gas saturation value

Focus is here made on some results of simulations achieved with isotropic intrinsic permeabilities, Millington Quirk tortuosity model, and gas phase relative permeability $k_{rg}$ expressed as in [KRG 2].

Figure 27 shows evolution with time of gas pressure and liquid saturation, for reference case, at points 2 through 7 as defined in benchmark description. Influence of pressure boundary condition appears on pressure distribution, especially for pressure in EDZ (point 5, 6 and 7). At 1 year, EDZ is partially unsaturated (points 5, 6 and 7). Interface facing canister appears to be resaturated between 45 years and 68 years (point 3), and from 12,000 years.

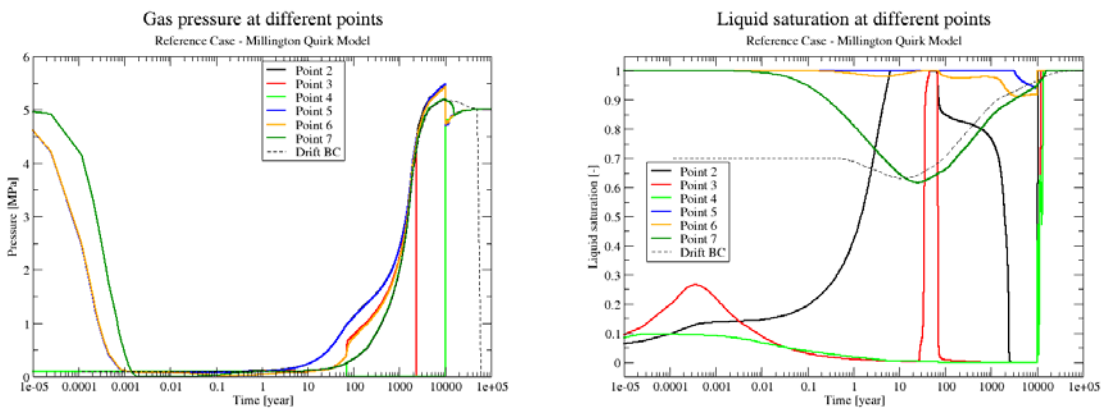


*Figure 27: Reference Case : evolution with time of gas pressure (left) and liquid saturation (right)*

Figure 28 shows same evolution with time, for sensitivity case 1 (modified intrinsic permeability for EDZ). EDZ remains saturated during the whole simulation (points 5, 6 and 7). Interface facing canister appears to be resaturated, for a longer time, between 20 years and 670 years (point 3), and from 12,000 years.

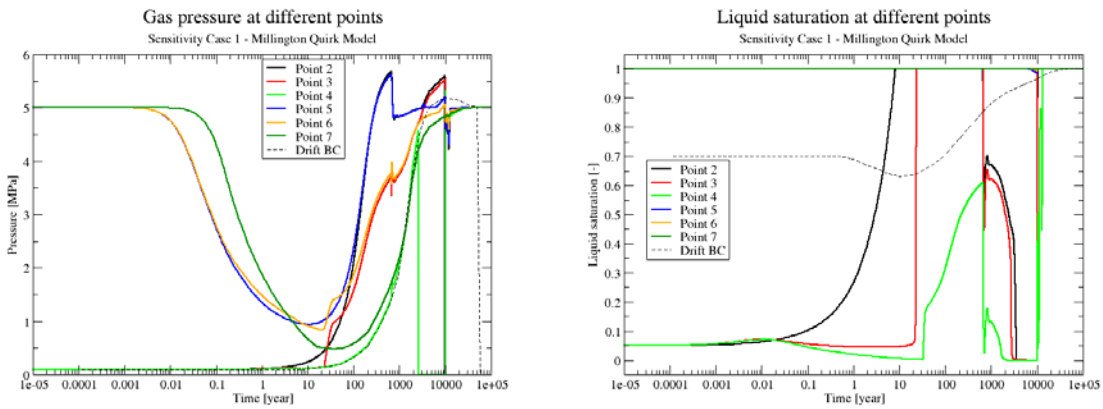


*Figure 28: Sensitivity case 1: evolution with time of gas pressure (left) and liquid saturation (right)*

Figure 29 shows same evolution with time, for sensitivity case 2 (cubic law for relative permeability –saturation relationship, for undisturbed argillites and EDZ).

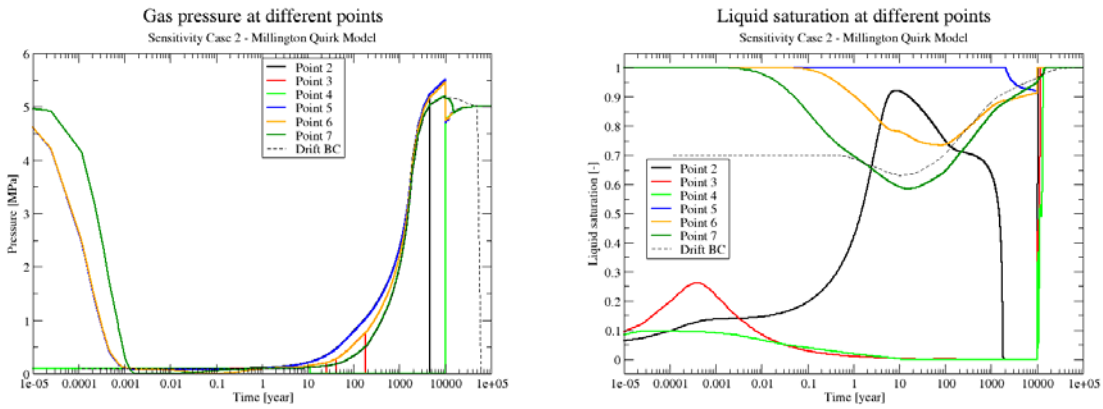


*Figure 29: Sensitivity case 2: evolution with time of gas pressure (left) and liquid saturation (right)*

Figure 30 shows same evolution with time, for sensitivity case 3 (modified molecular diffusion for dissolved hydrogen).

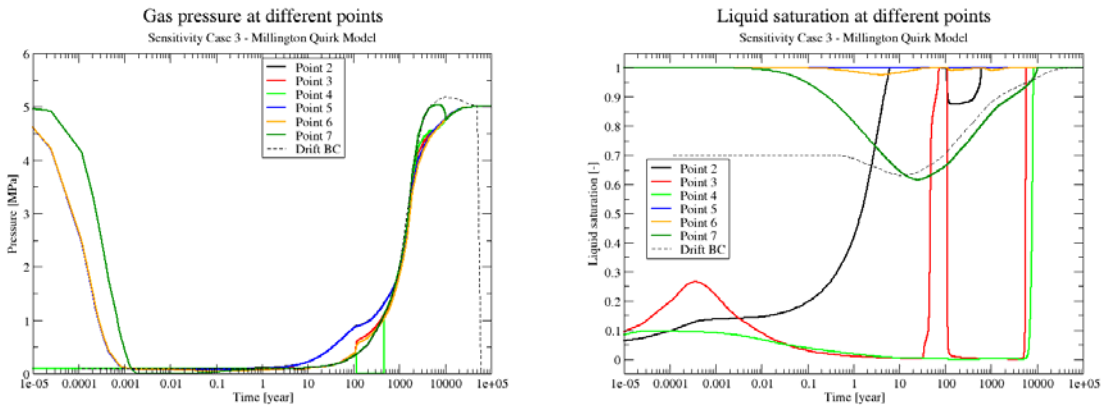


*Figure 30: Sensitivity case 3: evolution with time of gas pressure (left) and liquid saturation (right)*

## 3.4 IRSN contribution (M. DYMITROWSKA)

### 3.4.1 Simulation code

We use the MiGazTra code developed in collaboration with UPPA based on a conventional gas pressure – water saturation formulation. Keeping in mind the efficiency requirement, we have implemented a vertex centred finite volume scheme on an arbitrary triangular mesh. We have then tested the code on a 2D case of the Couplex-Gas benchmark (contribution submitted in January 2008) and in EU PAMINA WP3.2 in 2009.

***Mathematical model***

With this tool we simulate a classical two-phase flow without dissolution and evaporation effects. One of the phases and the solid matrix is assumed incompressible, and the other phase follows the ideal gas law. We start with classical mass conservation laws for both one-component phases supplemented by generalized Darcy equations for each phase. After some algebra we obtain the set of coupled non-linear diffusion-convection equations for **water saturation S** and **gas pressure P**:

$$\Phi\frac{\partial S}{\partial t}+div(f_w(S)\vec{q})+div(K\nabla\alpha_2(S))+div(\bar{\lambda}(S)(\rho-A(p)K\vec{g}))=\frac{Q_w}{\rho} \qquad (1)$$

$$\Phi\frac{\partial}{\partial t}\big(S(\rho-A(p))+A(p)\big)+div(G_1(S,p)K\nabla p)+div(\rho K\nabla\alpha_1(S))+div(G_2(S,p)K\vec{g}))=Q_w+Q_g \qquad (2)$$

Where the nonlinear functions of p and S are defined as follow:

$$G_1(S,p)=A(p)\lambda_g+\rho\lambda_w$$

$$G_2(S,p)=\big(A(p)\big)^2\lambda_g+\rho^2\lambda_w$$

$$\alpha_1(S)=-\int_S^1\lambda_w(s)P_c^{'}(s)ds$$

$$\alpha_2(S)=-\int_S^1\bar{\lambda}(s)P_c^{'}(s)ds$$

$$\vec{q}=\vec{q}_g+\vec{q}_w=-\lambda(S)K\nabla p+K\nabla\alpha_1(S)+\rho G_1(S,p)K\vec{g}$$

$$\lambda_\alpha(S)=\frac{k_{r\alpha}}{\mu_\alpha},\quad \lambda(S)=\lambda_g(S)+\lambda_w(S),\quad \bar{\lambda}(S)=\frac{\lambda_g(S)\lambda_w(S)}{\lambda(S)}$$

and A(p)=□g is the gas law which can be of any type.

We use Van Genuchten model for the relative permeability $\mathbf{k_{r\alpha}(S)}$ and capillary pressure $\mathbf{P_c(S)}$:

$$k_{rg}=\sqrt{1-S_{we}}\left[1-S_{we}^{1/m}\right]^{2m} \qquad k_{rw}=\sqrt{S_{we}}\left[1-(1-S_{we}^{1/m})^m\right]^2$$

$$S_{we} = \frac{1}{\left[1+\left(\frac{P_c}{P_r}\right)^n\right]^m} \quad \text{and} \quad S_{we} = \frac{S_w - S_{wr}}{1 - S_{wr} - S_{gr}}$$

A special attention has been paid to the treatment of the saturation S and of the capillary pressure $P_c$ on the interfaces between different materials. Since all the pressures are supposed to be continuous (mechanical equilibrium state) the saturation can be discontinuous if both materials have different capillary pressure curves. Given $\mathbf{S_j}$ on the interface it is possible to reconstruct two (or more) saturations corresponding to the materials entering into the control volume of the vertex **j**. We use an approach based on homogenization which allows a mass conservation on the interface and is compatible with existence of residual saturations and is equivalent to defining a "mean" capillary pressure curve in each interface point, see Figure 31.

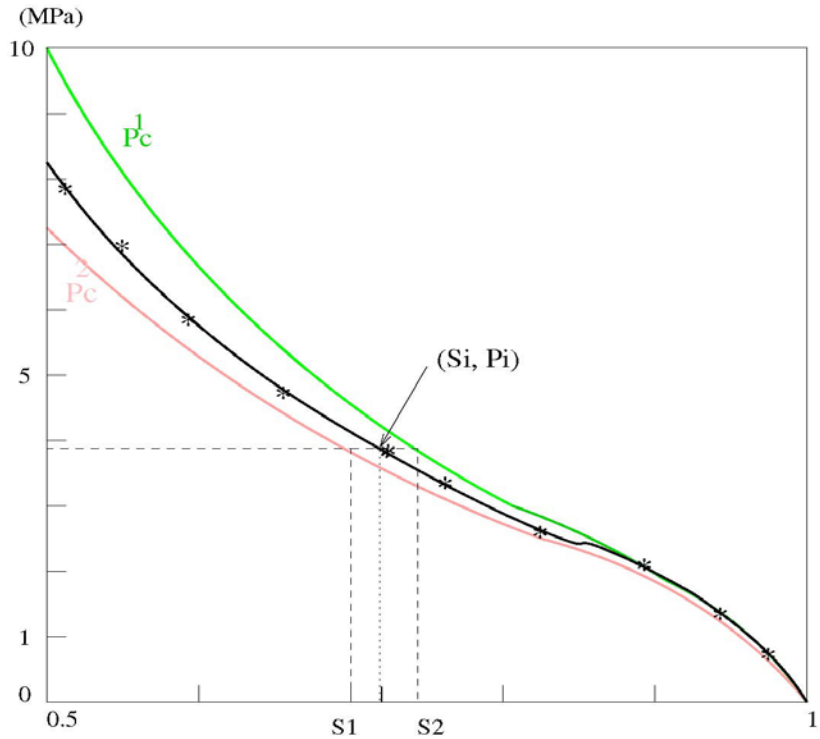


*Figure 31 : Effective cappilary pressure on the interface between two materials.*

### *Discretisation*

We use a finite element $P^1$ method for diffusion type terms and finite volume vertex centered Godunov scheme for convective type terms. An upwinding is applied to the two convection terms using the arithmetic means on the pressure values inside each element. The convection term arising from the gravity contribution contains a non-monotone function and therefore simple upwinding is not adequate. We need to use, for example, 1D Godunov scheme.
In order to avoid the CFL condition on the length of the time step arising with explicitly solved convection terms we use the sequentially implicit time discretisation. Being given $S^n$ and $p^n$, first, we calculate the field velocity $\overset{\rho}{\boldsymbol{q}}{}^n$ by piecewise linear conforming triangular finite elements. Then the couple ($S^{n+1}$, $p^{n+1}$) is calculated by solving (1-2) sequentially (predictor-corrector scheme). The fixed point method is used for the resolution of the nonlinear equations.

### 3.4.2 Differences with respect to the benchmark definition

***Physical model***

As mentionned before, the MiGazTra is not taking into account the mass exchanges between phases, (gas dissolution abd water evaporation). This implies also that no diffusion transport of dissolved hydrogen is present. However the solubility of hydrogen in water is very small and the geometry of the test case favors the convection phenomena. This should let us stay close to the models including hydrogen dissolution.

***Geometry and the source term***

We use a plane 2D geometry (the only one avaiable in our code). In order to be able to represent a similar process as the one from the initial test case we have to modify the original gas source term. There are many approaches allowing obtaining the reduction coefficient for the gas term. It can be made equal to the ratio between the accessible volumes in both cases or to the ratio of the corroding metal surface present in the systems (in the 2D case the depth of the model is taken to be equal to 1m). Since the most of volume accessible to gas is localised close the symmetry axis the second possibility is being adopted which gives us the following source terms:

- for 0 < t ≤ 10000 years, $\boldsymbol{Q_{H_2}^g} = 100 * 0.3224\, \boldsymbol{mol} / \boldsymbol{year} / \boldsymbol{cell}$
- for t > 10000 years $Q_{H_2}^g = 0\ mol / year / cell$

Also in contrast to the initial case the source term is not localised on the waste canister external surface, but has to defined within some volume; in our case the source term is distributed uniformly inside the material called the interface (“clearences”).

***Initial conditions***

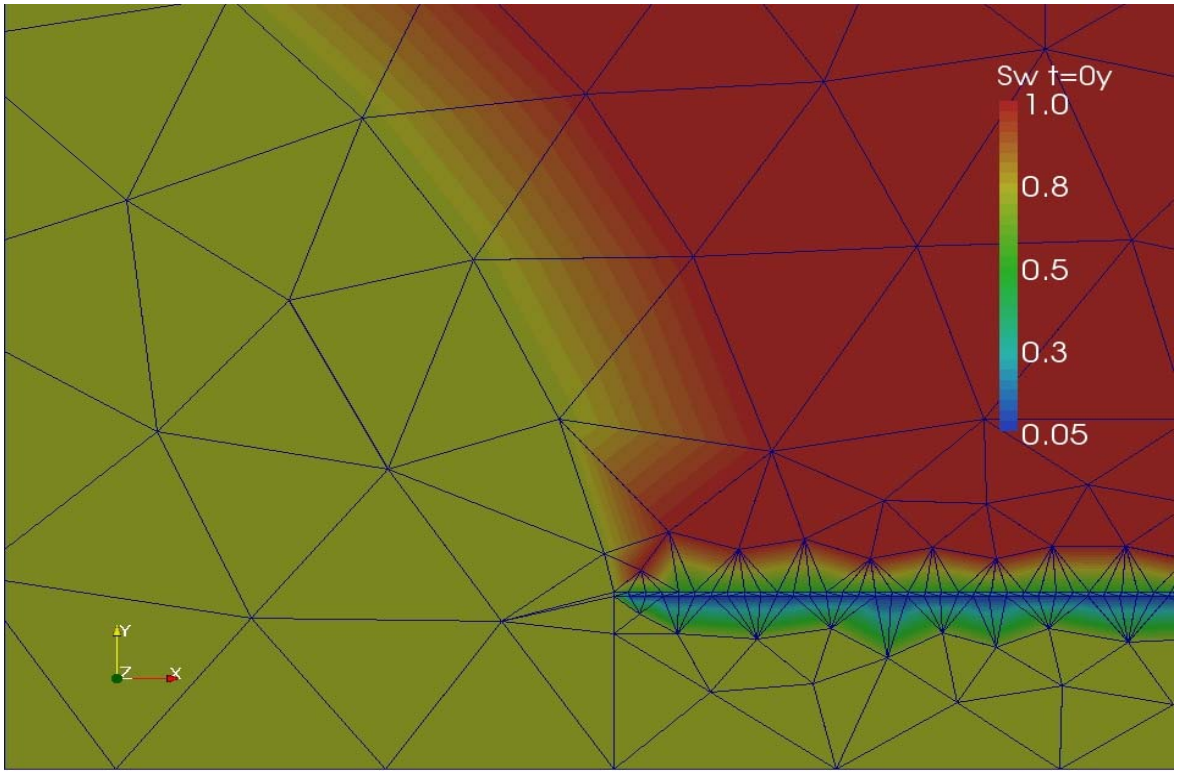


*Figure 32 : Zoom of the initial saturation field near the beginning the cell*

Two main problems appeared in order to take into account the benchmark definition inside our code. The initial water saturation in fully saturated media had to be transformed into 1-□, which is a standard way of avoiding the divergence of the derivative of the capillary pressure curve in the vinicity of S=1. In what follows the value of e=0.01 is used ( the lower the □ the longer is the simulation time). The second problem concerns the points situated on the borders between differents materials. If the saturation and pressure are to be imposed on both sides are different, which is the value to be given on the interface ? This question is solved in a pragmatic way, which is illustrated by Figure 32. The decision was made to imposed partially saturated conditions on the border of drift EDZ (S=0.7 and P=0.1Mpa as in the drift) and of the border between the interface and the cell EDZ (S=0.5 and P=0.1MPa, the saturation is the homogenised value corresponding to the approach proposed for interfaces treatement). It can also be noticed that inside the “interface” there is only one layer od triangular elements, which means that there are no points inside this material).

### 3.4.3 Simulations results

***Mesh***

We use triangular unstructured meshes generated with GMSH. We have three different degrees of refinement 3k 6k and 16k of nodes. Due to the geometrical constraints in representing the interface zone we find an important number of elements that are not respecting the Delaunay criteria (even after extensive optimisation):

| Mesh size | %bad elements |
|---|---|
| **16K** | 5 |
| **6K** | 3 |
| **3K** | 1,6 |

Due to its best quality we use the smallest mesh.

***Time step***

We use an automatic time stepping algorithm: if the iterations of the fixed point method fail to converge (the prescribed precision is of 0.001), the time step is dived by a factor of 4, if the convergence is obtained the time step is increased the same factor. The initial time step needed to obtain the convergence at early times has appeared to be very small: 1.e-6 year.
After 5 days of run on a standard PC the simulation has reached the time of 2.3 years and the actual time step is of 1.e-4 year.

The values of principal variables S and P are saved for prescribed points (or in the point nearest the requested location).Figure 33 shows that the pressure curves are smooth and with a well defined tendencies. The saturation curves, as seen in Figure 34, are less well behaving. Some small oscillations can be noticed in Point 4 and a more problematic behaviour of the Point 3. Both of these points are in fact situated on the border between three materials and the actual S value is the homogenisation result of the saturations in each of the materials. However the oscillation seen in Point 3 does not seem to lead to unphysical saturations fields in its vicinity, as can be seen on Figure 35.

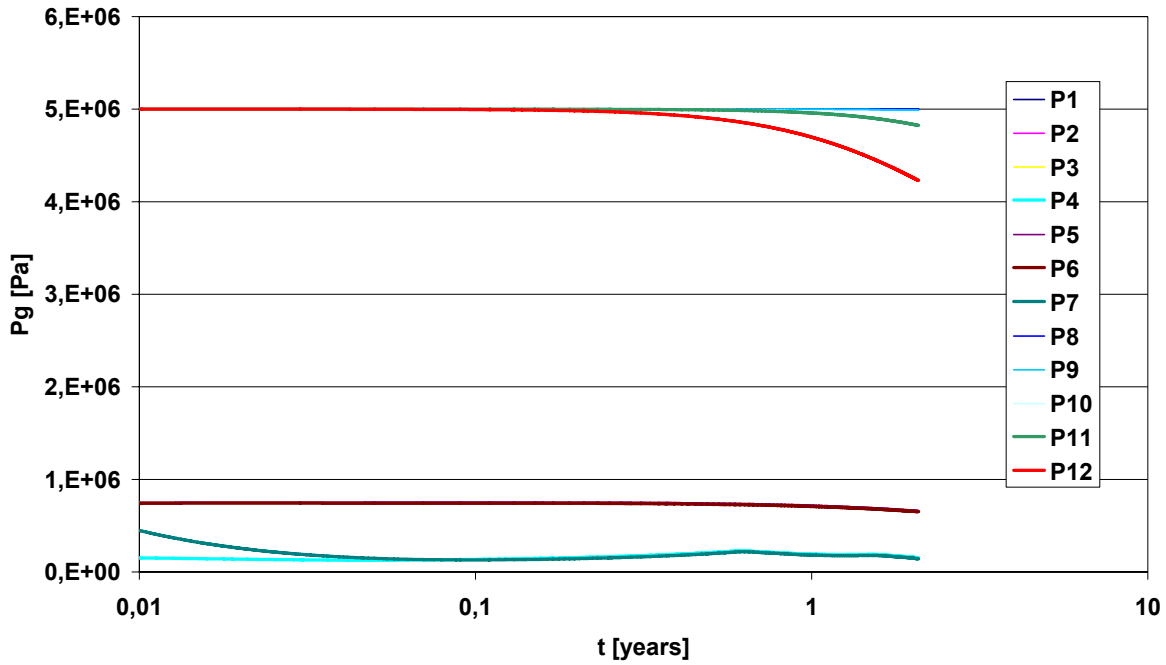


*Figure 33 : Gas Pressure evolution in observation points*

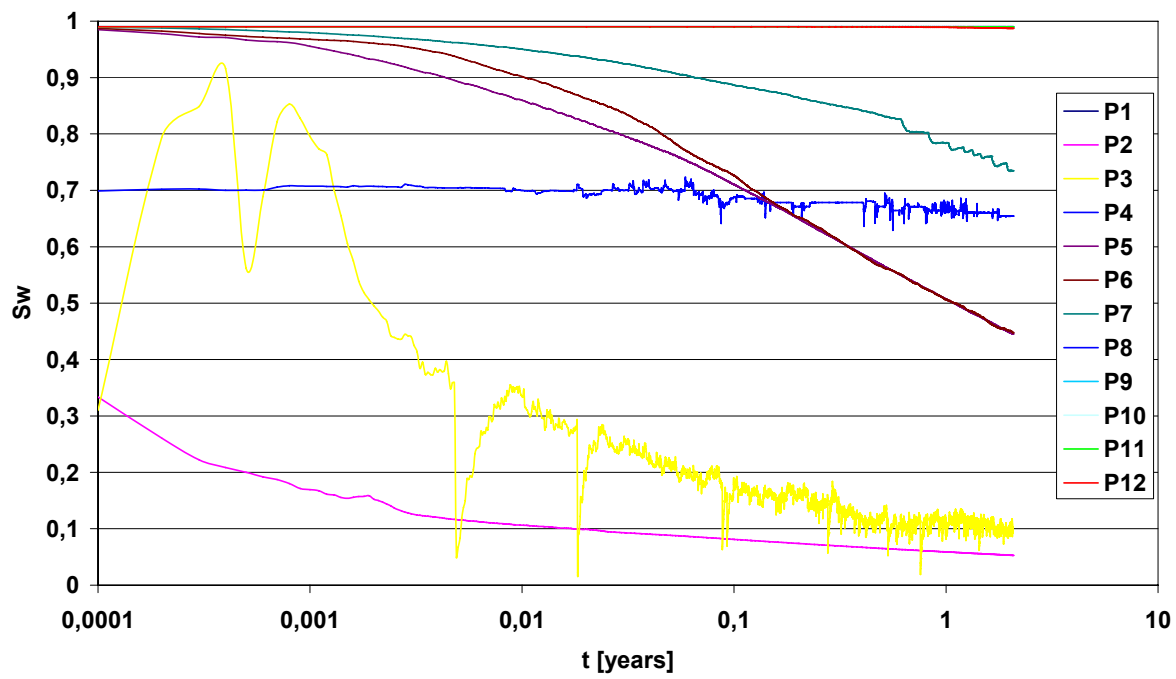


*Figure 34 : Water saturation evolution in the observation points*

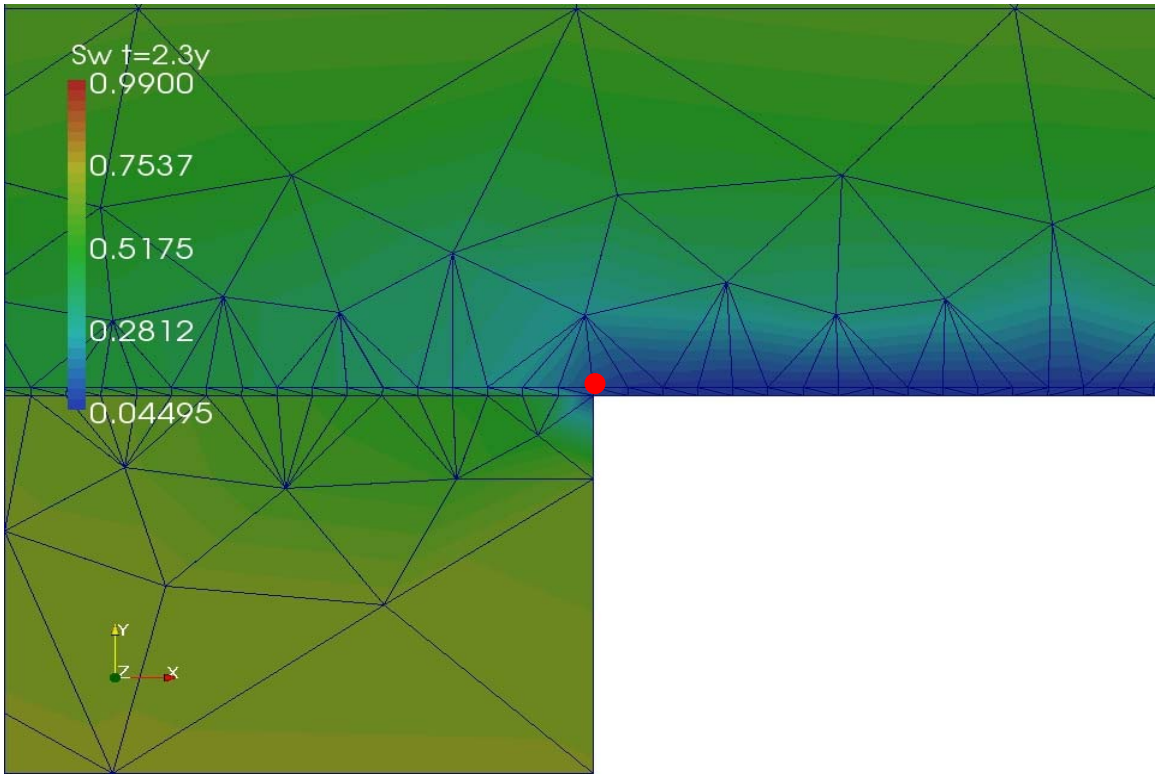


*Figure 35 Water saturation field at t=2.3years near the P3 point (red dot)*

Finally we give also some pressure and saturation fields around the gallery, see Figure 36

### 3.4.4 Conclusion and perspectives

We use the MiGazTra code to simulate the benchmark case proposed as a first stage of modelling work in FORGE WP1. We find this exercise more difficult than those proposed in the passed within the CouplexGaz and Pamina WP3.2. The main difficulties are connected with getting a good quality mesh and with the accurate representation the interface material which has very contrasting transport properties as compared to its neighbours. The initial conditions which are defined out of mechanical equilibrium require using very small time steps which make the simulation code running extremely slowly. Some additional tests have showed that the convergence behaviour is very much related to the exact definition of the initial conditions.
In the future work we will seek to optimise them in a way to get a quicker convergence and also to investigate the effect of the mesh size on the optimal time step.
In parallel we are developing a new 3D simulation tool taking into account mass exchanges between phases. We would like to use this new code in the further stages of the FORGE WP1 work.

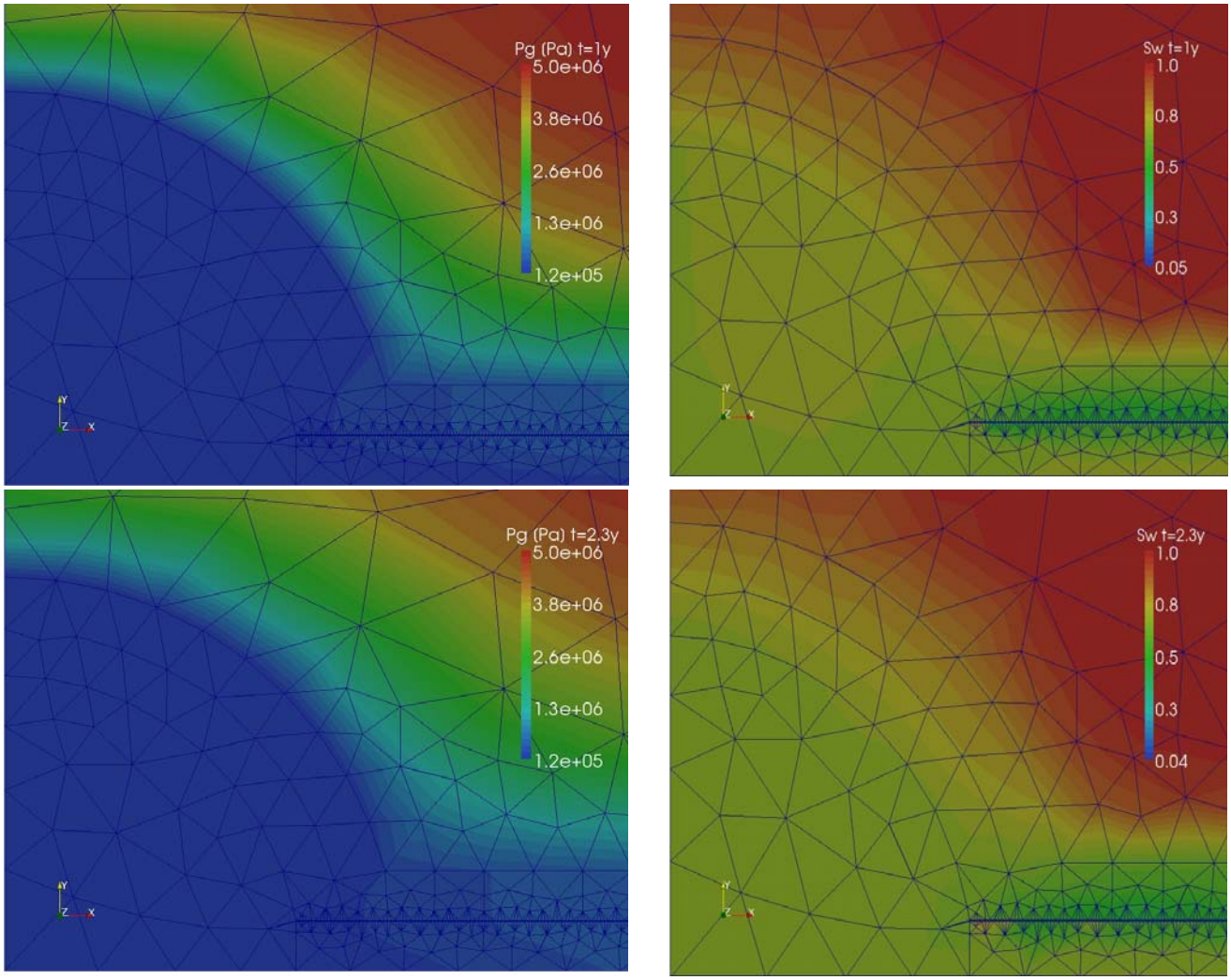


*Figure 36 Zoom of gas pressure and water saturation field at t=1y and t=2.3y*

## 3.5 LEI contribution

Up to now LEI team have made every effort to calculate the reference case of the benchmark studies with some simplification in the model using the numerical code TOUGH2 (USA). A lot of runs ended with the convergence problems of the numerical schemes. The reasons were related with the properties of different materials (high contrast of permeability - up to 9 orders of magnitude, porosity, gas entry pressure, retention and relative permeability functions). Besides, a lot of different materials were taken into account at scales between 1cm and several tens of meters – so it is a great challenge to create a valid mesh, with an emphasis to minimize the computing time. Key problematic issue appears when a transition from single phase conditions to two phase conditions occurs. Then the gas saturation appears to get a residual value, very much lower than 0.001 (for example about $10^{-5}$), the time step critically decrease and the calculation aborts. Nevertheless these problems, some converged results were achieved.

### 3.5.1 Numerical code

The gas transport calculations are performed with the TOUGH2 code using PetraSim as the graphical interface. PetraSim is new pre- and post-processor for TOUGH2. The EOS5 fluid property module is selected for the description of the thermodynamics of hydrogen gas.

### 3.5.2 Main Features of TOUGH2/EOS5

- Three Dimensional Transports of Water, Hydrogen and Heat in an Anisotropic Porous Medium;
- Mass Conservation Equations for each Mass Component (here: 2) including Advection and Diffusion in both Phases and considering Gas Solubility (Henry law);
- Darcy Equations for Liquid and Gas Phase including Relative Permeability's and Capillary Pressure depending upon Liquid Saturation;
- Water Properties using Complete Water Steam Table;
- Space Discretization employing Volume Elements;
- Liquid Phase: Water and Dissolved Gas;
- Gas Phase: Vapour and Gas;
- Primary Variables: Gas Pressure, Gas saturation, Temperature.

### 3.5.3 Modelling approach and the deviations from the definition of the benchmark:

1. Geometry:
   - Calculation domain is axisymetrical, as it is defined in the benchmark definition. The number of irregular rectangular Volume elements – 10534 (in radial x-direction: 46 elem. with a length between 0.01 and 1 m, in vertical z-direction: 229 elem. with a height between 0.01 and 0.25 m). <u>Vertical effects of gravity are neglected in computational domain.</u>
   - <u>Grid simplification</u> – PetraSim uses only rectangular grid. The reason for using a rectangular grid is that TOUGH2 uses Integrated Finite Volume approach. In order to satisfy convergence criteria, the grid must be a "voronoi grid". Essentially, this means that the cell volumes must be defined by planes normal to the lines drawn between the centres of the adjacent cells. The simplest grid that satisfies this criterion is a rectangular grid. Therefore, the zones defined as "Access drift" and "Drift EDZ" in benchmark model are not in circular grid (Figure 37).

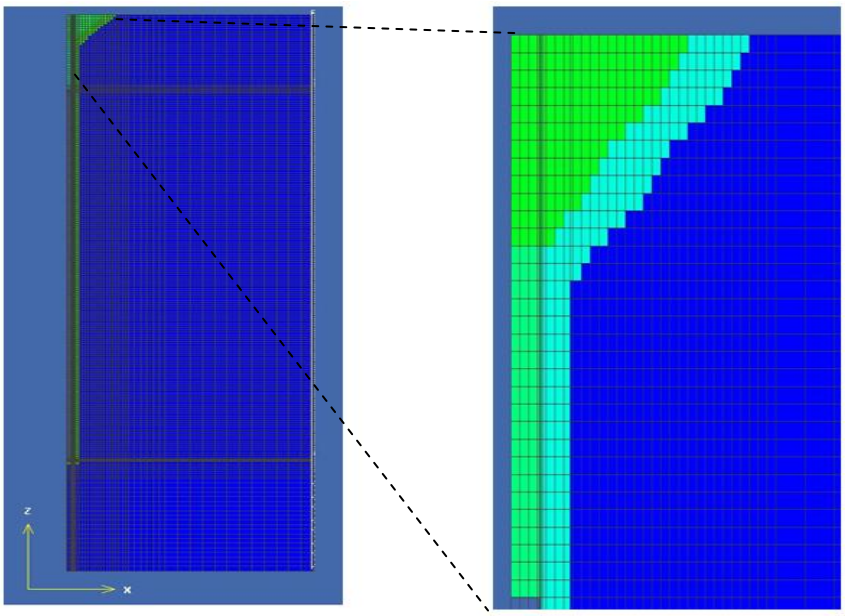


*Figure 37 : Schematic view of the geometry and mesh of the axisymetrical configuration*

2. Boundary Conditions:

   - Time-dependent boundary conditions were set as they are specified in the benchmark description for the access drift, are not available in Tough2. In our case no-flow boundary condition for the access drift were performed.
   - Waste disposal package are not defined as a part of computational domain (the canister surface has to be treated as the internal boundary in the domain and it means that no-flow boundary conditions were set around waste package.

3. Initial Conditions:

   To improve the model convergence performance, small initial gas saturation ($S_g$=0.01) is assigned to the fully water saturated materials (as it noted in benchmark definition) – geological medium and EDZ. It is reasonable, because full saturation of the host rock in repository is a rather unrealistic but conservative assumption.

4. Physical process:

   As the foregone investigations have shown (*K. Zhang at all*), comparing to the advection flow, the diffusion flux is relatively small at early stage. To facilitate the simulation run the diffusion effect was neglected for the first 5000 year simulation.

5. Physical parameters:

   The densities of the materials have to be provided in TOUGH2 input, but these parameters have not been described in benchmark definition, therefore the conservative assumption was made – all densities of different material were set equal to 2600 kg/m$^3$;

6. Sensitivity analysis:

   Only the reference case has been calculated (no sensitivity analysis).

The simulations were divided into several time periods. The results of the first time period was used as the starting points (initial conditions) for the second run and so on. To facilitate the simulation run the diffusion effect is neglected for the first 5000 year simulation. For this time period the results were recorded. Performing the simulations after 5000 years the diffusion was "switched on", but converged results were obtained only for additional 300 years. After that the

time step critically decreases and the simulation aborts. It seems what this is caused by the residual gas saturation values in particular grid elements.

Figure 38 is a schematic representation of the lines along which results are outputted. Figure 39 shows for exemple the evolution of gas saturation along L_int at different time up to 5 200 years.

Figure 40 is a schematic representation of the position of the points at which results are outputted. Figure 41 and Figure 42 show calculated evolution with time at different point respectively for gas saturation and capillary pressure.

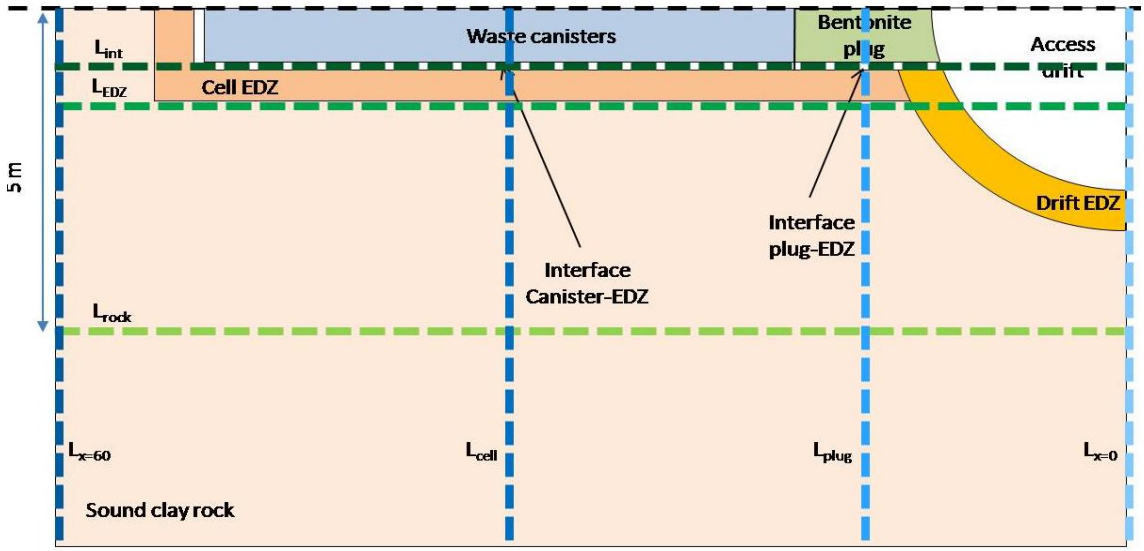


*Figure 38 : Schematic representation of the lines along which results should be given*

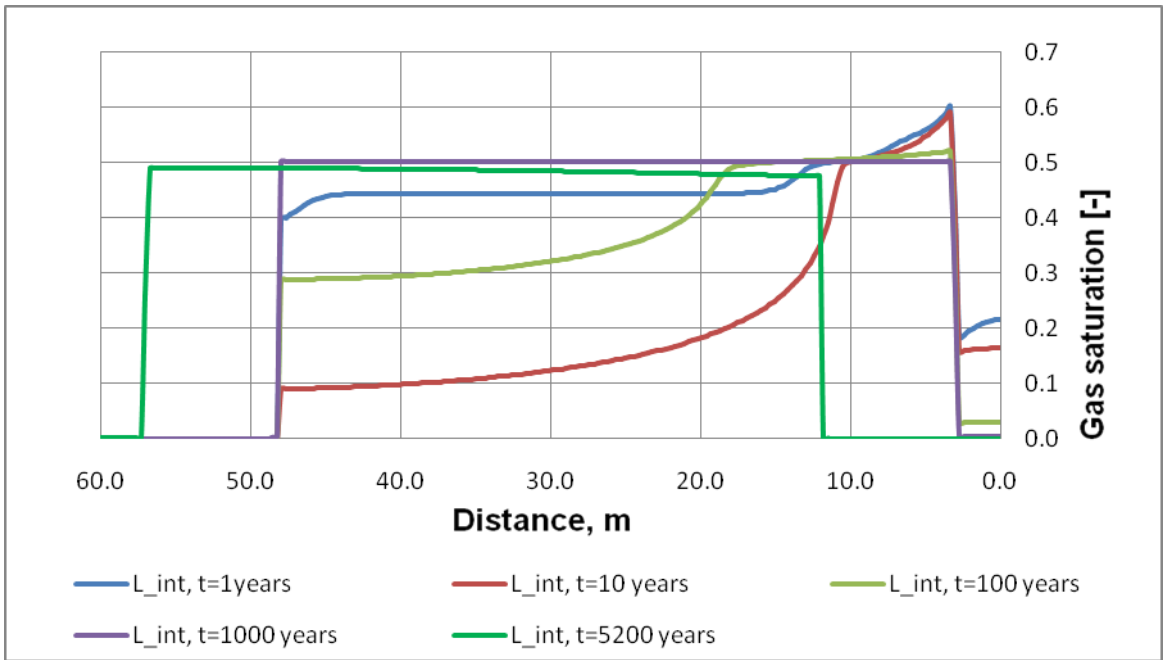


*Figure 39 :. Evolution of gas saturation along interface for different time periods*

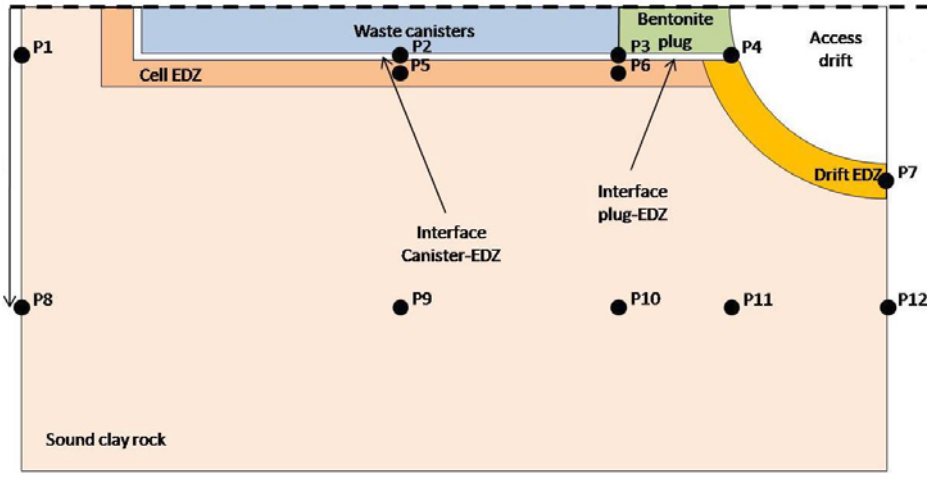


*Figure 40 :* *Schematic representation of the point where results should be given*

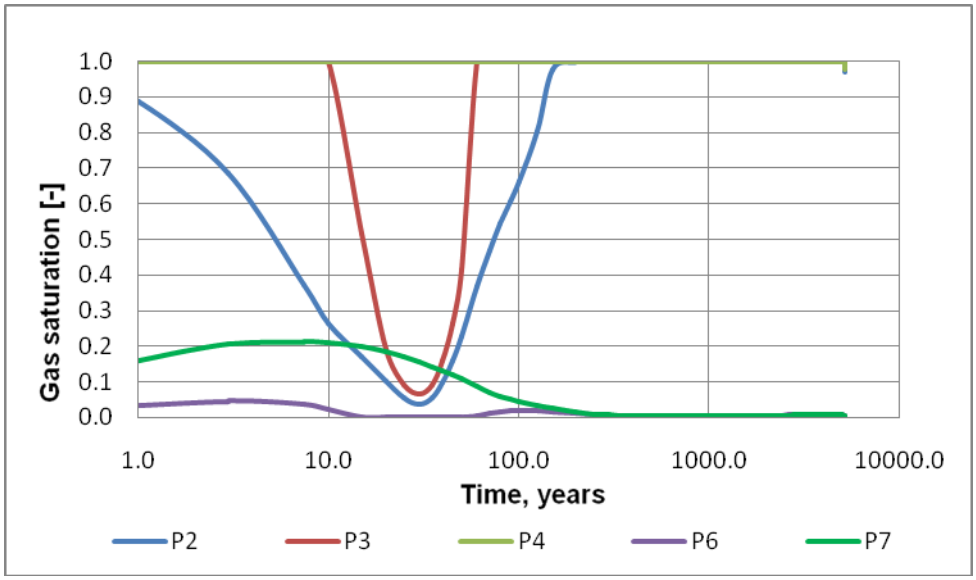


*Figure 41 : Evolution of gas saturation in different points*

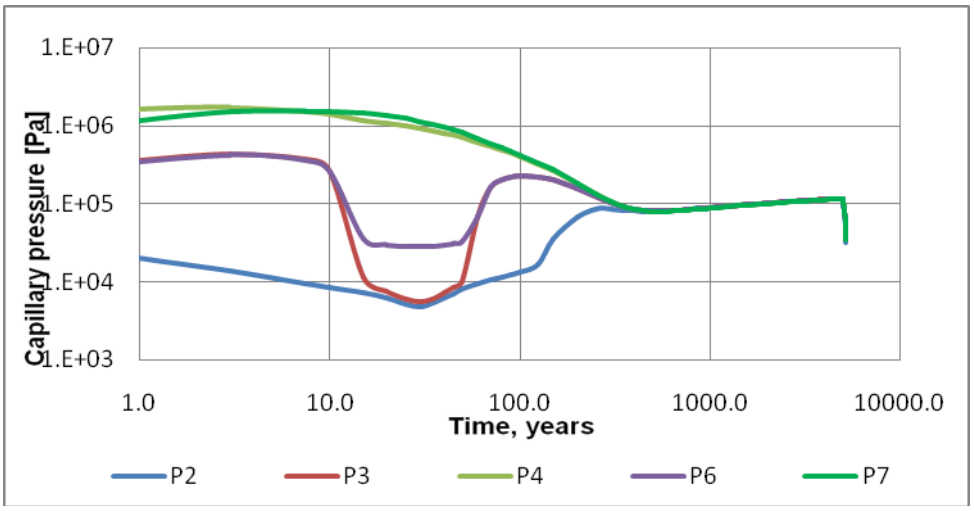


*Figure 42 : Evolution of capillary pressure in different points*

## 3.6 ENSI/IFSN contribution

### 3.6.1 Introduction

ENSI started in December 2009 with the preparations for the modelling of the first exercise within FORGE WP1.2. This period coincided with gas related calculations performed by ENSI for the ongoing review of the stage 1 of the sectoral plan. The sectoral plan is a process in three stages for a site selection of a geological repository for radioactive waste in Switzerland

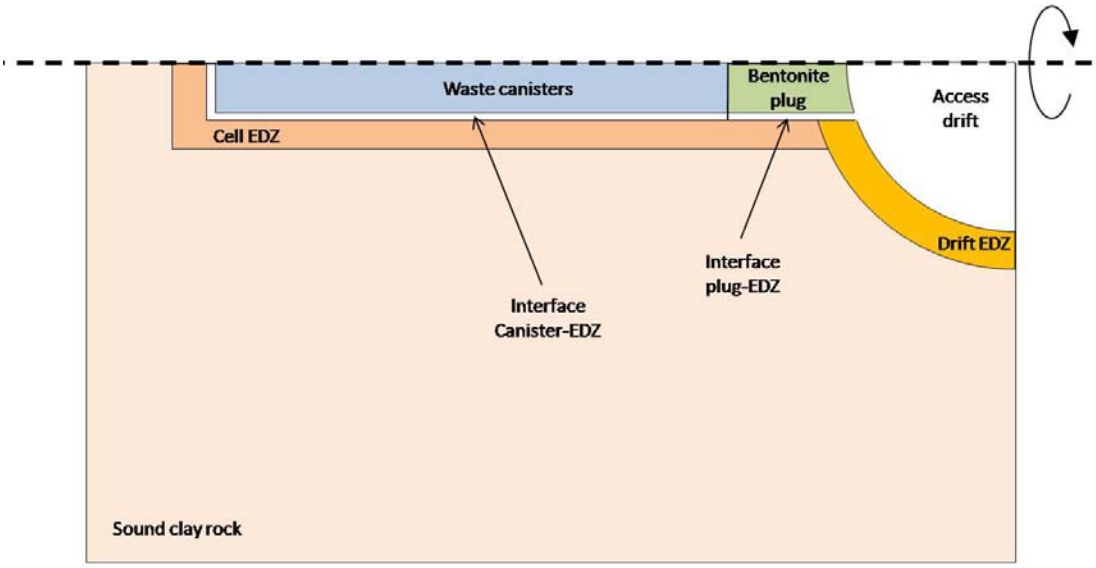


*Figure 43 Domain of the model proposed for the first exercise.*

The preparations for the calculations (Mesh for the model, installation and compilations of the used program, changes in the program, and preparation of the input file) and the calculation itself took longer than expected. Several problems were found as it will be explained in this report. The progress made with the simulations within FORGE WP1.2 will be shown in this report.

### 3.6.2 Programs used for the model

The code chosen to perform the numerical simulations is TOUGH2 (Transport of unsaturated groundwater and heat), a general purpose numerical simulation program for multi-dimensional fluid and heat of flows of multiphase, multicomponent fluid mixtures in porous and fractured media. It is applicable in geothermal reservoir engineering, nuclear waste isolation, environmental assessment and remediation and flow and transport in variably saturated media and aquifers. It is specially the two-phase flow capabilities, which are of concern in the calculations envisaged in this report. The program is being developed by the Lawrence Berkeley National Laboratory.

The simulations were started with TOUGH2 but quickly problems were found, such as the time-dependent boundary conditions or the long computational times. It was therefore decided to use the recently acquired program TOUGH2-MP to perform the numerical simulations for this exercise. TOUGH2-MP is a massively parallel version of the TOUGH2 code developed by the Lawrence Berkeley National Laboratory.

### 3.6.3 Implementation of the grid

The program Wingridder was used to create the mesh for the whole simulation domain (Figure 43) and for code for TOUGH2. Initially was created a very fine mesh of about 12000 elements, with three layers in the interfaces facing plug and canister. Due to these small volume elements

the simulations showed some numerical problems. It was then decided to use a coarser grid with about 8000 elements but still we found that the numerical simulations were still too slow. The mesh was again reduced to 6200 elements and the three layers in the interfaces were reduced to only one layer (Figure 44), additionally the program TOUGH2-MP was used for the calculations, which increased the speed of the simulations.

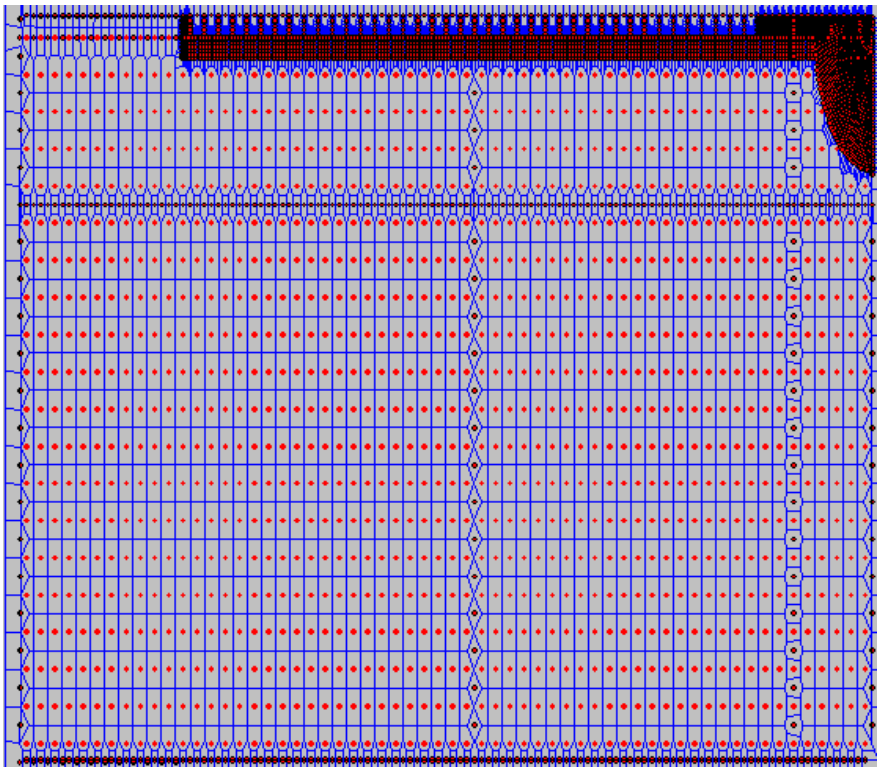

*Figure 44 Mesh used for the numerical simulations with TOUGH2 and TOUGH2-MP, the mesh consists of 6200 nodes.*

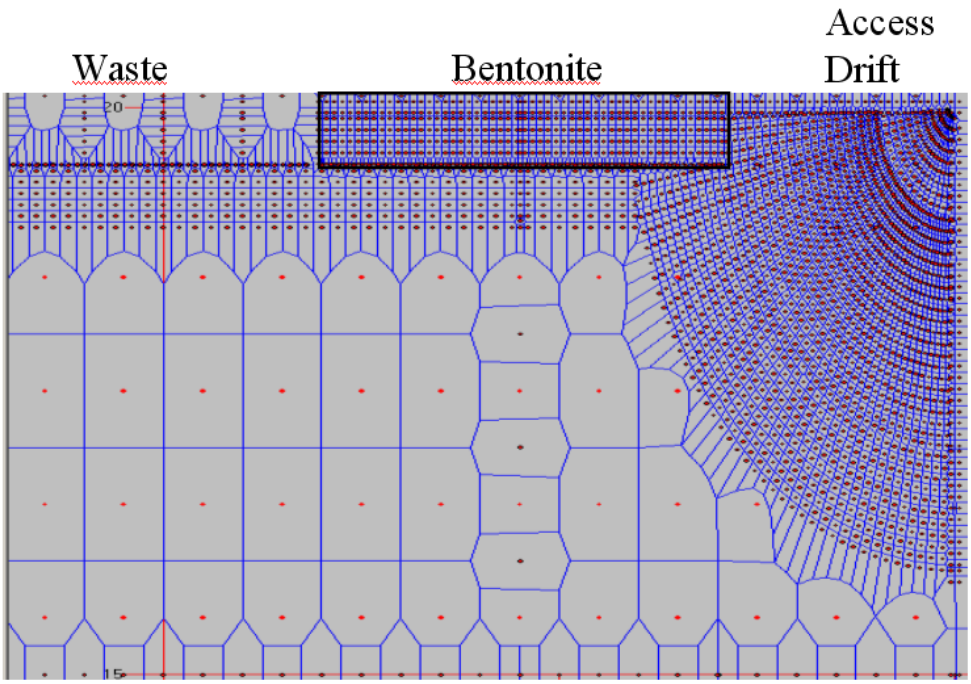


*Figure 45 Detail of the mesh in the common region of the EDZ, bentonite and access drift. The differences in sizes of the nodes for the different materials are noticeable.*

A detail of the mesh close to the bentonite plug is shown in Figure 45. The mesh in the less permeable cell domain is coarser than in the bentonite and in the access drift domain. The source term is integrated in volume elements all around the cell domain.

In the next figure a detail of the layer in the interface facing the cell is shown. Originally there were three layers in the interfaces facing the plug and the canister but due to numerical problems it was reduced to one layer as it can be seen in Figure 46.

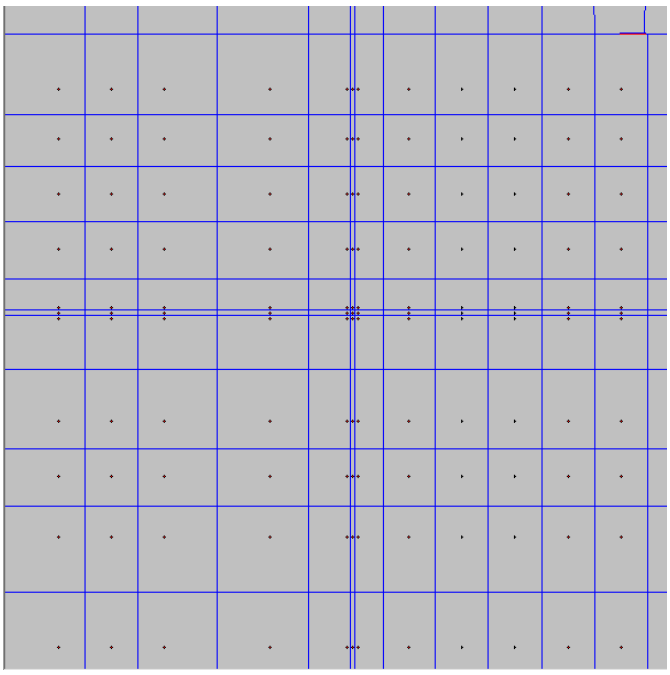

*Figure 46 Detail of the mesh close to the corner in the interface facing canister.*

The small volumes of the nodes, especially in the interfaces, may explain the numerical problems of the simulations; the volumes are in the order of $10^{-2}$ $m^2$. These volumes are situated in a region of wide change in the hydrological properties of the materials between the cell and the bentonite and thus some numerical instabilities are expected.

Great care was taken in order to implement the material domains with exactly the same area as specified in the exercise. In order to check this some scripts were created. One of the objectives of this exercise is to study whether the changes in the dimensions of the interface affect indeed the results. In which case, as the dimensions of the interfaces are so small, the use of other values for the areas of the interfaces than the specified may produce different results.

### 3.6.4 Initial conditions and boundary conditions

The boundary conditions as well as the initial conditions prescribed in the FORGE WP1.2 were implemented in the TOUGH2 input file. The behaviour of the system depending on the initial conditions was studied with numerical simulations. It was seen that the numerical convergence of the simulations were improved if the initial conditions through the different nodes in the interface, EDZ and rock change smoothly. The best convergence was obtained when the initial conditions of the EDZ and interface are the same.

The results of ENSI and of other teams confirm that initially a transient of pressure occurs during the first thousandth of a year as shown in Figure 47. The gas pressure in the EDZ changes during this transient from 5MPa to about 0.1 MPa. ENSI proposes therefore to change the initial conditions of the EDZ to this last value in order to avoid numerical problems at the beginning.

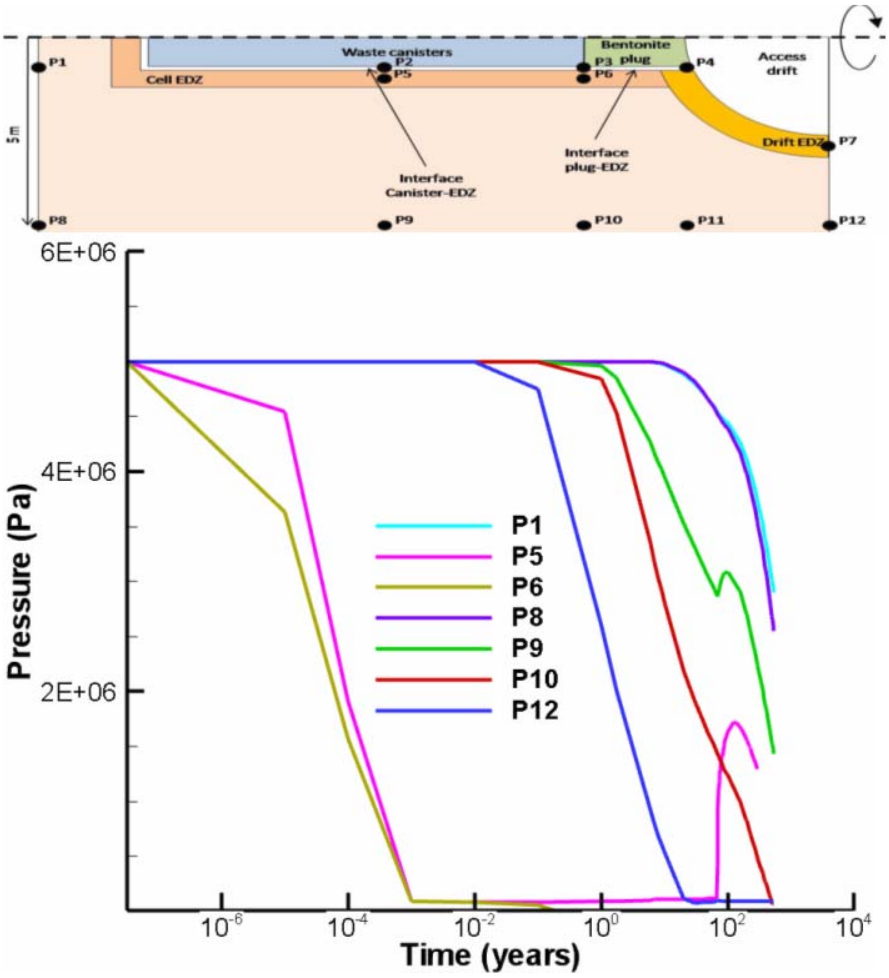


*Figure 47 ENSI Results for pressure values for the first hundred years in different points of the model.*

Initially the code TOUGH2 was used to perform the simulations for this exercise; the boundary conditions were implemented with a time-dependent source term. In this way the prescribed pressure and saturation variation was implemented but on the other hand also a variable mass of gas was introduced into the system, how this mass can affect the properties of the system has to be analysed.

To avoid possible problems with the inserted gas, the code TOUGH2-MP was used because this code includes a capability to implement time-dependent boundary conditions for the pressure. As in the exercise not only time-dependent boundary conditions for the pressure but also for the saturation were prescribed, the code had to be modified to allow the implementation of time-dependent saturation values.

The time-dependent boundary conditions cause the code to slow down. Comparisons were made between the calculation times of two inputs, one with boundary conditions and the other without them. The calculation time was extremely reduced for the case without time-dependent boundary conditions. Additional calculations will be performed to study the reason of this difference in computational time.

### 3.6.5 Installation of TOUGH2-MP and modifications in the code

ENSI acquired the program TOUGH2-MP in November 2009. In January 2010 it was decided to use TOUGH2-MP to implement the time-dependent boundary conditions and to perform the calculations faster. The compilation and installation of the code took longer than expected. Our

computer cluster consists of IBM AIX machines and this was not included among the systems in which the program was tested. Therefore the compiling options had to be adapted to our system and additional features had to be installed in our system. The code needs also the external libraries AZTEC and METIS. The compilation of these libraries was also system-dependent and compiling options were not specified for our system.

After the installation of TOUGH2-MP some tests were performed with inputs included in the distribution. The input for FORGE was implemented and adapted to the code TOUGH2-MP, there are some slight differences between the inputs for the two codes TOUGH2 and TOUGH2-MP. Unfortunately many problems were found sometimes related to the installation of the code and also related to the input file and the code did not work with the program TOUGH2-MP. The input file was refined and the installation and compilation options were optimize but there were still problems. The input file was checked by the authors of the code in LBNL and no problem was found except that it run a little slow. In the meantime the input was tested with the module EOS3 (TOUGH2 module in which the gas phase consists of air instead of hydrogen like in the EOS5 module) and the input worked. After some weeks of extensively checking of the code, a bug related to our computer architecture was found in the code, after the correction of this bug the input worked. The input run relatively well at the beginning but after more or less 100 years the code starts slowing down. That is something that has not yet been solved but we think that it is created by the small dimensions of the node elements of the grid. ENSI is still working on this issue.

ENSI had the intention from the beginning of its work on this exercise to implement the parameters and models as prescribed in the exercise. Some of them like the thin interfaces and like the time-dependent boundary conditions were extremely difficult to implement and without them, the calculations would have been much easier but on the other hand it would have been much more difficult to compare with other teams within the scope of this benchmark exercise. That is why ENSI proposes for next exercises to use identical specifications and if some specifications happen to be problematic to inform all the teams in order to change these specifications accordingly.

The parameters of the model according to Table 2 of the document with the definition of this exercise were implemented in the input of TOUGH2-MP. The code has to be changed to implement the diffusion coefficient, the gas relative permeability and slight changes have to be made also in the solubility coefficients for hydrogen in the Henry's law.

In the TOUGH2 code there are several options for the gas relative permeability, the relation of Van Genuchten is usually used:

$$k_r^g = (1 - S_{we})^2 \left[1 - S_{we}^2\right]$$

The prescribed gas relative permeability is given by the Van Genuchten-Mualem relation with γ=0.5:

$$k_r^g = (1 - S_{we})^\gamma \left[1 - S_{we}^{1/m}\right]^{2m}$$

This option is not available in TOUGH2, therefore the code was modified to make this option available.

Since the model is axisymmetric around the axis of the cell, each element of the grid includes all elements generated by rotating each planar element around this axis. Therefore the horizontal intrinsic permeabilities are implemented in the input as prescribed but the vertical intrinsic permeabilities have to include all the rotated elements. An average value around the rotation was

taken for the vertical intrinsic permeabilities. For the isotropic materials the prescribed intrinsic permeabilities did not change, for the anisotropic materials the following changes were made:

*Table 2 Changes made in the intrinsic permeabilities in order to fulfil the requirements of the axial symmetry.*

| | $k_x$ ($m^2$) | $k_y$ ($m^2$) | $k_z$ ($m^2$) |
|---|---|---|---|
| Interface facing plug | $1.0*10^{-17}$ | $7.49*10^{-18}$ | $7.49*10^{-18}$ |
| EDZ | $1.0*10^{-17}$ | $7.49*10^{-18}$ | $7.49*10^{-18}$ |
| Rock formation | $1.0*10^{-20}$ | $7.49*10^{-21}$ | $7.49*10^{-21}$ |

### 3.6.6 Scope of future work of ENSI in FORGE

The work of ENSI was so far dedicated to install and compile TOUGH2-MP, modifying the code, create the respective input and above all in making the code run faster. Results were obtained until about 10000 years but often under numerical simplifications. ENSI is now evaluating how these simplifications may affect the results. ENSI will create a much coarser grid and run the code with it and refine successively the size of the grid until obtaining convergence problems.

The first stage of the sectoral plan is now finished and ENSI expects to be able to dedicate more time for the simulations within the FORGE project. Despite having started later than other teams, ENSI has done a lot preparation work and some preliminary calculations useful for the next exercises. ENSI has the intention of finishing all required results for the first exercise and participate in the definition and calculations of the next exercises.

# 4. Global synthesis of the benchmark so far

This benchmark study is not aimed at comparing between codes, but rather aims to consider how relevant global phenomenological behaviour associated with gas generation and migration in a repository are considered by participating teams. However, as each team is using its own code, some code specificity has been introduced into the benchmark study regarding how it is represented in the participants' respective codes, especially in relation to boundary conditions. Therefore, direct comparison of all results produced by participants is not possible, and different level of comparison will be described in the following.

***N.B**: the fact that all teams have not complete the benchmark using exactly the same representation is a real issue, which is addressed in the discussion in paragraph 4.3.1*

## 4.1 Comparison of the available results and main phenomenological results

Despite some minor differences in the way to represent varying boundary conditions at the drift, the ways NDA RWMD/Quintessa and Andra have represented the model are quite comparable. The results for these two teams are in good agreement, for water and gas pressure, as well as for water saturation.

Figure 49 is representing the time evolution of water pressure at point 4 (see Figure 48 and annex for more details)

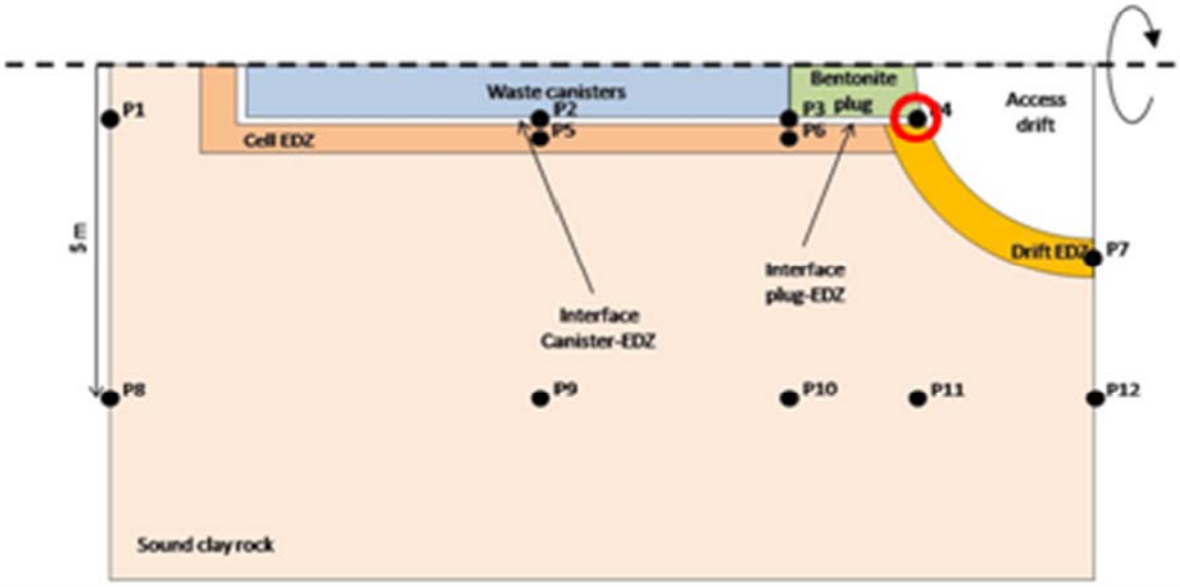


*Figure 48: position of point 4 in the model*

For both of these teams, results show that gas is not generating groundwater overpressures: the maximum pressure is reached after a long time, when water pressure is reaching initial undisturbed conditions at 5 MPa. This time is comparable for both teams (between 20,000 and 30,000 years for NDA/Quintessa and between 30,000 and 40,000 years for Andra) and correspond to the moment of saturation (gas pressure is equal to water pressure, e. g. capillary pressure is equal to zero). Gas pressure is never very high, the maximum being achieved just before resaturation at around 5 to 5.5 MPa.

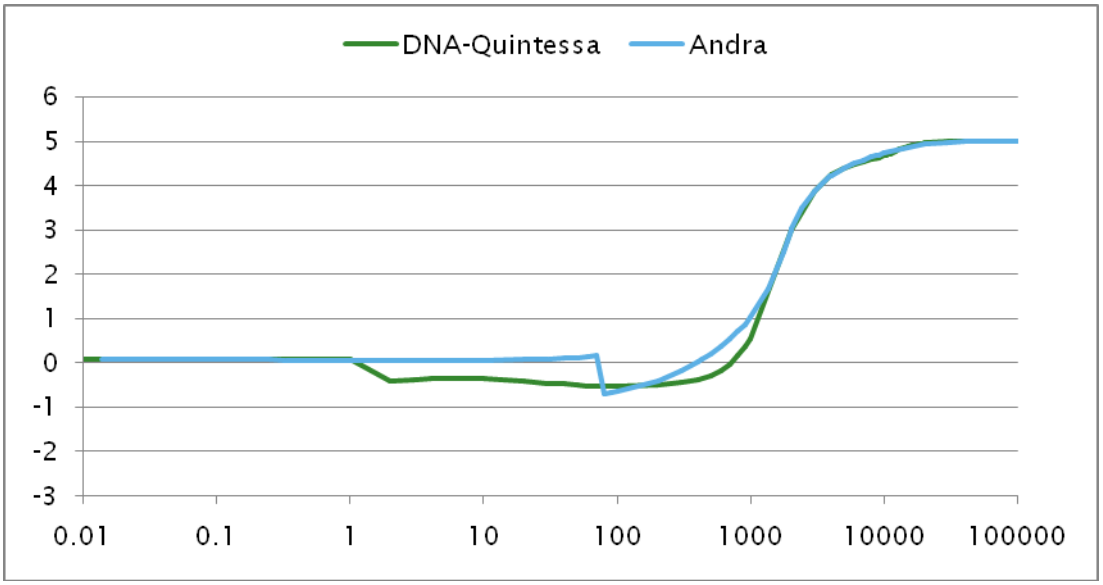


*Figure 49: evolution with time of water pressure at point 4*

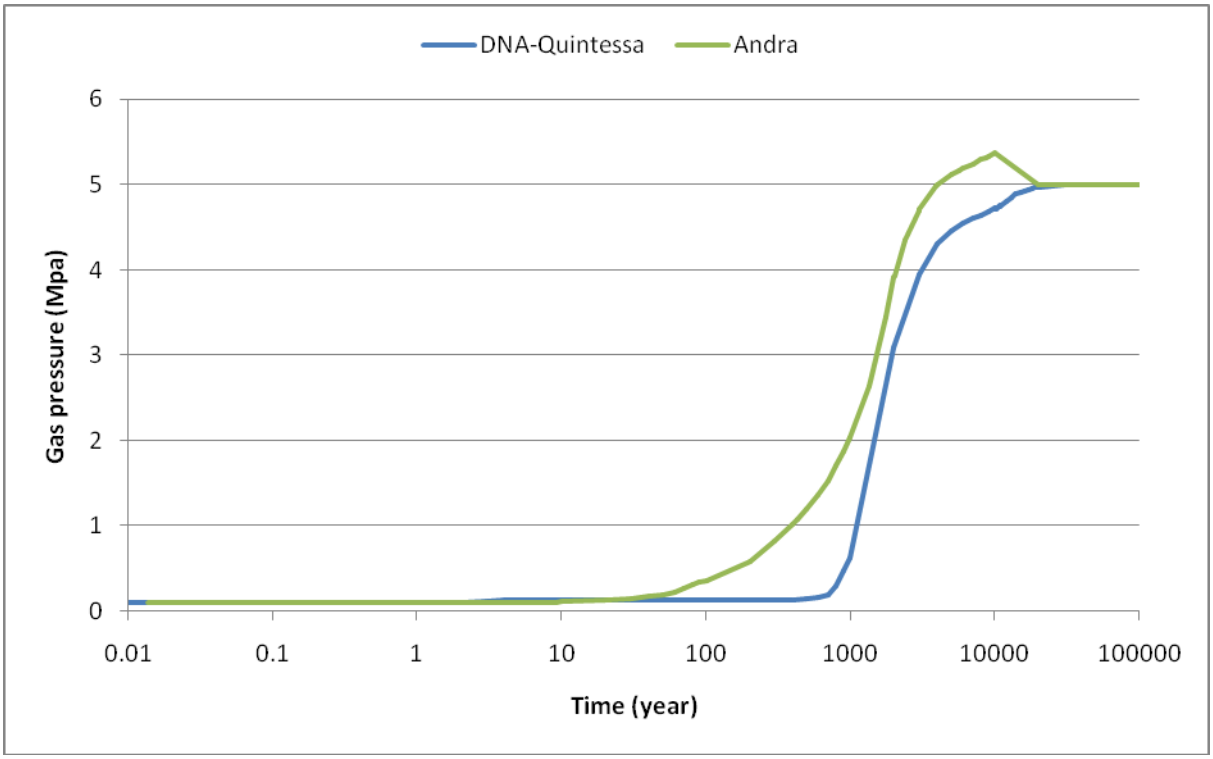


*Figure 50: evolution with time of gas pressure at point 4*

Another interesting result is the fact that a gas phase is maintained in the access drift during several tens of thousands of years after the end of the gas production phase (ended at 10,000 years) before dissolution/diffusion processes lead to its removal. Convection along the access drift is certainly also a dominant process during this period, but this will have to be tested at a bigger scale.

For points in the argillites far from the cell, the results are also coherent between the two teams. For example, point 9 (see Figure 51 for position) evolution of water pressure with time are really similar (Figure 52). The fact that water pressure only decreases by around 2 MPa from the initial

undisturbed natural pressure means that the media is not desaturation at all at this distance from the cell. In fact, due to the very small permeability of the argillites and to its high capillary entry pressure, desaturation is mainly occurring inside the cell and up to the radial end of the EDZ, but the undisturbed argillites are not significantly desaturated (a desaturation of some % is possible over some decimetres in the undisturbed argillites, but not more than this).

*Figure 51: Position of point 9 in the model*

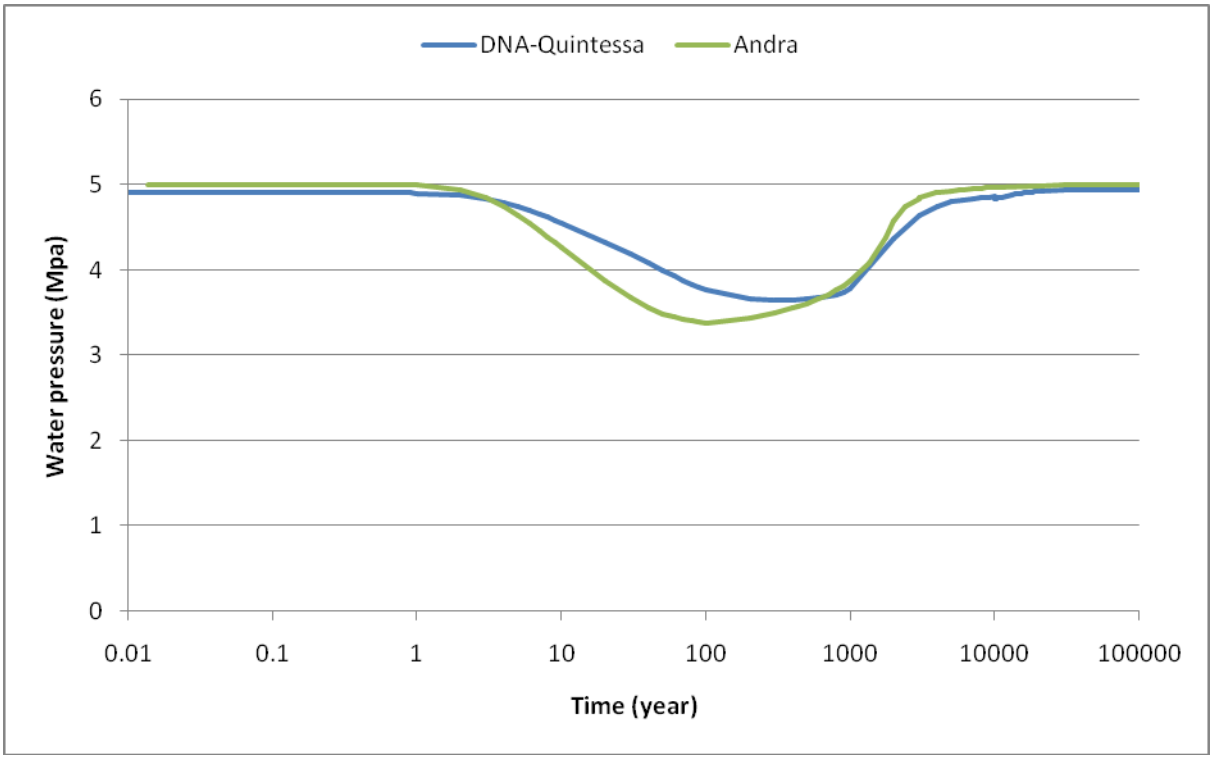


*Figure 52: evolution of water pressure with time at point 9*

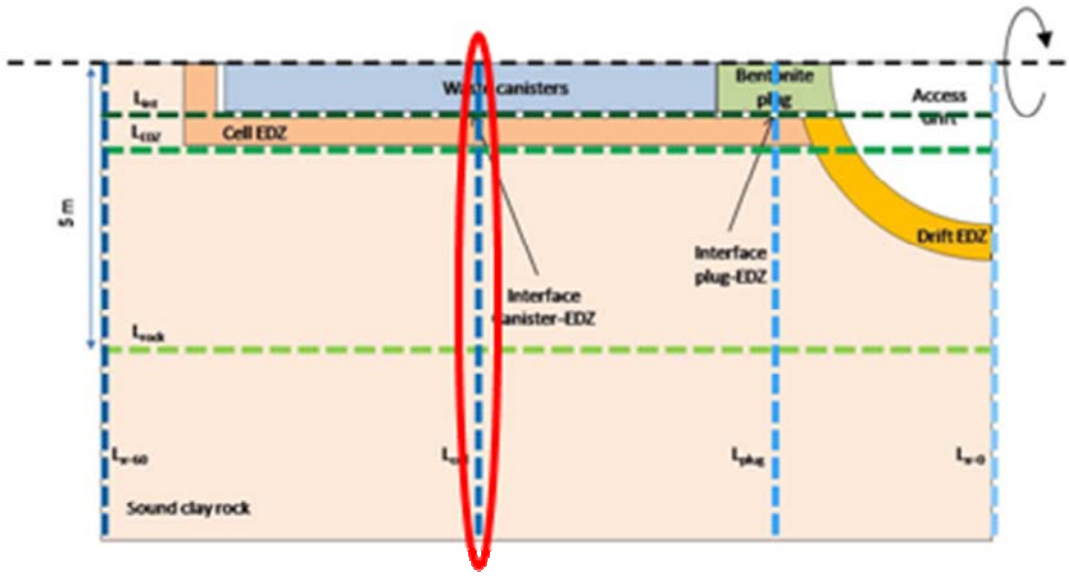


*Figure 53: position of mine Lcell in the model*

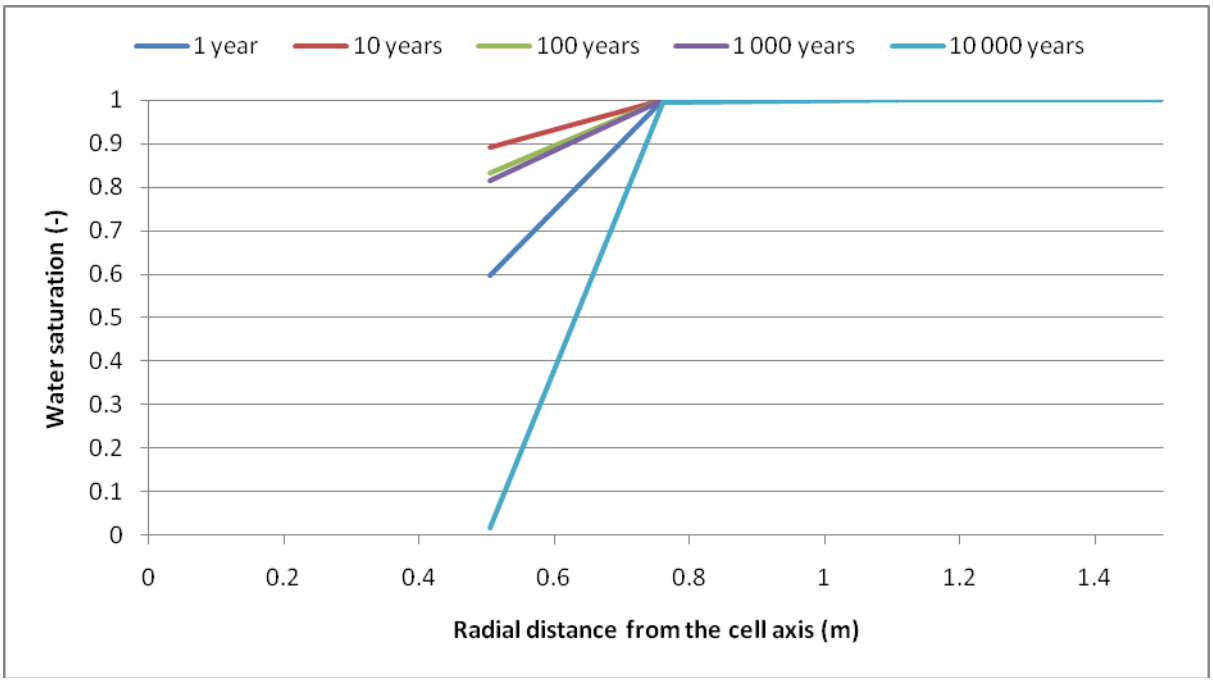


*Figure 54: evolution with time of the water saturation in the first on and a half meter radially from cell axis along line Lcell at different time. Results from NDA/Quintessa*

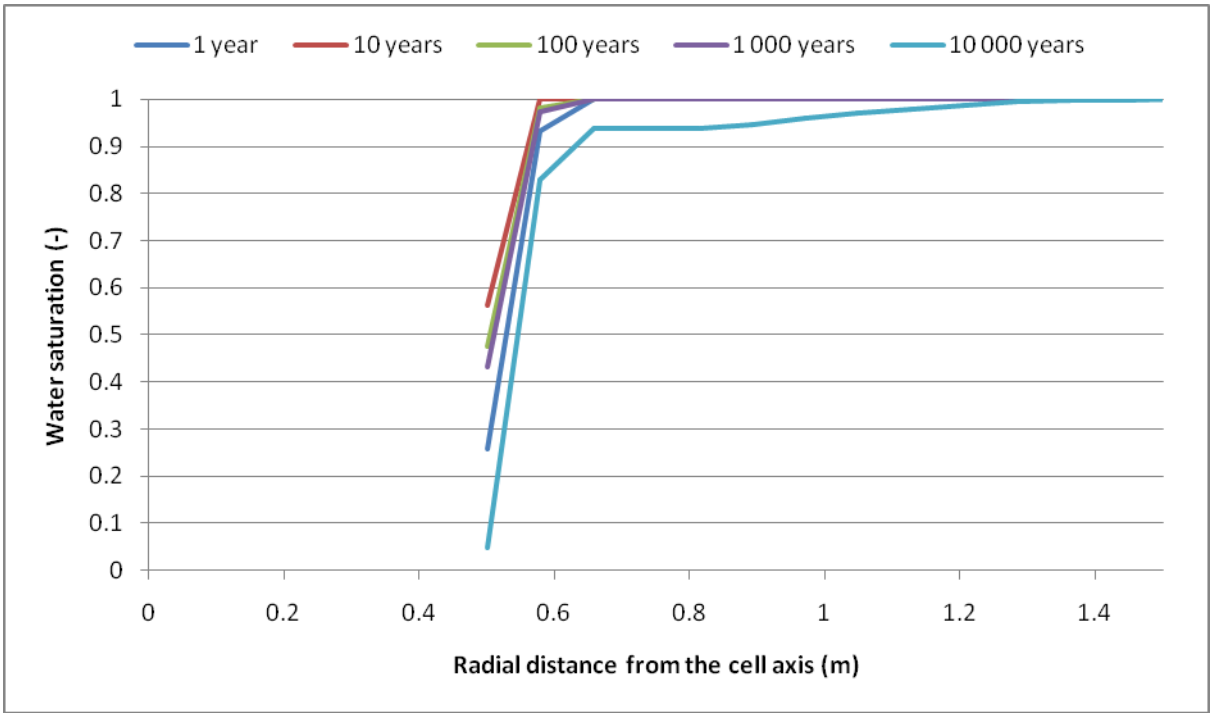


*Figure 55: evolution with time of the water saturation in the first on and a half meter radially from cell axis along line Lcell at different time. Results from Andra*

This is confirmed by the evolution of water saturation along Lcell line (see Figure 53 for position) reproduced inFigure 54 and Figure 55 . Although the values of water saturation in the interface between the canister and the EDZ are not the same for both teams (mainly due to the way this interface is simulated), the general behaviour is comparable for both results :

- Desaturation is limited to some decimetre in the EDZ. Even at long time (10,000 years) the desaturation in the undisturbed argillites (distance over 1.2 meter) is limited to some % at the most;
- Initially (1 year) the interface is highly desaturated but partial resaturation occurs quite rapidly (10 years) before a general desaturation lasting several thousands of years and leading to a residual saturation less than the initial one (10,000 years).

Concerning gas fluxes, the two simulations are also coherent as shown in Figure 57 (see Figure 56 for position of the interface on which the flux is calculated). Initially, for around one year, the gas (initially air brought during drilling of the cell) flux is directed from the access drift toward the cell, but rapidly, the gas ($H_2$) direction of the flux is inverted and hydrogen is going out of the cell toward the access drift. The maximum flux (around 0.1 to 0.14 kg/y) is reached after several hundreds of years. After this peak, the gas flux reaches a plateau from around 2'000 years up to the end of the gas generation period (10,000 years). The value of this plateau is relatively near production rate (0.8 kg/y). This implies :

- that most of the hydrogen is moving under gas phase and that only a small part is dissolving and diffusing in the argillites water around the cell;
- that the interface is playing an important role in enabling the gaseous hydrogen to move easily from the end of the cell toward the drift.

After the gas production period, the gas flux toward the drift is decreasing to zero over a timescale of some thousands of years. A reverse flow (from drift to cell) is eventually possible at a small rate for several tens of thousands of years, the gas stored in the drift moving back to the

cell as pressure drops due to the dissolution/diffusion process (which become dominant after gas production period).

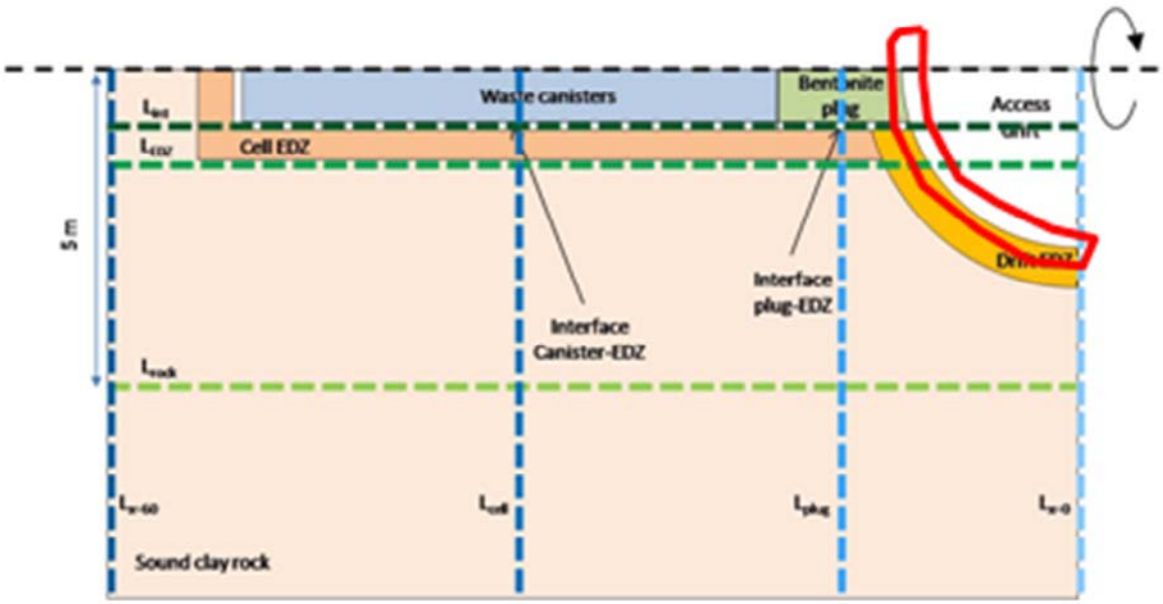


*Figure 56: position of the interface on with gas flux is calcultated*

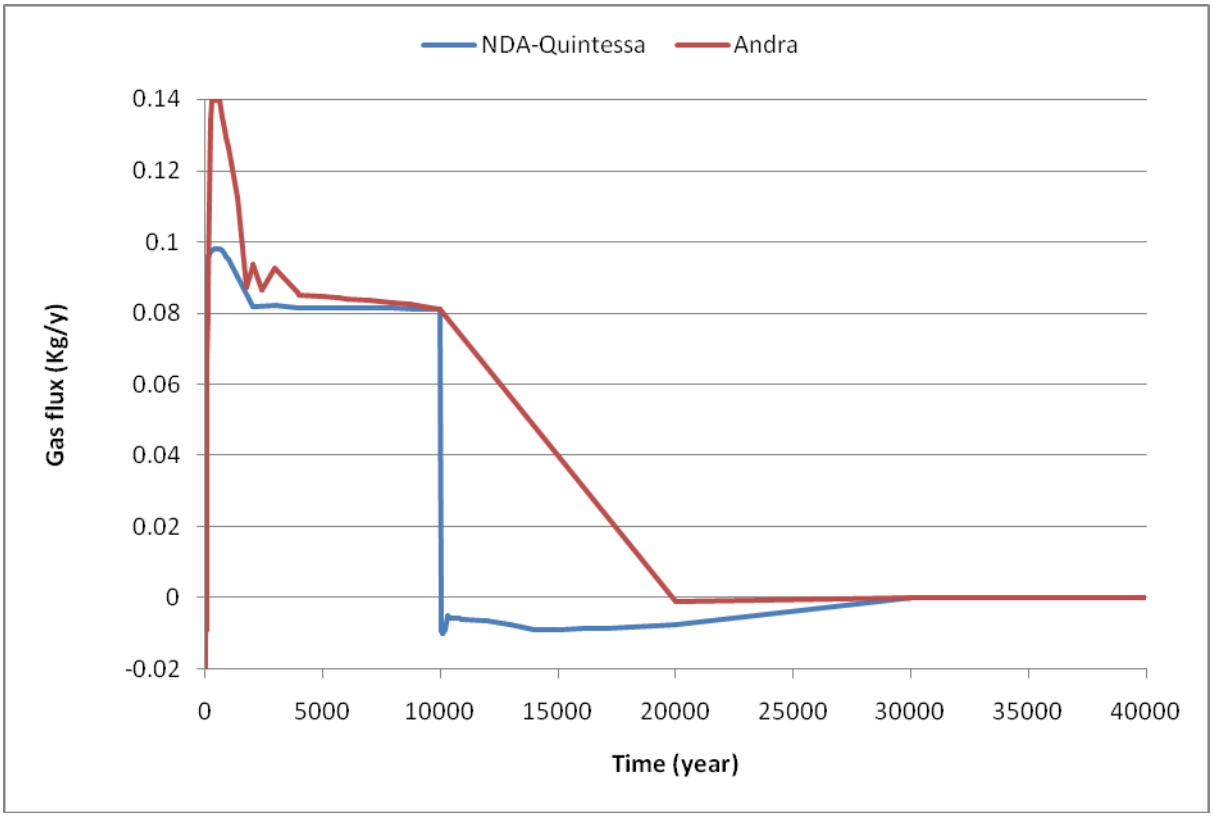


*Figure 57: evolution with time of the gas flux toward the access drift for both teams*

The work done by LEI and SCK-CEN enables us to compare the NDA RWMD/Quintessa and Andra results to a situation where the drift does not represent an important outflow for the gas generated in the cell. The main differences between these cases (see Figure 58) are:

- the increase of gas pressure in the cell commences much sooner;
- the gas pressure can be significantly higher;

The desaturation zone is increased, but desaturation always stays to some % at the most in the undisturbed argillites.

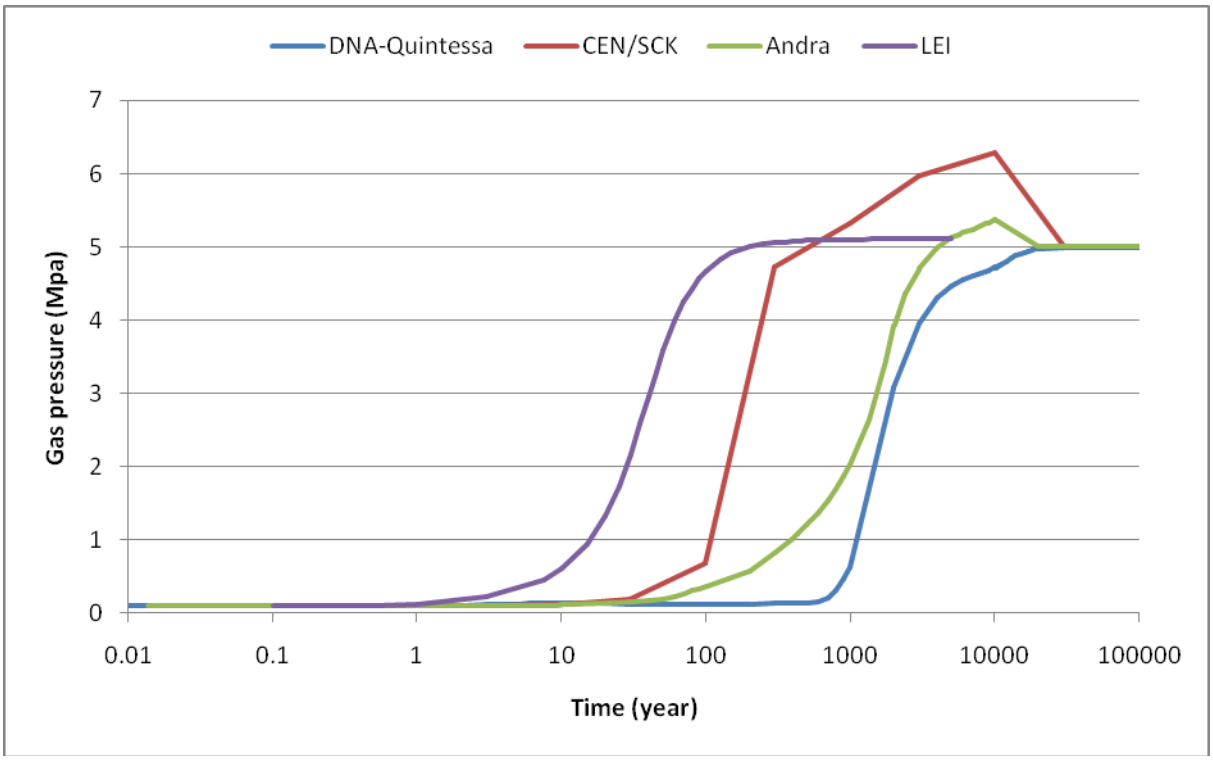


*Figure 58: Evolution with time of the gas pressure at point 4*

## 4.2 Sensitivity analysis results

For this first part of the benchmark exercise, three sensitivity analyses were performed (see benchmark definition in Annex). The impact of the changes to the model output, associated with these sensitivity analyses, on the phenomenological behaviour described in Section 4.1 is analyzed in the following sub-section only in consideration of for the reference case of the benchmark definition (and so mainly concerns NDA/Quintessa and Andra reference results).

### 4.2.1 Sensitivity 1 : Permeability of EDZ reduced to permeability of the undisturbed rock

This sensitivity analysis was proposed because some measurements, either in-situ in different underground rock laboratories (URL) or in surface laboratories on test samples, have shown that the permeability of the EDZ can be significantly reduced both by an increase of the mechanical stress (which will be the case at long term all around the cell, and especially around the bentonite seal once the bentonite swells on resaturation) and by a resaturation (which will be the case roughly after several tens of years) all around the cell part situated far from the ventilated drift EDZ.

As permeability of the EDZ is reduced, the pathway toward sound argillites along the cell is significantly reduced as well. Less gas is then entering the EDZ, and less gas is dissolving in the argillites. This implies that more gas is flowing along the interface increasing the global gas flux toward the drift (Figure 59 and Figure 60).

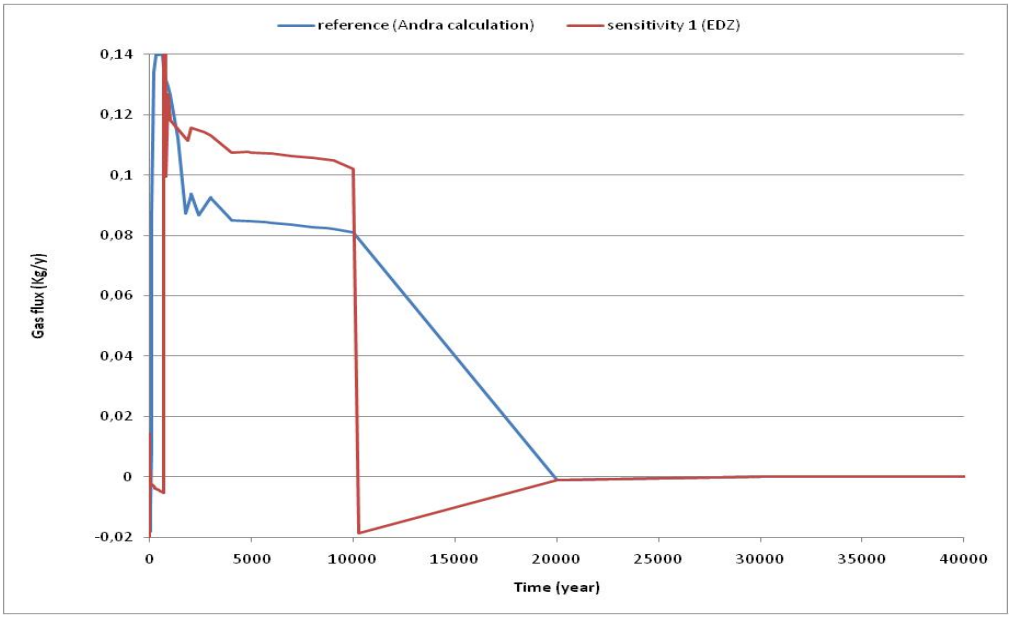


*Figure 59 : comparison of gas flux toward the drift between reference case and sensitivity 1 for andra's results*

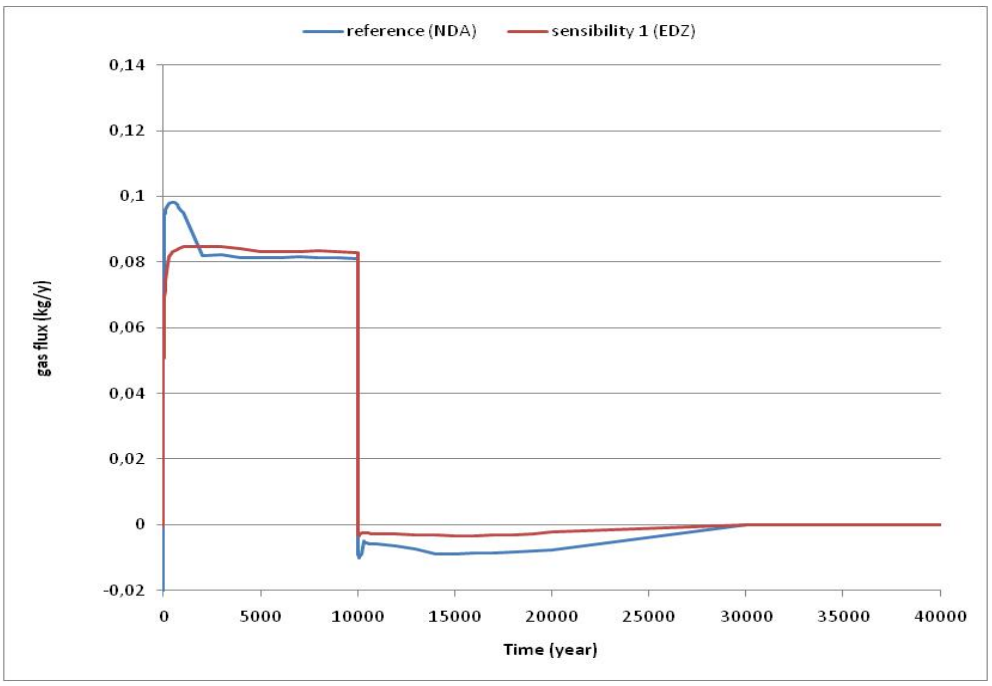


*Figure 60 : comparison of gas flux toward the drift between reference case and sensitivity 1 for NDA-RWMD's results*

As EDZ permeability is significantly reduced, permeability of the interface should be reduced as well due to mechanical constrains. This is not implemented in the calculation and can be a significant bias.

This sensitivity analysis shows that EDZ and interface permeability has a real impact on gas migration at the cell scale.

### 4.2.2 Sensitivity 2 : use of different relative permeability curves

This sensitivity analysis was introduced because experimental measurements on samples with permeabilities assumed in this benchmark study are difficult: effectively, water saturation in argillites and bentonite is mostly at over 90% and even 95%, and modern experimental methods

that are used to determine the relative permeability curves are borderline applicable under such saturations. Therefore, the uncertainty on the real behaviour of permeability as saturation changes at these relatively high saturation levels is itself quite high.

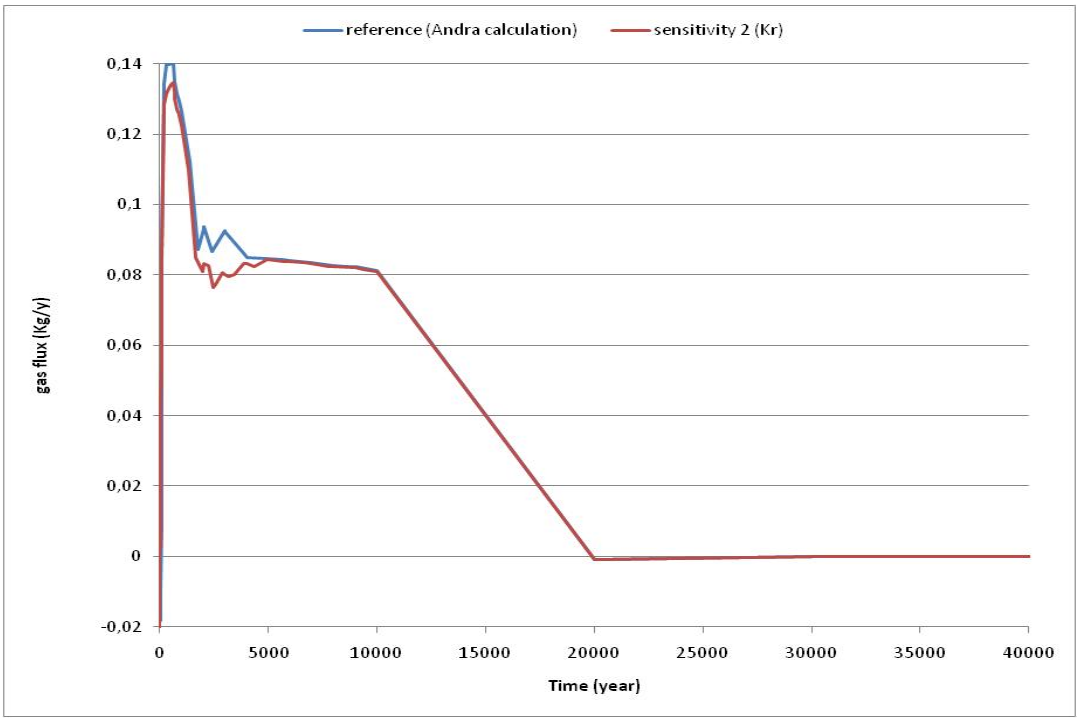


*Figure 61 : comparison of gas flux toward the drift between reference case and sensitivity 2 for andra's results*

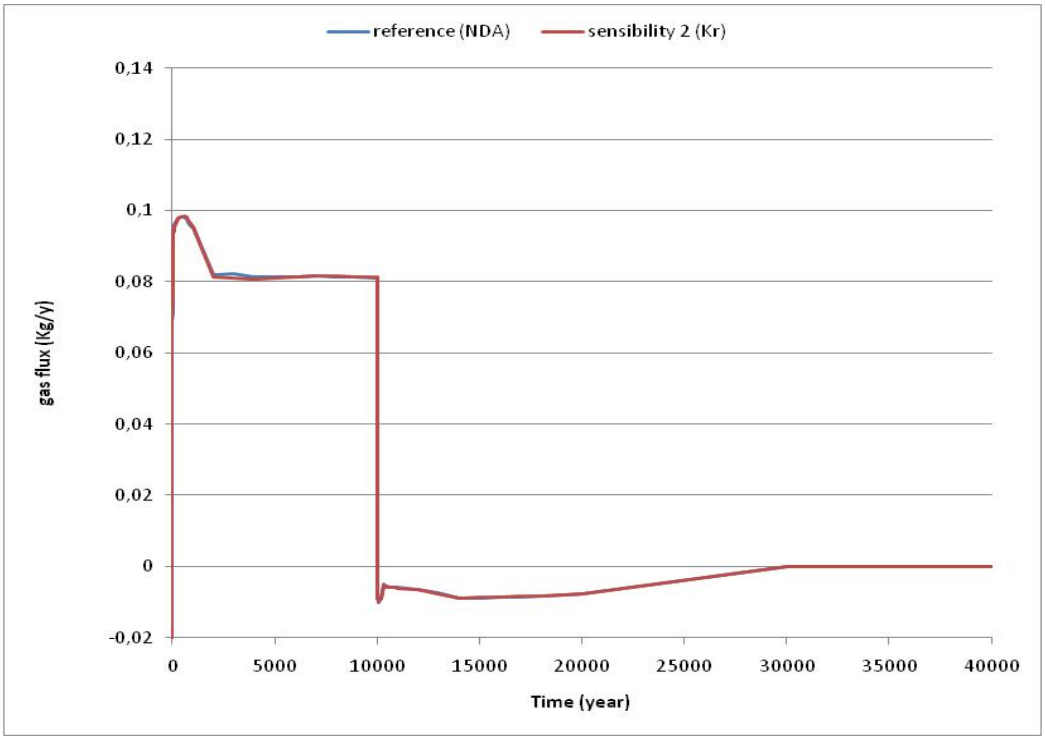


*Figure 62 : comparison of gas flux toward the drift between reference case and sensitivity 2 for NDA-RWMD's results*

For this benchmark, the influence of differing saturation – permeability relationships has shows no real impact (Figure 61 and Figure 62). This is a bit contradictory with some other results, showing that the choice of the permeability curve has a real effect on gas migration, but can be

explained by the fact that in previous calculations the interface was not explicitly modelled. In such a case, the pathway towards the drift was then less important, and more gas has to go through the EDZ or argillites: the relative permeability curves of these materials in this case therefore have more importance in the overall behaviour of the gas than results from the current NDA/Quintessa and Andra sensitivity analyses suggest.

### 4.2.3 Sensitivity 3 : Diffusion coefficient of dissolved gas multiplied by 10

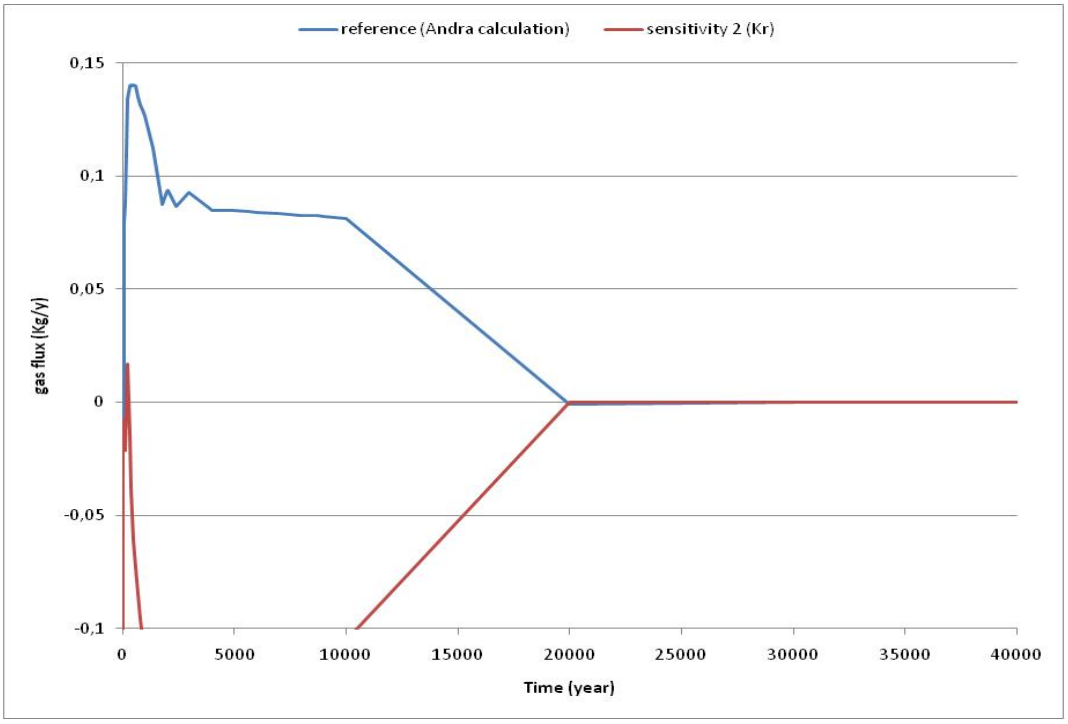


*Figure 63 : comparison of gas flux toward the drift between reference case and sensitivity 3 for andra's results*

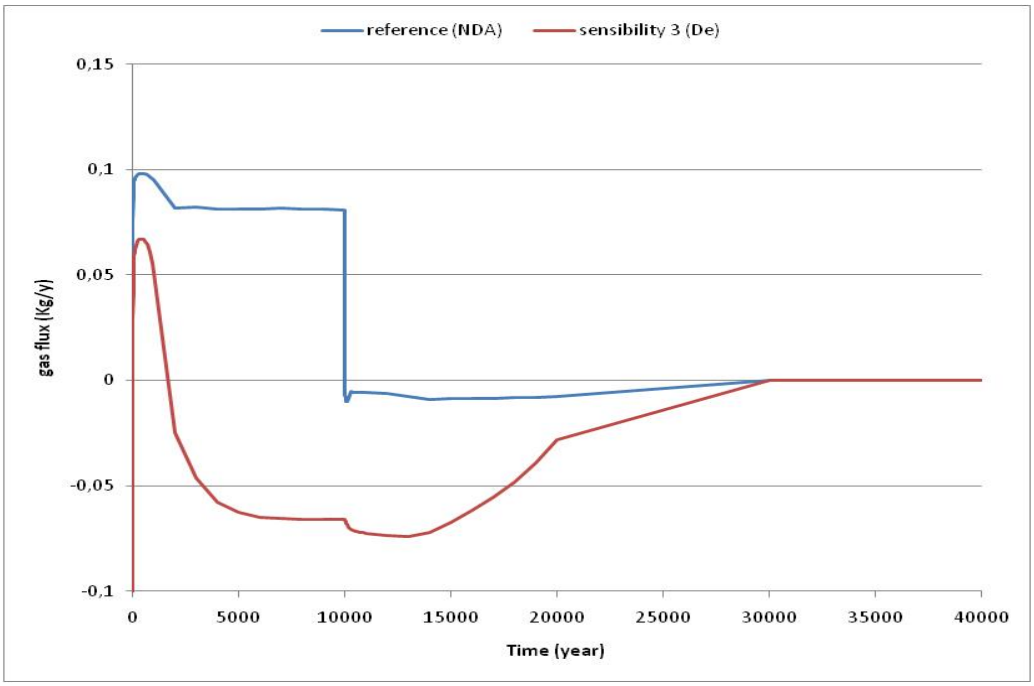


*Figure 64 : comparison of gas flux toward the drift between reference case and sensitivity 3 for NDA-RWMD's results*

This sensitivity analysis was proposed because the diffusion process for gas, and especially for hydrogen - one of the most mobile gases - is really difficult to derive precisely. Depending on the procedure used, and on the teams making the experience, one order of magnitude difference in the rate of diffusion of hydrogen can be found in available data. One other point is that, due to the potential health and safety danger associated with working with this gas, there is little data on measurement made in-situ in a URL; only samples measurement are at hand for the moment.

Due to boundary conditions expressed in pressure and deduced from another simulation at complete storage scale (but with less geometrical details) the results are showing a gas flux from the drift toward the cell (Figure 63 and Figure 64). This is a bias of the simulation, but what is to keep in main is that the uncertainty on diffusion coefficient can imply significant changes in the way hydrogen is behaving, e.g. the higher the diffusion coefficient, the smaller the gaseous flux toward the drift. This can make a real difference concerning high hydrogen pressure at storage scale especially at on long time.

## 4.3 Main problems encountered

On the basis of input from all participating teams, the main problems encountered with the current benchmark study can be subdivided into 3 major groups, all closely linked with numerical issues:

### 4.3.1 Boundary conditions representation

For some teams, it was a real challenge to take into account the varying prescribed pressure boundary conditions, because their specific code does not allow the integration of these types of boundary conditions. In such a case, the boundary conditions had to be adapted to the code capabilities and the results were therefore affected, sometimes significantly.

A way to resolve this problem is to transform pressure-varying boundary conditions into time-dependent flux boundary conditions: this type of boundary condition is more widely supported by the codes used for this exercise.

### 4.3.2 Time step management

Although the benchmark geometry is not very complicated, its definition is really demanding in terms of numerical behaviour. The main difficulties are the highly heterogeneous properties of the different material, especially in terms of permeability (interface $10^{-12}$ $m^2$, argillite $10^{-21}$ $m^2$). A second difficulty, linked to model geometry, is the different size of the different materials (thickness of the interface is 0.01 m whereas radius of the domain is 20 m).

This causes numerical problems especially in the management of the shift between water saturated flow and two-phase flow. Sometimes a cell is near the shift from one situation to another and depending on the internal numerical iteration there is a movement back and forth between the two stages. Trying to solve this uncertainty, the code reduces the numerical time step and this can result in a time step so small that a simulation over thousand year period is computationally impossible to manage; for extreme situations, the model-run can stop cease.

This problem is linked to several factors :

- Specific complexity of the model (high heterogeneity of parameters, high differences in characteristic dimension, …);
- Mesh optimization (see next point) : the smallest the numerical elements, the higher the number of elements where this type of problems can appear;
- Code capability to cope with this type of numerical problem.

The two first items can be modified by the user when working on a specific simulation, but the third one is more difficult to modify and can needs specific numerical development within in the code structure.

### 4.3.3 Mesh optimisation

This problem is related to the preceding point, and is a real issue in its own right. There are several ways to define meshes that are coherent with the numerical requirement of the code and the model to simulate (Figure 65 and Figure 66). Simple regular meshes can be defined by hand, but complex unstructured and/or non uniform meshes can only be generated by specific numerical codes and sometimes it is difficult to optimize the parameters of these codes.

If the mesh is not sufficiently refined, the numerical diffusion can be high, and the results are no longer representative of the physics that the code is trying to solve. On the other hand, if the mesh is too refined, the time needed for the simulation can be too high for practical use (due to power limitation of the computers) or numerical problems occur, like time step reduction (see preceding point), can occur.

To solve this problem, one approach is to use an automatic and adaptive mesh generator, optimizing the mesh at each numerical time step by refining it where fronts are present and coarsening it where refinement is less necessary (front has passed or is not yet arrived).

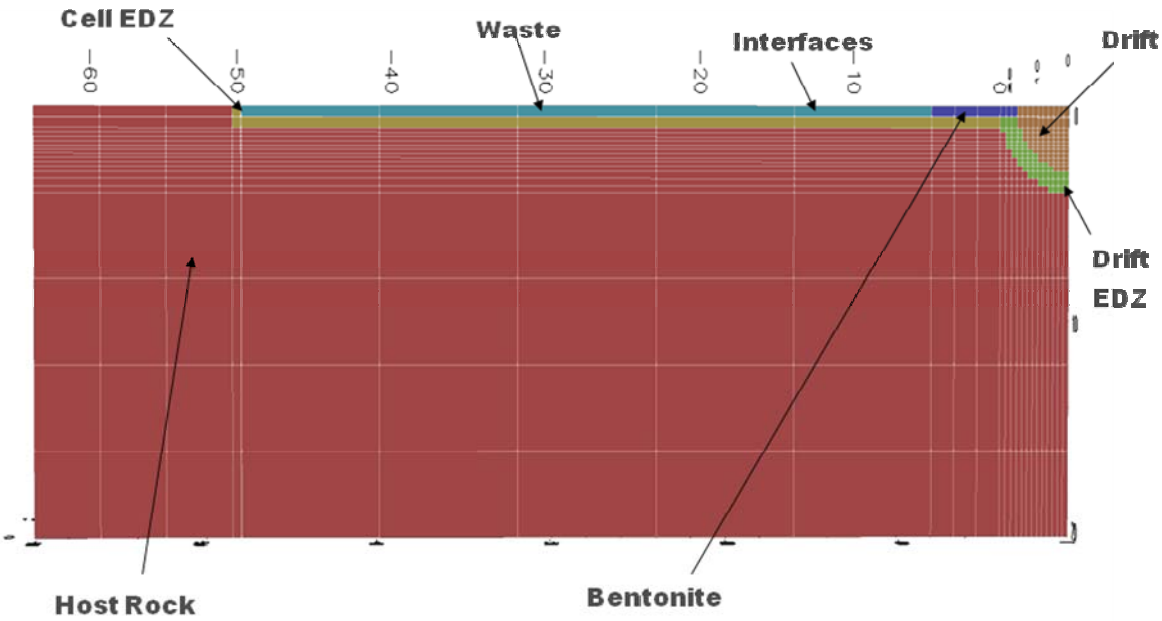


*Figure 65: example of a coarse regular mesh*

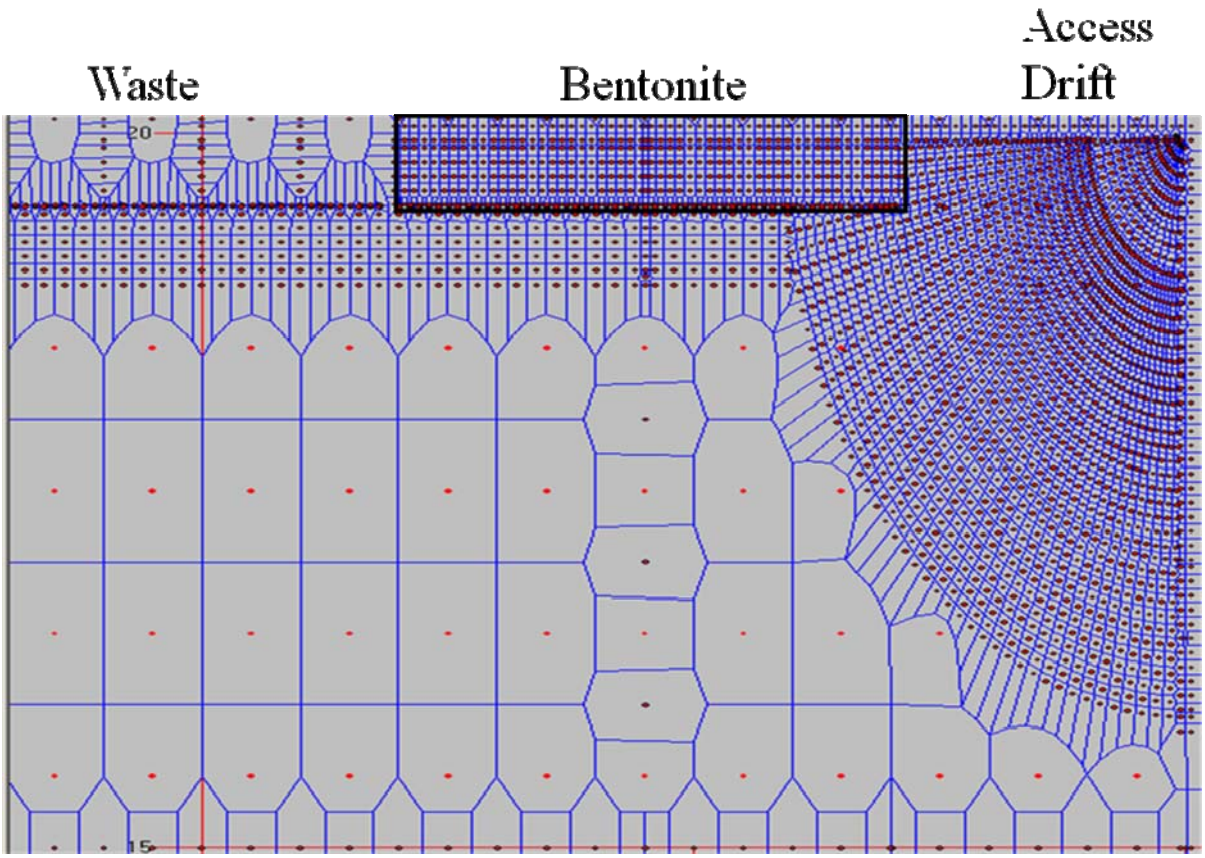


*Figure 66: example of a refined unstructered non conform mesh*

# 5. Interactions with other FORGE WP's

Some conclusions of these first results from Work Package 1.2 can be directly linked to the work done in other FORGE Work Packages, or in the work that will be done in WP1.2 in the future :

- The interface between canisters, cell liner or cell seal (bentonite or concrete) and EDZ is a very important feature for gas behaviour at an HLW cell scale in argillite media. Thus improving the knowledge about these interfaces is really important. This links to part of the work done in WP3 and WP4.
- The EDZ permeability is also an important parameter concerning gas migration at an HLW cell scale in argillite media. Having more confidence in hydraulic parameters in this material is of real importance, especially for intrinsic permeability, initial values but also its evolution with time. This links to part of the work done in WP4.
- Another potentially important process is diffusion. A good estimation of the parameters defining this process is to be found especially in the EDZ and in the undisturbed argillites. This links to part of the work done respectively in WP4 and WP5.
- Numerical optimization, and especially for the mesh generation, are an important issue to increase the confidence in the numerical results, only way to have estimation of gas behaviour for large time and space. This links to part of the work to be done in WP1.2.

# 6. Future work

The production of this first intermediate report from FORGE Work Pacakge 1.2 also corresponds to the end of the first part of the work defined at the launch meeting of WP1.2. Considering the work achieved by the different teams, it has been decided to continue work for a further six months on the same benchmark exercise, with two main objectives :

- To have all participating teams reach the same level of achievement
- To increase the number of sensitivity analyses undertaken on this benchmark relating to a HLW cell in argillite media.

Three more sensitivity analyses are therefore defined :

- **Impact of mesh refinement on results** (no more specification can be given as mesh generation is participating team-dependent). The aim is to find the "best mesh" (i.e., one that is as coarse as possible, without impact on the phenomenological results) and to compare the way to find it and the mesh itself obtained by each team.
- **Sensitivity analysis on the time of initiation of gas production**. In the first part of the benchmark, gas generation was initiated at the beginning of the simulation, when interface was not saturated, so gas could flow easily from the cell to the drift. As the interface is assumed as resaturating quite rapidly with time on repository closure, assuming that gas production initiates only once it is completely full of water could change the kinetics of gas migration during the exploitation phase (at least during some years). Simulations will therefore be undertaken for an initiation of gas production at T=1 year and T=2 years (everything else being the same as in the reference case)
- **Sensitivity analysis on interface properties**. Intrinsic permeability of "interface facing canister" is at $10^{-12}$ $m^2$ in the reference case (compared to more or less $10^{-18}$ $m^2$ for the EDZ), and all the gas is flowing along it. In these sensitivity analysis, the intrinsic permeability of this material will be put to $10^{-15}$ $m^2$ at first and then at the same permeability as the EDZ.

In order for each team to work on models as closely reflecting the benchmark definition as possible, time-varying boundary conditions considering gas flux instead of gas/water pressure will be provided to each team

In addition to this new set of simulations at HLW cell scale level, reflections on two points will be produced, respectively on:

- **"Simple mechanical coupling"** - As a base of this reflection, the work done in PAMINA EC project could be useful.
- **Upscaling process**: what type of "upscaling" do we want/need ("lumping" form, High performance computing needing code development and reducing the upscaling problem, ...) ? For what purpose (concentration, time characteristic, pressure, ..., phenomenological understanding, PA/SA approach, ...) ? As the interface seems to be an important feature, not yet modelled, a special focus will be consideration on how to upscale it. Another point is to discuss the actual methods used to model global storage with good cell representation but simplifications on the intermediate levels (modules, drift, …)

Depending on the results, especially in consideration of upscaling, the next component of the benchmark studies to be considered in FORGE Work Package 1.2 will be defined after the next WP1.2 meeting of WP1.2, which is scheduled for June 2010. Note that the overall aim of WP1.2 is to achieve a benchmark intercomparison of the representation of gas migration at the repository scale.

# ANNEX

# 7. ANNEX : Full description of the benchmark

## 7.1 CONTEXT AND OBJECTIVES

From WP1 participants point of view, the aim of the benchmark should less be a comparison of numerical codes then an exercise trying to answer some precise questions in a PA logic (for example, which could be the relative role of the EDZ, interfaces, backfill in the migration of gas at storage scale?). This clearly includes numerical considerations, but they are a mean and not an objective.

One of the difficulties is to find a common playground for all participants, which allows bringing some add-on for each one. After discussion, a general agreement was that the reference exercise will be as generic as possible (without targeting precisely on national concepts) and to propose sensitivity analyses making it possible to cover national specificities. What is aimed is more to feel how the systems react and why they can react differently rather than an inter-comparison of codes. A second agreement was that, although the final aim of the benchmark studies is to represent repository-scale simulations, the first exercise should be rather simple and at cell scale.

In this context, one of the major problems in representing gas transfers in a repository for radioactive waste is to model simultaneously all gas sources (generally located in the disposal cells) and the transfer pathways constituted by the network of interfaces, plugs and undergrounds drift.

## 7.2 REFERENCE TEST CASE

The objective of this first test case is to simulate the gas production and migration in a disposal cell and a portion of the drift (Figure 67).

The calculation domain is axisymetric. In the direction of the cell axis, the extension takes into account the length of the cell, the distance between the bottom of two adjacent cells in this direction and the radius of the access drift (Figure 68 and Table 3). The radius of the axisymetric domain is a compromise between the inter-cell distance along the access drift and the thickness of the geological layer.

A gas-production term is provided for the disposal cell. It is imposed on the external surface of the cylinder that represents schematically the canisters. The cell is constituted of a material impermeable to both water and gas, and is not explicitly represented in the model (the external surface of the canister is a no flux boundary). The materials to be taken into account in that simulation include the EDZ of both the cell and the access drift, the cell plug, the backfill of the access drift and the geological medium. Moreover the interface between the cell and the cell EDZ should be represented (general retention behaviour similar to a sand), taking into account a different behaviour whether the interface is facing the bentonite plug (same permeability as EDZ) or the canisters (same permeability as a sand).

The aim of this test case is to better understand the mechanisms of the gas migration (transport, diffusion and dissolution) at the cell scale and in particular to analyze the effect of the presence of different material and interfaces on such mechanisms.

For this first exercise, isothermal hypothesis at 20°C were considered, even in the sensitivity analysis.

The main constraints of the case are to give a detailed representation of all the elements of the proposed problem and to maintain compatible calculation times with the simulation tools while complying with the physics of the problem. Moreover special attention should be paid at the effect of the size and form of the mesh on the results of the simulation.

The simulations should be performed using a full physical model (multiphase darcy's law, with interaction between each phase: dissolution/evaporation and diffusion), a consistent example can be found in paragraph 7.5 "Mathematical model proposed for the exercise".

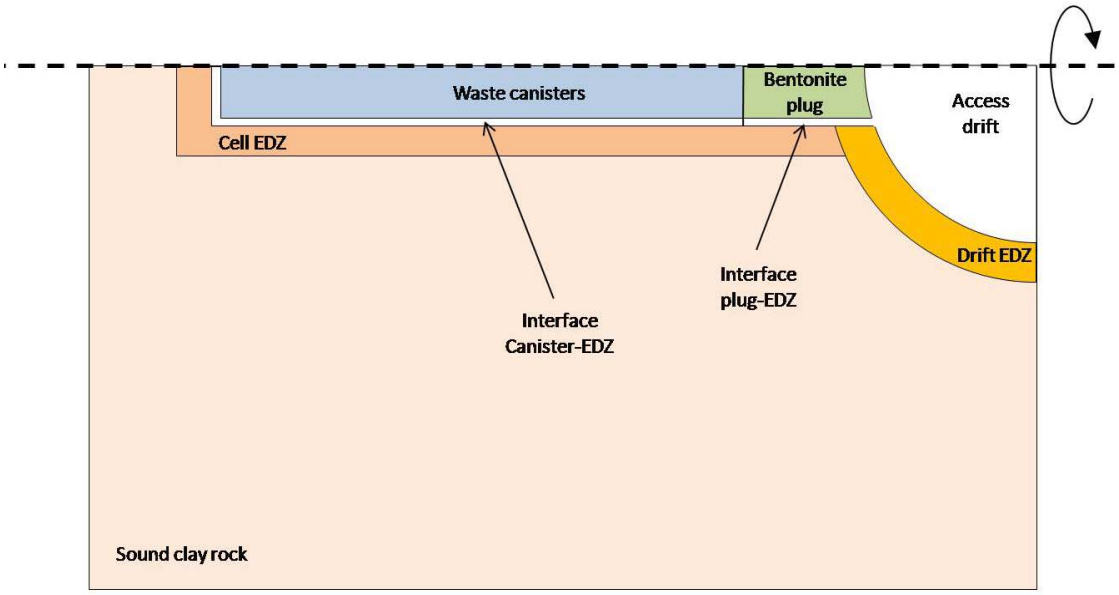


*Figure 67: Representation of the axisymetric calculation domain*

### 7.2.1 GEOMETRY

The canister and the plug share the same circular section.

The section of the access drifts is circular. Disposal cell is positioned at half-height in the access drift.

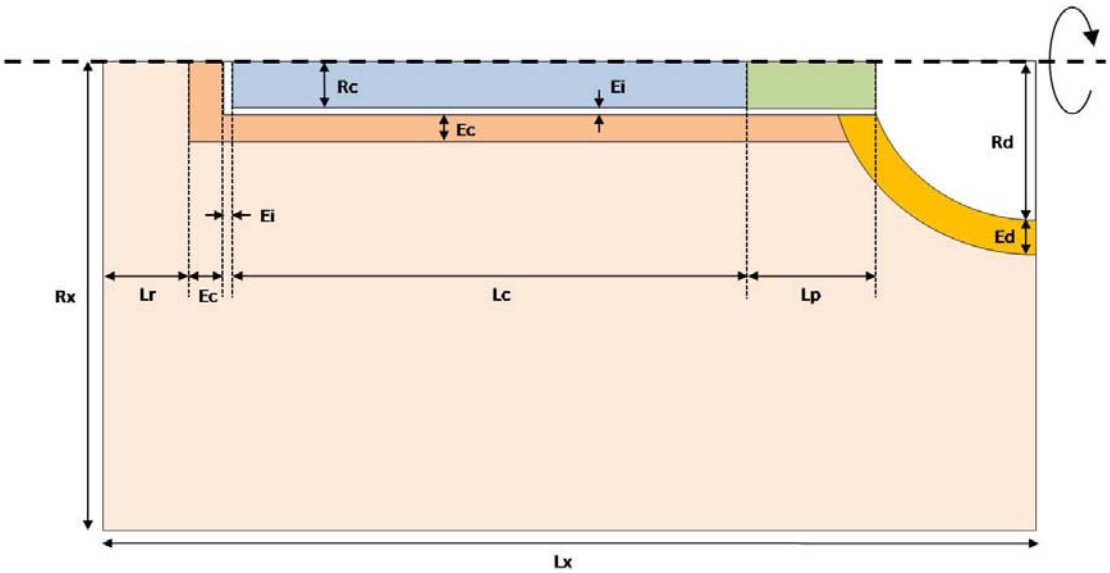


*Figure 68: Dimensions in the calculation domain*

Table 3 : Size of items in the calculation domain

| Name of parameter | Parameter | Value |
|---|---|---|
| Length of the domain (cell axis direction) | Lx | 60 m |
| Radius of the domain | Rx | 20 m |
| Radius of access drift | Rd | 3 m |
| Thickness of the access drift EDZ | Ed | 1 m |
| Length of the plug | Lp | 5 m |
| Length of the canister zone | Lc | 40 m |
| Thickness of the cell EDZ | Ec | 0.5 m |
| Plug and canisters radius | Rc | 0.5 m |
| Thickness of the interface | Ei | 0.01 m |
| Distance between end of cell EDZ and boundary | Lr | 11.5 m |

### 7.2.2 PHYSICAL PARAMETERS

Physical parameters at 20°C are shown in Table 4 (for this first exercise, all calculations are isotherm and temperature is set at 20°C throughout the simulation period).

Table 4 : Physical characteristics of materials

| Parameter (at 20°C) | Materials | | |
|---|---|---|---|
| | Interface facing plug | Interface facing canister | Backfill (access drift) |
| $K_v$ [m²] | $5.0\ 10^{-18}$ | $1.0\ 10^{-12}$ | $5.0\ 10^{-17}$ |
| $K_h$ [m²] | $1.0\ 10^{-17}$ | Kv=Kh | |
| Porosity [%] | 30 | 100 | 40 |
| Specific storage coefficient [m⁻¹] | $4.6\ 10^{-06}$ | $4.6\ 10^{-06}$ | $1.0\ 10^{-05}$ |
| Two-phase flow parameters | | | |
| $S_{gr}$ [%] | 0 | 0 | 0 |
| $S_{wr}$ [%] | 0 | 0 | 0 |
| Van Genuchten parameters | | | |
| n [-] | 4 | 4 | 1.5 |
| $P_r$ [Pa] | $10^4$ | $10^4$ | $2\ 10^6$ |
| □ (Tortuosity) | 1 | 1 | 2 |

| Parameter (at 20°C) | Materials | | |
|---|---|---|---|
| | Bentonite plug | EDZ | Geologial Medium |
| $K_v$ [m²] | $1.0\ 10^{-20}$ | $5.0\ 10^{-18}$ | $5.0\ 10^{-21}$ |
| $K_h$ [m²] | Kv=Kh | $1.0\ 10^{-17}$ | $1.0\ 10^{-20}$ |
| Porosity [%] | 35 | 15 | 15 |
| Specific storage coefficient [m⁻¹] | $4.4\ 10^{-06}$ | $2.3\ 10^{-06}$ | $2.3\ 10^{-06}$ |

| Parameter (at 20°C) | Materials | | |
|---|---|---|---|
| | Bentonite plug | EDZ | Geologial Medium |
| Two-phase flow parameters | | | |
| $S_{gr}$ [%] | 0 | 0 | 0 |
| $S_{wr}$ [%] | 0 | 0 | 0 |
| Van Genuchten parameters | | | |
| n [-] | 1.6 | 1.5 | 1.5 |
| $P_r$ [Pa] | $1.6\ 10^7$ | $1.5\ 10^6$ | $1.5\ 10^7$ |
| □ (Tortuosity) | 4.5 | 2 | 2 |

- Viscosity of the gas mixture:

The viscosity of the gas mixture (water vapour + hydrogen) can be estimated by a classical Wilke approximation or by a simplified formula as follows:

$$\mu_g = \frac{1}{\dfrac{X^g_{H_2}}{\mu^g_{H_2}} + \dfrac{X^g_{wvap}}{\mu^g_{wvap}}} \quad \text{with} \quad \mu^g_{H_2}(T = 293K) = 9\ 10^{-6}\ Pa.s \quad \mu^g_{wvap}(T = 293K) = 10^{-5}\ Pa.s$$

- Diffusion coefficient of dissolved $H_2$ in water:

$$D_{H_2/water} = 1.57\ 10^{-14}\ \frac{T}{\mu_{water}(T)} \quad (m^2/s)$$

- Diffusion coefficient of gaseous $H_2$ in water vapour:
($T_0$=293 K and at $P_0$=1.0·$10^5$ Pa: $D_0$=9.5·$10^{-5}$ $m^2$/s)

$$D^g_{H_2-H_2O} = D_0\left(\frac{P_0}{P}\right)\left(\frac{T}{T_0}\right)^{1.75} \quad (m^2/s)$$

- Diffusion coefficient of dissolved $H_2$ in the water of the porous medium:

$$D^w_{H_2} = S_w\left(\frac{\omega}{\tau^2}\right)D_{H_2/eau}$$

- Diffusion coefficient of dissolved $H_2$ in the binary $H_2$/water-vapour mixture of the porous medium:

$$D^g_{H_2/vap} = (1 - S_w)\left(\frac{\omega}{\tau^2}\right)D^g_{H_2-H_2O}$$

- Solubility of hydrogen in water: $H_{H_2}(T = 293K) = 7.610^{-6}\ mol.Pa^{-1}.m^{-3}$

*Note:* Temperature in diffusion models is stated in Kelvin.

### 7.2.3 Initial conditions

Water saturation:

- in the geological medium is equal to 100%;
- in the cell and drift EDZ is equal to 100%
- in the interface (facing canister and plug) equal to 5%;
- in the bentonite plug is equal to 70%;
- in the backfill of the access drifts is equal to 70%.

Pressure:

- in the water-saturated materials at 100%, the water and gaz pressure are equals to the value at radial outer boundary (respectively 5 MPa and 0.1 MPa, see Boundary limits);
- in partially-saturated materials, the gas pressure is equal to 1 atmosphere. The water pressure is deduced from the gas pressure and the saturation by applying Van Genuchten models associated with each material.

### 7.2.4 Boundary conditions

Figure 69 is a schematic representation of the boundary conditions to be used.

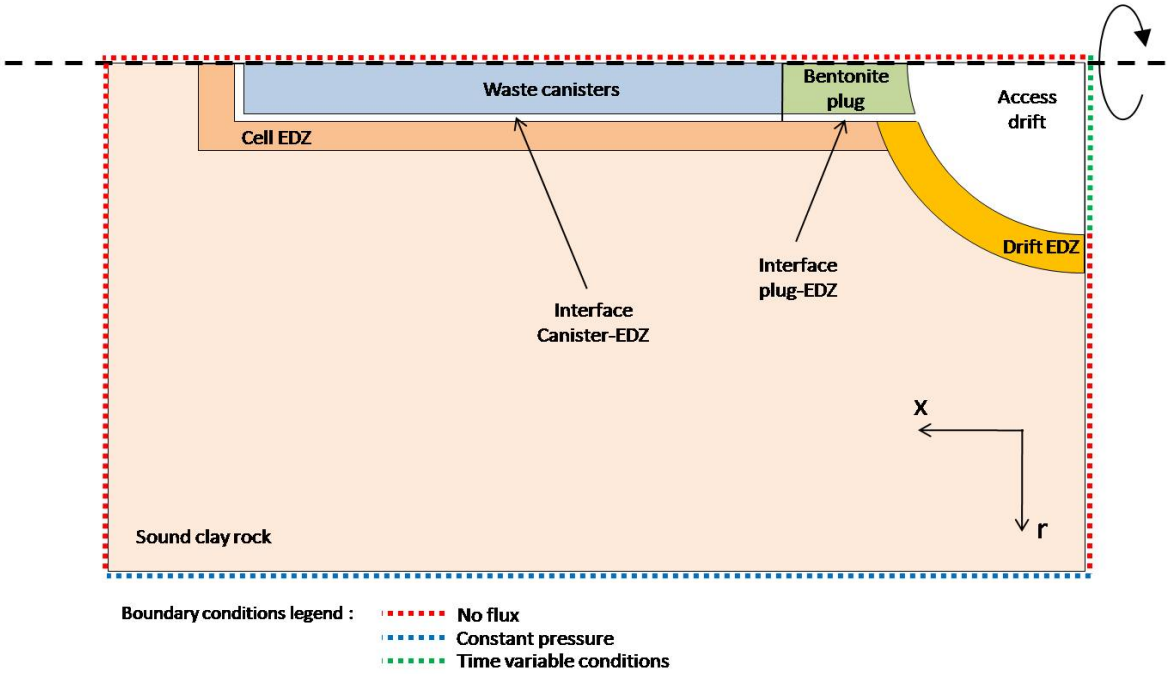


*Figure 69: schematic representation of the boundary conditions*

- Conditions at the outer radius of the calculation domain:

$$P_w(x,r=20,t)=5.0\,10^6\,Pa \quad S_w(x,r=20,t)=1 \quad P_g(x,r=20,t)=1.0\,10^5\,Pa \quad x\in[0,60],\ t\in[0,t_{fin}]$$

As gaseous phase is not expressed, the gas pressure corresponds also to a concentration via Henry's law (see "Mathematical model proposed for the exercise" for details).

- Conditions at the centre (r=0) of the calculation domain:

$$Flux_w(x,r=0,t)=0 \quad Flux_g(x,r=0,t)=0 \quad x\in[0,60] \quad t\in[0,t_{fin}]$$

- Conditions on the lateral side, x=60 of the calculation domain:

$$Flux_w(x=60,r,t)=0 \qquad Flux_g(x=60,r,t)=0 \qquad r\in[0,20] \qquad t\in[0,t_{fin}]$$

- Conditions on the lateral side, x=0 of the calculation domain:

$$Flux_w(x=0,r>3,t)=0 \qquad Flux_g(x=0,r>3,t)=0 \qquad r\in]3,20] \qquad t\in[0,t_{fin}]$$

For r ≤ 3, the boundary conditions are variable in time for water and gas. The representation of these variations can be found in Figure 70.

The boundary conditions represented in Figure 70 are extrapolated from a study made by Andra at a module scale (several hundred of cells). The hypothesis used in this study are a bit different from the one assigned here (especially, the generation term for hydrogen is more complex), but the general behaviour should be the same.

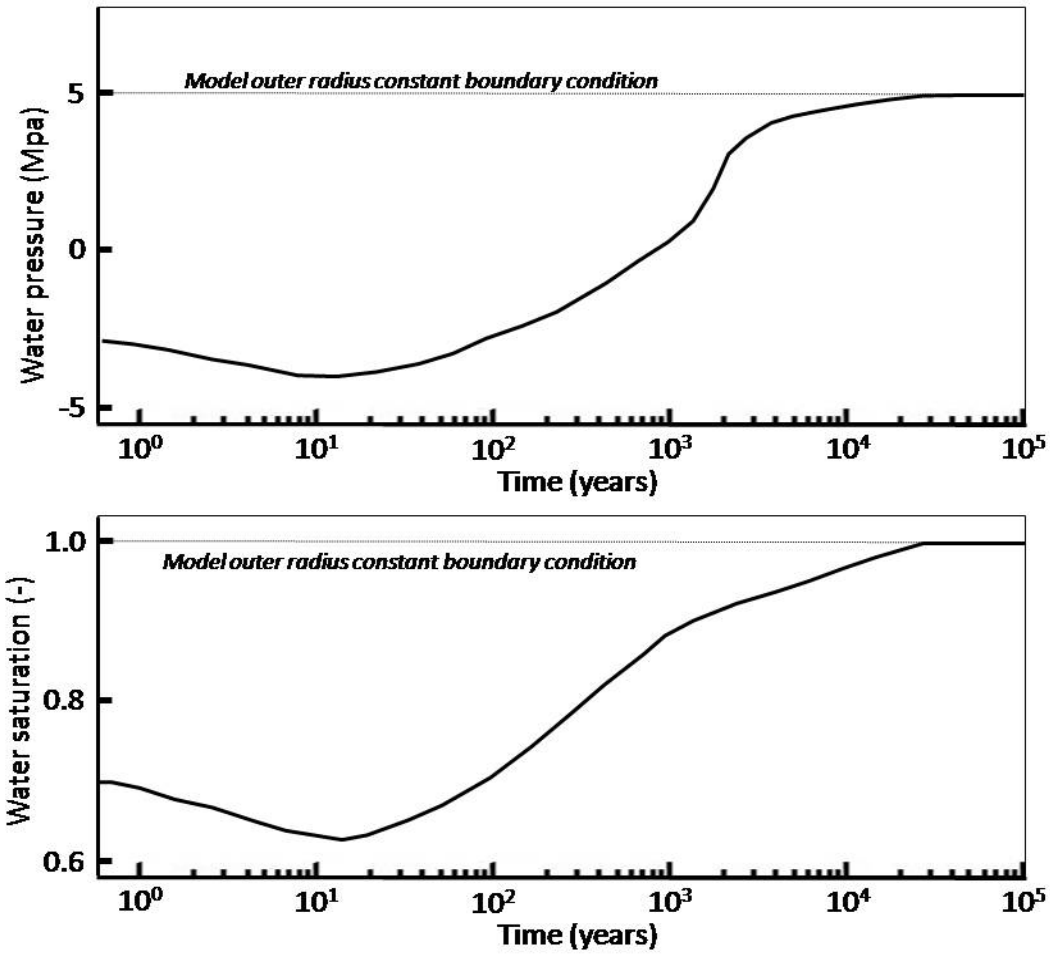


*Figure 70: Time variable boundary conditions to be used in the drift*

### 7.2.5 Production term for hydrogen

The hydrogen-production term is to be distributed over the external surface of the cell, as follows:

- for 0 < t ≤ 10000 years, $Q^g_{H_2} = 100\ mol\ /\ year\ /\ cell$ $\quad Q^w_{H_2} = 0$
- for t > 10000 years $Q^g_{H_2} = 0\ mol\ /\ year\ /\ cell$ $\quad Q^w_{H_2} = 0$

### 7.2.6 Simulation period

The simulation will be performed between moment $t_0=0$ and moment $t_{fin}$=100.000 years.

## 7.3 SENSITIVITY ANALYSIS

For this first exercise, the sensitivity analysis is concentrated oround uncertainties concerning the EDZ, the host rock permeability and the diffusion of H2 in porous media :

- Sensitivity 1 :

The evolution of the EDZ intrinsic permeability with time is not well known, some data however show a reduction of permeability with time down to values similar to those of the undisturbed rock. Concerning the evolution with time of the retention and relative permeability curve of the EDZ, no consistent data are available.

For this sensitivity analysis, everything else being equal to the reference case, EDZ intrinsic permeability (for both drift and cell) is supposed equal to undisturbed rock permeability

- Sensitivity 2 :

Depending of the type of clay rock, Mualem / Van Genuchten curve is not always the best choice for relative permeability of the host rock and EDZ. For certain data a power law fits quite well the measures.

For this sensitivity analysis, everything else being equal to the reference case, relative permeability curve for water and gas of undisturbed host rock and EDZ (for both drift and cell) is supposed to follow saturation at the power 3 :

$$K_r^w = S_w^3 \qquad K_r^g = S_g^3 = (1 - S_w)^3$$

- $K_r^w$ : Relative permeability for water (-)
- $K_r^g$ : Relative permeability for the total gas phase (-)
- $S_w$ : saturation for water (-)
- $S_g$ : saturation for the total gas phase (-)

- Sensitivity 3 :

Uncertainties for the diffusion coefficient of dissolved hydrogen in porous media is quite high and this parameter can have a real impact on the percentage of H2 turning effectively to gas.

For this sensitivity analysis, everything else being equal to the reference case, the diffusion coefficient of dissolved hydrogen under water saturated conditions will be multiplied by 10 for all simulated porous media.

## 7.4 OUTPUT RESULTS

The output will be the same for the reference case and the sensitivity cases.

- Evolution with time of fluxes through surfaces (see Figure 71)

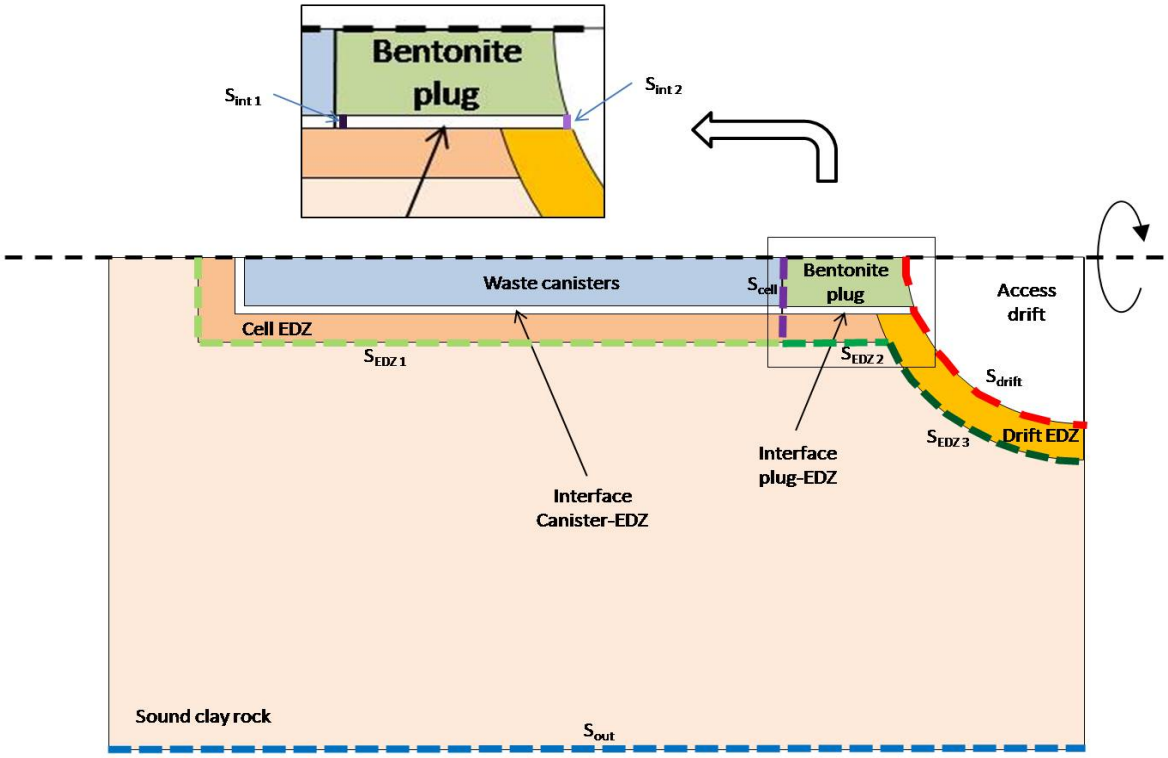


*Figure 71: schematic representation of the surfaces trough which fluxes will be calculated*

Type of fluxes :

- Liquid water flux
- Water vapor
- Gaseous H2
- Dissolved H2

Type of surfaces :

- Outer boundary of the model at r=20 m ($S_{out}$ in Figure 71), fluxes counted positively out of the model.
- Drift wall ($S_{drift}$ in Figure 71), fluxes counted positively toward the drift
- Outside surface of the EDZ, separated in 3 sections (see Figure 71): $S_{EDZ1}$ (around canister), $S_{EDZ2}$ (around plug), $S_{EDZ3}$ (drift EDZ). Fluxes counted positively out of the EDZ toward the undisturbed rock
- Inner cell surfaces (see Figure 71) : Scell (section including interface and EDZ at canister-plug junction), Sint1 (interface at canister-plug junction), Sint2 (interface at the drift wall). Fluxes counted positively toward the drift.

- Evolution with time along lines (see Figure 72)

Evolution with time of :

- Water saturation
- Water pressure
- Gas pressure (in the gas phase when it exists)
- Dissolved H2 pseudo-pressure (see Henry's law in paragraph 7.5 "Mathematical model proposed for the exercise" for details)
- Capillary pressure

Type of lines

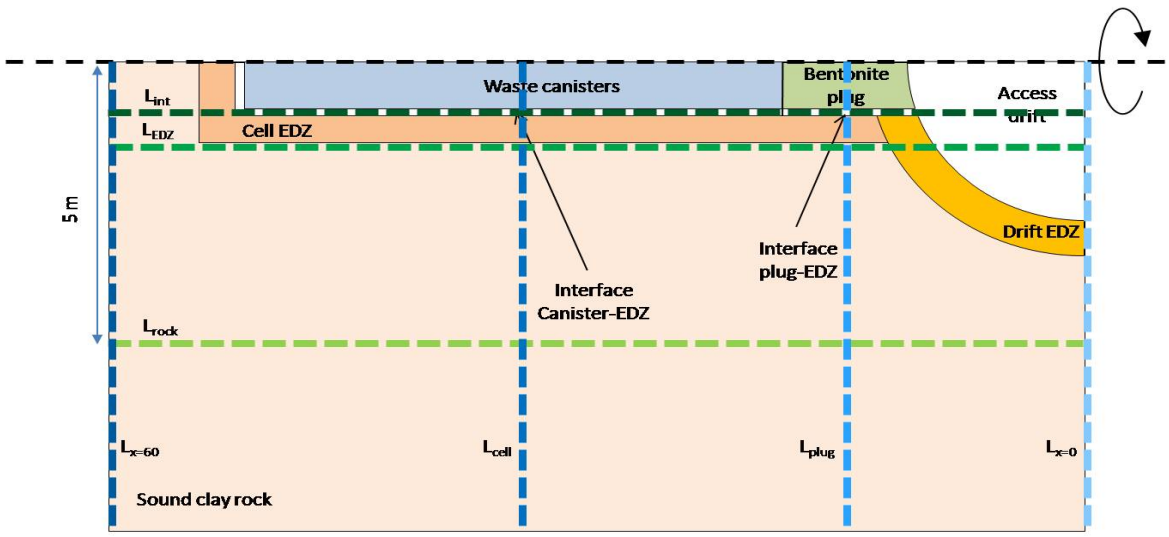


*Figure 72: schematic representation of the lines along which results should be given*

- Lines at constant radius (see Figure 72) : $L_{int}$ (passes through the interface), $L_{EDZ}$ (just outside the cell EDZ), $L_{rock}$ (inside the rock at a 5 m radius)
- Lines at constant x (see Figure 72) : $L_{x=0}$ and $L_{x=60}$ (boundaries of the model), $L_{plug}$ (in the middle of the plug), $L_{cell}$ (in the middle of the canister)

- Evolution with time at given points (see Figure 73)

Evolution with time of :

- Water saturation
- Water pressure
- Gas pressure (in the gas phase when it exists)
- Dissolved H2 pseudo-pressure (see Henry's law in paragraph 7.5"Mathematical model proposed for the exercise" for details)
- Capillary pressure

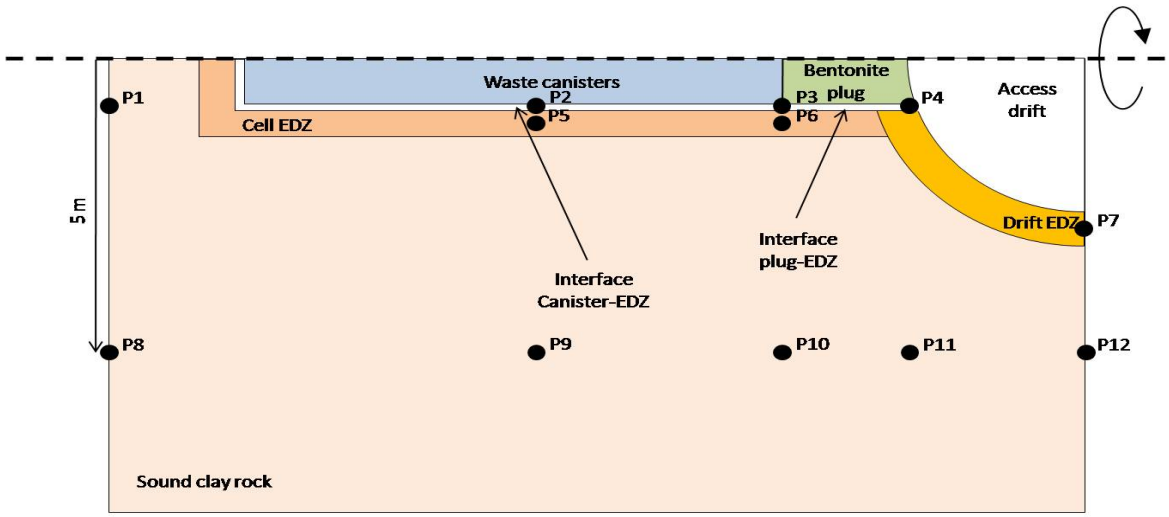

*Figure 73: schematic representation of the point where results should be given*

Type of points :

- Points 1 to 4, at the same radius as the centre of the interface (see Figure 73) : P1 and P4 (at the boundaries), P2 (in the middle of the canister), P3 (in the middle of the plug)
- Points 5 and 6, at the same radius as the centre of the cell EDZ (see Figure 73) : P5 (in the middle of the canister), P6 (in the middle of the plug)
- Point 7 (see Figure 73) in the middle of the drift EDZ on the x=0 boundary
- Points 8 to 12, at a 5 m radius (see Figure 73) : P8 and P12 (at the boundaries), P9 (at the same x as the middle of the canister), P10 (at the same x as the middle of the plug), P11 (at the same x as the intersection of the drift and the interface)

## 7.5 MATHEMATICAL MODEL PROPOSED FOR THE EXERCISE

The capillary pressure is defined as the difference between gas pressure and water pressure :

$$P_C = P_g - P_w \qquad (1)$$

- *Pc* : capillary pressure (Pa)
- *Pg* : total pressure of the gas phase(Pa)
- *Pw* : water pressure (Pa)

The dependence between water and gas saturation in each porous media is expressed by :

$$S_g + S_W = 1 \quad \text{with} \quad S_g = \frac{V_g}{V_p} \text{ and } S_w = \frac{V_w}{V_p}$$

- Sg : gas saturation (-)
- Sw : water saturation (-)
- Vg : gas volume (m3)
- Vw : water volume (m3)
- Vp : pore volume (m3)

Van Genuchten model is used to express capillary pressure function of the effective saturation in a given porous media :

$$S_{we} = \frac{S_w - S_{wr}}{1 - S_{wr} - S_{gr}} \qquad (2)$$

$$S_{we} = \frac{1}{\left[1 + \left(\frac{P_c}{P_r}\right)^n\right]^m} \qquad (3)$$

- Swe : Effective water saturation (-)
- Swr = residual water saturation (-)
- Pr : reference pressure for Van genuchten law (Pa). Generally the value for this coefficient is higher than the gas entry pressure for a given porous media
- n, m : coefficient for Van genuchten law. We have $m = 1 - \frac{1}{n}$

The relative permeability for water is expressed by integrating the Mualem prediction model in the Van Genuchten capillarity model :

$$k_r^w = \sqrt{S_{we}}\left[1-\left(1-S_{we}^{1/m}\right)^m\right]^2 \quad (4)$$

- $k_r^w$ : relative permeability for water (-)

The relative permeability for gas is expressed similarly :

$$k_r^g = \sqrt{1-S_{we}}\left[1-S_{we}^{1/m}\right]^{2m} \quad (5)$$

- $k_r^g$ : relative permeability for gas (-)

The water and gas movement in a porous media is represented by the mass conservation law and the energy conservation law (reduced to the generalized Darcy law) :

$$U_w = -\frac{kk_r^w(S_w)}{\mu_w}(\nabla P_w + \rho_w g \nabla z) \quad (6)$$

$$U_g = -\frac{kk_r^g(S_g)}{\mu_g}(\nabla P_g + \rho_g g \nabla z) \quad (7)$$

- K : intrinsic permeability of the porous media (m2)
- μg : viscosity of the total gas phase (kg.s-1.m-1)
- μw : viscosity of water (kg.s-1.m-1)
- ρg : volumetric mass of the total gas phase (kg.m-3)
- ρw : volumetric mass of water (kg.m-3)

$$\rho_w(P_w) = \rho_{atm}\exp\left[S_s(P_w - P_{atm})\right] \quad (8)$$

ρatm : volumetric mass of water at atmospheric pressure (kg.m-3)
Patm : atmospheric pressure (Pa)
Ss : specific storage (Pa-1)

- g : gravity (m.s-2)
- z : altitude (m)
- Ug : Darcy velocity for the gas phase (m.s-1)
- Uw : Darcy velocity for water (m.s-1)

Equation of conservation for water :

$$\frac{\partial(\rho_w \omega S_w)}{\partial t} + \nabla(\rho_w U_w) = Q^w \quad (9)$$

- ω : porosity (-)
- Qw : consumption/production of water (kg.m-3.s-1)

Equation of conservation for the total gas phase :

$$\frac{\partial(\rho_g \omega S_g)}{\partial t} + \nabla(\rho_g U_g) = Q^g \quad (10)$$

- Qg : consumption/production for the total gas phase (kg.m-3.s-1)

The mass fraction of gaseous hydrogen is expressed as :

$$X_{H_2}^g = \frac{\rho_{H_2}^g}{\rho_g} \quad (11)$$

With $\rho_{H_2}^g = \frac{m_{H_2}^g}{V_g}$ and $\rho_g = \frac{m^g}{V_g}$

- $X_{H_2}^{g}$ is the mass fraction of hydrogen in the total gas phase (-)
- $m_{H_2}^{g}$ is the hydrogen mass in the gaz phase (kg)
- $m^{g}$ is the total mass of the gas phase (kg)
- $\rho_{H_2}^{g}$ is the volumetric mass of gaseous hydrogen in the gas phase (kg.m-3)

Mass conservation law for gaseous hydrogen :

$$\frac{\partial}{\partial t}(\omega S_g \rho_g X_{H_2}^{g}) + \nabla(\rho_g X_{H_2}^{g} U_g - J_{H_2}^{g}) + \Omega_{H_2}^{g/l} = Q_{H_2}^{g} \qquad (12)$$

- $\Omega_{H_2}^{g/l}$ is the exchange term from the gaseous phase to the liquid phase for H2 (kg.m-3.s-1)
- $Q_{H_2}^{g}$ is the consumption/production term for gaseous hydrogen (kg.m-3.s-1)
- $J_{H_2}^{g}$ is the diffusive term for gaseous hydrogen (kg.m-2.s-1)

Diffusive flux for a binary mixture of gas (H2 and water vapor) can be expressed by Kick law :

$$J_{H_2}^{g} = \rho_g D_{H_2 vap}^{g} \nabla X_{H_2}^{g} \qquad (13)$$

- $D_{H_2 vap}^{g}$ is the diffusion coefficient for gaseous hydrogen in water vapor (m2.s-1)

The mass fraction of dissolved hydrogen is expressed as :

$$X_{H_2}^{w} = \frac{\rho_{H_2}^{w}}{\rho_w} \qquad (14)$$

With $\rho_{H_2}^{w} = \frac{m_{H_2}^{w}}{V_w}$ and $\rho_w = \frac{m^{w}}{V_w}$

- $X_{H_2}^{w}$ is the mass fraction of dissolved hydrogen (-)
- $m_{H_2}^{w}$ is the dissolved hydrogen mass (kg)
- $m^{w}$ is the total mass of the liquid phase (kg)
- $\rho_{H_2}^{w}$ is the volumetric mass of dissolved hydrogen in the liquid phase (kg.m-3)

Mass conservation law for dissolved hydrogen is expressed as :

$$\frac{\partial}{\partial t}(\omega S_w \rho_w X_{H_2}^{w}) + \nabla(\rho_w X_{H_2}^{w} U_w - J_{H_2}^{w}) + \Omega_{H_2}^{l/g} = Q_{H_2}^{w} \qquad (15)$$

- $\Omega_{H_2}^{l/g}$ is the exchange term from the liquid phase to the gas phase for H2 (kg.m-3.s-1)
- $Q_{H_2}^{w}$ is the consumption/production term for dissolved hydrogen (kg.m-3.s-1)
- $J_{H_2}^{w}$ is the diffusive term for dissolved hydrogen (kg.m-2.s-1)

The exchange terms from between liquid and gaseous phase are linked by the following relation :

$$\Omega_{H_2}^{l/g} = -\Omega_{H_2}^{g/l} \qquad (16)$$

Diffusive flux for dissolved hydrogen can be expressed by Kick law :

$$J_{H_2}^{w} = \rho_w D_{H_2 vap}^{w} \nabla X_{H_2}^{w} \qquad (17)$$

- $D_{H_2 vap}^{w}$ is the diffusion coefficient for dissolved hydrogen in water vapor (m2.s-1)

Part of the gas will be dissolved in the pore water. The solubility limit for the gas depend mainly on thermodynamic conditions and can be expressed by Henry's law :

$$C_{H_2}^{w} = H_{H_2}(T) P_{H_2}^{g} \quad (18)$$

Where $C_{H_2}^{w} = \dfrac{X_{H_2}^{w} \rho_w}{M_{H_2}}$

- $C_{H_2}^{w}$ is the maximum concentration of hydrogen in water (mol.m-3)
- $H_{H_2}$ is the constant of Henry's law for hydrogen (mol.m-3.Pa-1)
- $P_{H_2}^{g}$ is the partial pressure of hydrogen in the total gaseous phase (Pa)
- $M_{H_2}$ is the molar mass for hydrogen (kg.mol-1)

The relation between partial pressure of each gas present in the total gas phase and total gas pressure is given by Dalton law that writes for a binary mixture (H2 and water vapor) :

$$P_g = P_{H_2}^{g} + P_{wvap}^{g} \quad (19)$$

- $P_{wvap}^{g}$ is the partial pressure of water vapor in the total gas phase (Pa)

Each of the gas is supposed perfect :

$$P_{H_2}^{g} = \frac{\rho_{H_2}^{g}}{M_{H_2}} RT \text{ and } P_{wvap}^{g} = \frac{\rho_{wvap}^{g}}{M_{wvap}} RT \quad (20,21)$$

For the gas mixture this writes :

$$P_g = \frac{\rho_g}{M_g} RT \quad (22)$$

- Mg : molar mass for the total gaseous phase (H2 + water vapor) (kg.mol-1)
- R : constant of the perfect gas (J.mol-1.K-1) : R = 8.314 J.mol-1.K-1
- T : temperature (°K)

Saturation pressure for water vapor is only depending on temperature and can by expressed by :

$$\log_{10}(P_{sat}) = 2.786 + 0.031514 T_c - 1.2373x10^{-4} T_c^{\,2} + 4.2267x10^{-7} T_c^{\,3} - 8.1308x10^{-10} T_c^{\,4} \quad (23)$$

- Psat : saturation pressure for water vapor (Pa)
- Tc : Temperature (°C)

Kelvin law is giving a relation between saturation pressure for water vapor, effective pressure for water vapor and capillary pressure :

$$P_{wvap}^{g}(T, S_w) = \exp\left(\frac{M_w P_c(S_{w)}}{\rho_w RT}\right) P_{sat}(T) \quad (24)$$